Parameter optimisation for the improved modelling of industrial-scale gas explosions

Anna-Lena Both

Thesis for the degree of Philosophiae Doctor (PhD)
University of Bergen, Norway
2019

UNIVERSITY OF BERGEN

Parameter optimisation for the improved modelling of industrial-scale gas explosions

Anna-Lena Both

Thesis for the degree of Philosophiae Doctor (PhD)
at the University of Bergen

Date of defense: 17.06.2019

Year: 2019

Title: Parameter optimisation for the improved modelling of industrial-scale gas explosions

Name: Anna-Lena Both

Print: Skipnes Kommunikasjon / University of Bergen

Preface

In the submitted version of the thesis, Paper 3 was listed as "submitted [...]". Since submission of the thesis, the article has been published by the journal. Please find the details here:

Both, A.-L., Atanga, G. & Hisken, H. (2019). CFD modelling of gas explosions: optimising sub-grid model parameters. *Journal of Loss Prevention in the Process Industries*, **60**, 159–173, doi: https://doi.org/10.1016/j.jlp.2019.04.008.

Acknowledgements

Special thanks are offered to my research supervisors. Prof. Dr Jan J. Rückmann, thank you for your professional guidance and for keeping my progress always organised and on schedule. Prof. Dr Trond Steihaug, your patient advice in the theoretical, mathematical part of my thesis has been much appreciated. Thank you!

My very deep gratitude is given to my colleague, supervisor and best friend, Dr Helene Hisken. Thank you for your valuable knowledge and constructive support during the planning, development and writing of this research thesis. Your willingness to give your time so generously has been great. Without you, this thesis would not have been written.

I would like to thank my colleague and supervisor, Dr Michał Folusiak. Thanks a lot for your continuous assistance especially concerning my many questions about coding and writing.

My grateful thanks are extended to all my former and present colleagues at Gexcon – with a special mention to Dr Gordon Atanga, Dr Trygve Skjold, Lorenzo Mauri, Djurre Siccama, Dr Deiveegan Muthusamy, Idar Storvik, Dr Kees van Wingerden, Dr Lars Pesch, Dr Sunil Lakshmipathy, and Dr Scott G. Davis. Thank you for fruitful discussions, constructive critiques and enthusiastic encouragement during all those years. I have greatly enjoyed working together with my fellow PhD students, Marika Ivanová, Helene Hisken, Laurence Bernard, and Maryam Ghaffari. Thank you for sharing this unique experience with me.

Thanks to everybody who proofread my work. Your friendly, pushing comments and help had a profound impact on the final result.

The financial support from the Research Council of Norway through the industry PhD scheme, grant no. 246167, is gratefully acknowledged.

My deepest thanks goes to my whole family and friends. Without you, I would not be the person I am today. Jakub, thank you so much for always believing in me, your love and endless support. Isak, I thank you for all the laughter and happiness you bring to our lives. We love you so much!

Abstract

This thesis presents work on improving the predictive capabilities of a numerical model by parameter optimisation. The numerical model is based on computational fluid dynamics (CFD) and predicts the consequences of industrial-scale gas explosions. CFD models are, in general, approximate representations of real phenomena of interest; often, the agreement between model output and relevant experimental data can be improved through optimising parameters in the model. In this work, the parameters considered for optimisation are contained in sub-grid models for turbulence and combustion.

The doctoral project focuses on the gas explosion module of the commercial CFD tool FLACS. Explosion predictions of the tool are utilised in risk management for safer design of industrial facilities handling combustible gases. The challenge of simulating gas explosions with the CFD tool is that the predictions have to be reliable for many different explosion scenarios in extremely different large-scale geometries. This thesis presents an optimisation approach that considers this wide application range of the CFD model.

Four papers constitute the main part of the thesis; they propose a methodology for formulating and solving the optimisation problem (Paper 1, 2 and 4) and present examples of application (Paper 3). Additionally, the thesis comprises scientific contributions that have not been presented in the papers.

Amongst several candidates, suitable model outputs are identified as optimisation targets. The problem has first been formulated as a least-squares problem (Paper 4); this formulation did not appear to be appropriate for improving model predictions in gas explosions. Thus, in Paper 2, a problem formulation is developed that assesses under- and over-predictions as in model validation processes. This validation-based formulation is shown to be closely connected to another formulation in which the solution is the maximum likelihood estimator in the case of log-normally distributed errors in the measurements. It is shown that in contrast to a traditional least-squares problem formulation, the validation-based formulation yields an overall better improvement of the specific model outputs. The thesis presents three methodologies for selecting gas explosion experiments to be included in one optimisation process.

Running simulations is time-consuming. To enable a practical optimisation runtime, the model output is approximated by surrogates, which are fast to evaluate. Surrogates are explicit functions representing parameter-output relations. In Paper 1, surrogates based on neural networks are compared to polynomial response surfaces. Due to the satisfactory overall approximation quality of the neural networks in this application, these are employed as surrogates in subsequent optimisation processes. Furthermore, the smoothness of the surrogates allows for employing gradient-based optimisation routines; the resulting surrogate-based optimisation problem is solved by a trust

region method embedded in a multi-start approach that has originally been intended for non-linear least-squares problems. As the developed optimisation problem is not a least-squares problem, the convergence of the routine for this problem with respect to the first order necessary optimality conditions is proven in Paper 2. In the end, to ensure that it is not a blind fit of the optimisation targets, but that characteristic physical phenomena of gas explosions are represented by the model, a comprehensive sanity check of the model is performed after optimisation.

The optimisation approach is used for two purposes: i) to obtain optimal parameter values that lead to reliable predictions for a wide range of applications, and thus can be implemented in the CFD tool; ii) to analyse physical models and detect their strengths and limitations. In this thesis, the second purpose is illustrated by an exemplary analysis of a flame folding model; optimisation for the first purpose is examined in more detail. In particular, the optimisation approach is tested and applied successfully to several versions of the CFD tool FLACS at different stages in the development process: a version released for commercial use and an in-house development version. The applicability of the optimisation approach is shown by testing it on the release version in Paper 2 and Paper 4. The in-house development version comprises models that have been updated recently with parameter values that have been set to an initial 'best guess', and thus requires optimisation. The in-house development version comprises updated models in which parameter values have been set to an initial 'best guess' and thus requires optimisation. Optimising the development version in Paper 3 improves the predictions significantly.

It is important to note that the optimisation process cannot compensate for models that do not capture the physical mechanisms of gas explosions. Thus, optimisation processes cannot replace further efforts in CFD modelling. However, the optimisation process has proven to be highly useful for supporting modelling efforts (Paper 3); analysing predictions of the optimised model may give information about the model's predictive capabilities, may suggest updated user guidelines, or may enable a discussion on how to progress within the development of the physical models. Such conclusions for recently updated model systems had been impossible to draw before model parameter optimisation.

List of papers

1. Braatz, A.-L.* & Hisken, H. (2017). Response surfaces for advanced consequence models: Two approaches. *Journal of Loss Prevention in the Process Industries*, **49**, Part B: 683–699.

2. Both, A.-L.*, Hisken, H., Rückmann, J.-J. & Steihaug, T. (2019). Surrogate-based model parameter optimization based on gas explosion experimental data. *Engineering Optimization*, **51**(2):301–316.

   Supplementary material.

3. Both, A.-L.*, Atanga, G. & Hisken, H. (2019). CFD modelling of gas explosions: optimising sub-grid model parameters. *Submitted to Journal of Loss Prevention in the Process Industries*.

4. Braatz, A.-L.*, Hisken, H. & Rückmann, J.-J. (2016). Surrogate-based optimisation of model parameters for the improved modelling of industrial-scale gas explosions. *Proceedings 5th International Conference on Engineering Optimization (EngOpt), 19–23 June 2016, Iguassu Falls, Brazil*, Published by E-papers Serviços Editoriais Ltda: 398–398. ISBN: 978-85-7650-548-8.

*The candidate changed her name from Anna-Lena Braatz to Anna-Lena Both in 2017.

List of papers not included in the present dissertation

1. Bau, U., Braatz, A.-L.*, Lanzerath, F., Herty, M. & Bardow, A. (2015). Control of adsorption chillers by a gradient descent method for optimal cycle time allocation. *International Journal of Refrigeration*, **56**: 52–64.

2. Braatz, A.-L.* & Hisken, H. (2016). Response surfaces for advanced consequence models: two approaches. *Proceedings Eleventh International Symposium on Hazards, Prevention and Mitigation of Industrial Explosions (ISHPMIE), 24–29 July 2016, Dalian, China*: 893–910. ISBN: 978-7-89437-165-2.

Scientific environment

The work presented in this thesis was conducted as part of the PhD studies at Gexcon AS and the Department of Informatics, University of Bergen. The doctoral project was funded by the Research Council of Norway (RCN) through the Industrial PhD scheme, grant number 246167, and Gexcon. The project period spanned four years, from which three years were reserved for the doctoral study and one year for work assignments in Gexcon. The candidate has been enrolled in the Research school in Information and Communication Technology (ICT Research School) at the Department of informatics, University of Bergen, and has been supervised by Professor Jan-J. Rückmann and Professor Trond Steihaug (co-supervisor).

The candidate has been employed as a Research Engineer in the Research and Development (R&D) department at Gexcon since January 2015. Co-supervisors at Gexcon have been Dr Michał Folusiak and Dr Helene Hisken. The R&D department of Gexcon develops and maintains the computational fluid dynamics (CFD) solver Flacs which is able to simulate gas dispersion, fires and explosions in large-scale realistic geometries. Flacs is an integrated part of the commercial software product FLACS.

The doctoral study evolved from a previous study by Dr Helene Hisken at Gexcon. In that study, Dr Helene Hisken worked with Dr Scott G. Davis from the Gexcon US office who developed (together with co-workers) an optimisation technique for detailed chemical kinetics models. Dr Helene Hisken applied it to parameter optimisation in FLACS. As part of a summer intern ship 2014, the candidate contributed to this study.

During the doctoral study, the candidate has followed up the idea of parameter optimisation in FLACS. She developed and implemented an approach for optimising parameters in the model system in FLACS. Through the work as Research Engineer, the candidate has optimised various development versions of the model system. Additionally, she has contributed to the joint industry project (JIP) "Modelling Escalating Accident Scenarios and the Use of Risk-reducing technology for Explosion safety (MEASURE)" (2013–2016). The candidate has also been involved in customer support in 2016–2017.

Abbreviations

AMF	Approximation Management Framework
AMMF	Approximation Model Management Framework
AMMO	Approximation Model Management Optimisation
ANN	Artificial Neural Network
BFETS	Blast and Fire Engineering for Topside Structures
CFD	Computational Fluid Dynamics
DNS	Direct Numerical Simulation
GP	Gaussian Process
JIP	Joint Industry Project
LES	Large Eddy Simulation
MARS	Multivariate Adaptive Regression Splines
MEASURE	Modelling Escalating Accident Scenarios and the Use of Risk-reducing technology for Explosion safety
MERGE	Modelling and Experimental Research into Gas Explosions
MG	Geometric Mean bias
MLE	Maximum Likelihood Estimator
MLP	MultiLayer Perceptrons
PDR	Porosity/Distributed Resistance
PRS	Polynomial Response Surface
QRA	Quantitative Risk Assessment
RANS	Reynolds-Averaged Navier–Stokes equations
RBF	Radial Basis Function
RCN	The Research Council of Norway
RSM	Response Surface Methodology
RSNN	Response Surface based on Neural Networks
SMF	Surrogate Management Framework
SVM	Support Vector Machines
SVR	Support Vector Regression
VG	Geometric mean Variance

Contents

Preface i

Acknowledgements iii

Abstract v

List of papers vii

Scientific environment ix

Abbreviations xi

1 Introduction 1
- 1.1 Consequence modelling of hazardous accidental gas explosions 1
- 1.2 Empirical sub-grid model calibration 2
- 1.3 Need for parameter optimisation in a CFD tool 2
- 1.4 Research literature and context 3
- 1.5 Scope of the thesis 4
- 1.6 Thesis outline 6

2 Formulating the optimisation problem 9
- 2.1 Sub-grid models and their parameters 9
- 2.2 Relevant model responses 10
- 2.3 Selecting gas explosion experiments 11
  - 2.3.1 Selecting experiments for improving modelling 11
  - 2.3.2 Selecting experiments for testing the optimisation approach . . 13
  - 2.3.3 Experimental campaigns considered in this work 14
  - 2.3.4 Covering a wide range of validation categories 14
  - 2.3.5 Experimental uncertainty 15
- 2.4 Assessing over- and under-predictions 17
  - 2.4.1 The validation-based problem formulation 17
  - 2.4.2 The VG formulation – minimising the geometric mean variance 17
  - 2.4.3 The statistical point of view – maximum likelihood estimator . . 18
  - 2.4.4 Relation of the VG formulation to the validation-based formulation 19
- 2.5 Weighting strategies and multi-objective optimisation 19
- 2.6 Outlier robust optimisation 20

3 Surrogate-based optimisation **23**
3.1 Surrogate modelling – a general overview . . . 23
3.2 Surrogates considered in this work . . . 24

4 Solving the optimisation problem **27**
4.1 Gradient-free vs gradient-based optimisation . . . 27
4.2 Adaptive sampling vs one-shot solution . . . 28
4.3 Trust region optimisation with a multi-start strategy . . . 28
4.4 Regularisation . . . 29

5 Application to the CFD tool FLACS **31**
5.1 Optimising the standard model within a single validation category . . . 31
5.2 Optimising the standard model across validation categories . . . 32
5.3 Optimising the development model across validation categories . . . 32
5.3.1 Testing different weights in the objective function . . . 32
5.3.2 Testing the VG problem formulation . . . 35
5.4 Optimisation for analysing the flame folding model . . . 37

6 Concluding remarks and future work **39**

Appendices **43**

A Approximation quality of surrogates **45**
A.1 Flame speed . . . 45
A.2 Pressure rising time . . . 45

B Trust region algorithm **49**
B.1 Without box constraints . . . 49
B.2 With box constraints . . . 51

C Optimisation of the standard model for a wide range of experiments **53**
C.1 Optimisation within validation categories . . . 54
C.2 Optimisation for experiments across validation categories . . . 55
C.3 The optimal parameter values . . . 62
C.4 Including outliers in the optimisation . . . 62
C.5 Conclusion . . . 63

D Optimising the flame folding model **65**
D.1 The Gaps project . . . 65
D.2 Sensitivity analysis . . . 65
D.3 Optimal parameter values and validation results . . . 68

Bibliography **71**

Papers **77**

List of Figures

2.1 Experimental variability for the repetitions of the BFETS, Phase 3A, series 'Alpha' and 'Beta'. 16

5.1 Overpressure-time histories for MERGE E with a propane-air mixture for the development model optimised for different weighted sums. . . . 35
5.2 Validation of the development and optimised model for the VG problem formulation. 36

A.1 Validation of surrogates for the flame speed of experiment MERGE B with propane-air at several monitor points. 46
A.2 Validation of a surrogate for the pressure rising time of experiment MERGE B with propane-air. 46
A.3 Switch in the strength of the pressure peaks for varying parameter values from the uncertainty space for MERGE B with propane-air. 47

C.1 Validation of the standard model optimised for validation categories separately. 54
C.2 Validation of the standard model optimised for all selected experiments together. 56
C.3 Validation of the surrogates at the overall optimal parameter values. . . 56
C.4 Validation of the overall optimised model, separately for each campaign. 59
C.5 Maximum overpressure across the rig for BFETS Phase 2 experiments for the standard and overall optimised model and experimental data. . . 60
C.6 Overpressure-time histories for BFETS Phase 2 experiments for the standard model, overall optimised model and experimental data. 62
C.7 Validation of the standard model optimised for all selected experiments together including outliers. 63

D.1 First order local sensitivities for DNV GL 182 m^3 vented enclosure tests. 67
D.2 First order local sensitivities for Gaps project tests. 68
D.3 Validation of the model optimised for flame folding for the DNV GL 182 m^3 vented enclosure experiments. 69
D.4 Validation of the model optimised for flame folding for the Gaps project experiments. 70

List of Tables

2.1 Functioning of the optimisation approach. 12

5.1 Optimal parameter values of the development model for different weights in the aggregated objective function. 34
5.2 Optimal parameter values for the development model for different problem formulations. 35

C.1 Optimal parameter values for different optimisation cases for the standard model. 62

D.1 Experimental configurations for selected tests of the Gaps project. . . . 66
D.2 Optimal parameter values for different optimisation cases. 69

Chapter 1

Introduction

1.1 Consequence modelling of hazardous accidental gas explosions

An inherent part of risk analysis in industries dealing with combustible gases is to assess the consequences of potential accidental gas explosions. According to Cant et al. (2004), numerical models based on computational fluid dynamics (CFD) are increasingly employed in consequence modelling to design safer structures. CFD models solve partial differential equations for the conservation of mass, momentum, energy, and fraction of chemical species.

Three main approaches can be distinguished: direct numerical simulation (DNS), large eddy simulation (LES) and Reynolds-averaged Navier–Stokes simulation (RANS). The approaches differ in defining the threshold of the scale below which the flow is assumed to be isotropic, i.e., uniform in all directions independent from the geometry. Turbulent flow below the defined scale, also called filter scale or grid scale, is described by an isotropic turbulence model. Above the filter scale, the flow is assumed to be geometry-dependent, and the Navier–Stokes equations are solved (Warnatz et al., 1996). In DNS, the filter scale is set below the Kolmogorov scale (the size of the smallest turbulence structures), and thus all scales are computed. As the scales in turbulent flow may be small compared to laminar flow, the computational grid is required to be relatively fine – invoking large computational times. An example can be found in (Warnatz et al., 1996). In contrast to DNS, in RANS the filter scale is implicitly assumed as a large scale. Hence, turbulence models are employed for a wide range of scales. In LES, the filter scale is placed in between the ones defined in DNS and RANS. Consequently, the computational time is typically less than for DNS and more than for RANS. A discrete solution obtained from DNS is the most accurate one. However, up to today, only small systems and low Reynolds number flows can be simulated with DNS due to limitations in practical simulation time and memory storage. In the context of simulating industrial-scale gas explosions as part of quantitative risk analyses (QRAs), the solution is, in general, not required to be that detailed; thus, in commercial CFD tools, RANS is employed most often (Skjold et al., 2018).

FLACS[1] is a CFD tool that relies on a turbulence model based on RANS equations (Gexcon AS, 2019). Geometries are represented on the computational grid using the porosity/distributed resistance (PDR) concept, cf. (Hjertager, 1986; Patankar and

[1] FLACS (FLame ACceleration Simulator) is a commercial CFD tool distributed by Gexcon AS.

Spalding, 1974; Sha et al., 1982). According to the PDR concept, for each control volume cell and cell face, a volume and an area porosity value is assigned, respectively. The porosity values lie between 0 and 1 and define the blockage of a cell or cell face by geometry. Taking into consideration the detailed geometry layout, especially for sub-grid geometries (smaller than the grid cell size), is a key requirement for estimating explosion loads in medium- and large-scale gas explosions. The primary mechanism for flame acceleration in congested geometries is the positive feedback between the expansion of combustion products, turbulence generated in the un-reacted mixture, especially in shear and boundary layers from flow past obstacles and walls, and enhanced combustion rates (Hjertager, 1984). Therefore, the success of the CFD tool FLACS depends on the implementation of sub-grid models (Skjold et al., 2014) accounting for under-resolved governing physical phenomena on scales smaller than the grid cell size.

1.2 Empirical sub-grid model calibration

Sub-grid models are, in general, less fundamental than the Navier–Stokes equations; the latter are based on fundamental physical laws derived from first principles, while sub-grid models are often phenomenological correlations (with little or no theoretical backing) based on measurements. Sub-grid models often contain constants called model coefficients or parameters. In empirical studies, suitable observations are used to determine the parameter values that have the maximum likelihood of being accurate within an acceptable tolerance. This process is called model calibration or estimation. An example is given by Bradley et al. (2013, 2011a) modelling the correlation for the turbulent burning velocity. The correlation can be found in the Appendix of Paper 3. To estimate parameters in the correlation, Bradley et al. (2013, 2011a) employed measurements of the turbulent burning velocity during an implosion in a fan-stirred spherical bomb. Several other examples for empirical model calibration for combustion modelling are discussed by, e.g., Cant et al. (2004) and the references therein.

1.3 Need for parameter optimisation in a CFD tool

For the CFD tool to give accurate predictions, the sub-grid model parameters normally require adjustments within their uncertainty ranges or physically allowable bounds. This is mainly due to the following:

- Extrapolating beyond the validity of the sub-grid models might be necessary. Sub-grid model calibration processes are mainly conducted for basic small-scale experiments, in which the quantity of interest can be adequately measured. For example, the bomb that was used to calibrate the correlation for the turbulent burning velocity (Bradley et al., 2013, 2011a) was of 19 cm internal radius. The CFD tool FLACS is used to predict gas explosion behaviour for a range of large-scale accident scenarios. Thus, the experiments used for model calibration are most often not relevant to the final application.

  Furthermore, other assumptions or settings in the experiments from model calibration may not be fulfilled in the application scenarios of the CFD tool. The

correlation for the turbulent burning velocity serves again as an example. Expressing the turbulent burning velocity as a function of the flow stretch rate and the Markstein number presumably gives a correlation with a wide applicability range (Bradley et al., 2011b). However, the derivation of the turbulent burning velocity correlation itself is associated with considerable uncertainty. The experimental value of the turbulent burning velocity for specific flow and mixture properties depends on how it is measured, such as the configuration of the apparatus, which flame surface is used in the analysis, or how quench effects and dynamic strain effects are accounted for (Bradley et al., 2011b). Additionally, the modelled turbulence velocity and integral length scale (used to correlate the turbulent burning velocity to the properties of the turbulent flow) likely is significantly different from the quantities used to derive the correlation. Due to the uncertainties, in this work, an uncertainty interval of a factor of 2 is found reasonable for the proportionality constant in the turbulent burning velocity correlation, cf. Equation (A.9) in Paper 3; see (Ciccarelli and Dorofeev, 2008) for a similar conclusion. Consequently, model parameters require adjustments for large-scale experiments relevant to the application area of the CFD tool.

- In gas explosion scenarios that are simulated with the CFD tool in a final application, one physical mechanism of a gas explosion may most often not be isolated from the other mechanisms. In this way, the application scenario differs from an experiment used in model calibration. Thus, in the CFD tool, the sub-grid model accounting for one single mechanism is embedded in the fundamental equations in the PDR formulation and coupled with several other sub-grid models. Consequently, parameter values from model calibration might not be optimal in this context.

To overcome the subjective and time-consuming nature of trial-and-error methods of manual parameter adjustment, an approach for systematic optimisation of model parameters is developed in this doctoral study. The objective is to obtain a better fit between relevant experimental data and model output of the corresponding simulation. The approach is based on surrogates that approximate the model output to accelerate the optimisation process.

1.4 Research literature and context

In this section, a few words are given to place the present project in relation to other works. Parameter optimisation appears in many applications. In particular, surrogate-based parameter optimisation is widely employed to create efficient engineering designs. Examples in the field of aeronautics and astronautics can be found in the work of Forrester et al. (2006) and Queipo et al. (2005). Another example is given by Huang and Li (2018). They improve the performance of a liquefied natural gas (LNG) hydraulic turbine, simulated with a CFD tool, by optimising the shape of an impeller. Castelletti et al. (2010) optimise the size and location of water quality rehabilitation technologies like surface mixers. When optimising design parameters or operating conditions, numerical models are only utilised to simulate quantities incorporated in the objective function or the constraints; the optimisation does not change the numerical model.

Changing model parameters and thus the models, however, is addressed in the present doctoral study.

The term 'model calibration process' is not only employed for empirical calibration of model constants as discussed in Section 1.2; it may refer to the optimisation of parameters in models that are designed for a wide range of applications but shall be used for a particular application context (Kennedy and O'Hagan, 2001). One example is given by distributed rainfall-runoff models for predicting river discharges in large drainage basins. Feyen et al. (2007) calibrate the model based on two years of measured daily discharges in the Meuse catchment upstream of Borgharen in the Netherlands.

In the following, some examples of calibrating CFD models are given. Guillas et al. (2014) present a calibration of a CFD tool for simulating airflow in a regular street canyon against wind tunnel observations. They focus on constants in the standard $k-\varepsilon$ turbulence model and the uncertainties related to these values. The experimental data for calibration originated from a wind tunnel experiment with two rectangular blocks on both sides representing the buildings on the street. Edeling et al. (2014) calibrate the Launder–Sharma $k-\varepsilon$ model for 13 wall-bounded turbulent boundary layer flows at a variety of pressure gradients. Morgut and Nobile (2012) calibrate a CFD model to simulate cavitating flow around model scale propellers. In particular, they consider models that regulate the mass transfer rate from liquid to vapour and back.

The main difficulties with simulating gas explosions with the CFD tool FLACS arise from the vast range of applications with respect to both, possible accident scenarios, and complex, large-scale geometries in which the explosions are likely to occur (Cant et al., 2004). Consequently, it is not sufficient to optimise model parameters for a specific single application as in the calibration processes mentioned above. Therefore, the approach for parameter optimisation that is developed in the present doctoral project considers the wide application range of the CFD tool.

1.5 Scope of the thesis

This dissertation focuses on the research question: "*How can the predictive capabilities of a numerical model for simulating gas explosions be improved by model parameter optimisation?*". The question is addressed in four scientific presentations, which are further expanded on in this dissertation. The main contributions are summarised as follows:

- A methodology is proposed for optimising model parameters in a CFD tool for simulating gas explosions. The objective is to obtain a better fit between relevant experimental data and model output of the corresponding simulation. Three model outputs amongst several candidates are found suitable as optimisation targets. Furthermore, different methodologies are developed for selecting gas explosion experiments to be included in an optimisation process.

- Paper 4 describes a least-squares problem formulation from an early stage of this doctoral project. As the project proceeded, the first formulation did not appear to be appropriate for improving model predictions in gas explosions. Thus, in Paper 2 a problem formulation is developed that assesses under- and over-predictions as in model validation processes.

The problem formulation is tailored with respect to the specifically targeted model output. Thus, the optimisation problem is not formulated as a least-squares problem, but to account for assessing under- and over-predictions as in model validation. It is shown that this validation-based formulation is closely connected to another formulation for which the solution is the maximum likelihood estimator in the case of log-normally distributed errors in the measurements.

- To speed up the numerical optimisation process, surrogates are employed that approximate the model output-parameter relations. Surrogates based on neural networks are tested and compared to polynomial response surfaces. The satisfactory approximation quality of the neural networks for the entire parameter space is shown numerically. As the approximation quality of the neural networks is in total better than for the polynomials, the neural networks are used as surrogates in the optimisation.

- The resulting surrogate-based optimisation problem is solved with a trust region routine from MATLAB ® (The MathWorks, Inc., 2015) embedded in a multi-start approach. The optimisation routine has been intended for non-linear least-squares problems and is based on the interior trust region algorithm for general non-linear objective functions subject to bounds proposed by Coleman and Li (1996b). In this doctoral project, the convergence of the routine for the present validation-based optimisation problem with respect to the first order necessary optimality conditions is proven.

- The approach is tested and applied successfully to several versions of the CFD tool FLACS at different stages of the development process and for different experimental data. The standard version that is released for commercial use is utilised to test the applicability of the optimisation approach. The model parameter values have been tuned manually over years of model validation; hence, optimisation improves the predictions just moderately. An in-house development version is optimised for various experiments together representing a wide range of physical phenomena. The in-house development version comprises models that have been updated recently, with parameter values that have been set to an initial 'best guess'; optimisation improves the predictions significantly. The optimisation process is highly useful for supporting modelling efforts; analysing predictions of the optimised model may suggest updated user guidelines, and may enable the discussion on how to progress with the development of the physical models. Such conclusions for recently updated model systems can only be drawn after model parameter optimisation.

- The optimisation approach is not only used to obtain optimal parameter values that can be implemented in the tool, but also for analysing strengths and limitations of the sub-grid models in FLACS. In complex models, it is challenging to investigate whether the models account for every aspect in every possible gas explosion scenario. However, by optimising one sub-grid model and its parameters for several experiments separately, the sub-grid models can be analysed. An example is given in this thesis for modelling the flame folding around sub-grid obstacles.

- Extensive model validation against experimental data is required to ensure that a gas explosion simulation tool can confidently be used for process safety. This is outside the scope of the present dissertation. However, optimisation results are analysed carefully in sanity checks. Through pressure-time histories, for example, it is investigated whether the optimised model represents the physical mechanisms of gas explosions.

The usability of an optimisation process is, in general, limited by two factors: i) the availability of experimental data and ii) the models itself: If sufficiently reliable and relevant experimental data that covers a wide range of scenarios is not available, optimal parameter values will not be of any practical use. Furthermore, it is important to emphasise that only models that are able to capture the physical mechanisms of a gas explosion can be optimised to give satisfactory predictions – with optimal parameter values that can be implemented in the tool. Thus, the optimisation processes cannot replace further efforts in CFD modelling.

1.6 Thesis outline

This section outlines the structure of this thesis.

Chapter 2 elaborates on the formulation of the optimisation problem presented in Paper 2 and Paper 4. In particular, information about the model and parameters is summarised. Furthermore, model responses that have been investigated but did not qualify to be fitted in the optimisation process are introduced. The framework for selecting experimental data for optimisation is extended to three methodologies. Moreover, the validation-based problem formulation from Paper 2 is examined and justified with respect to the following aspects: measuring the fit between model response and experimental data, weighting the model responses, and handling of outliers.

A general overview of surrogate modelling and references to review articles are provided in Chapter 3. Furthermore, the justification for the choice of the considered surrogates presented in Paper 1 is strengthened.

Chapter 4 presents how the surrogate-based optimisation problem is solved in this work. The literature review on commonly employed optimisation approaches is extended. Additionally, regularisation of ill-posed problems is addressed.

Various applications of the optimisation approach during the doctoral project are summarised in Chapter 5. Optimising the standard model within a single validation category presented in Paper 2 is reviewed; the work is extended in this chapter by the optimisation across validation categories. Results for optimising the development model are given in Paper 3. This chapter expands on the work considering testing different weights in the objective function and testing another, related problem formulation. Furthermore, this chapter gives an example of utilising the optimisation approach as a tool to analyse sub-grid models; a model for flame folding around obstacles is analysed.

Chapter 6 contains the main conclusions of the scientific results and open questions for future work.

Appendix A presents the approximation quality of two additional model responses, and thus provides a basis for the decision on including or excluding them from optimisation. Appendix B provides background information on the trust region routine

employed to solve the optimisation problem. Appendix C shows detailed results from application of the optimisation approach to the standard model for experiments from a wide range of validation categories; it supports the findings presented in Section 5.2. Appendix D supports the analysis from Section 5.4; it provides results from optimising a sub-grid model for flame folding around obstacles.

Finally, the four papers that are part of this thesis are given.

Chapter 2

Formulating the optimisation problem

Paper 4 describes a problem formulation from an early stage of this doctoral project. As the project proceeded, this first formulation did not appear to be appropriate for improving the specific model predictions. Thus, the formulation was tailored to gas explosion applications and presented in Paper 2. The main steps that are required for formulating the optimisation problem are documented in Paper 1, Paper 2 and Paper 4. The following sections expand on some concepts to provide a wider background.

The objective of the model parameter optimisation is to yield the best fit between certain outputs of a CFD model, also called model responses, and corresponding experimental data.

2.1 Sub-grid models and their parameters

Within this project, several versions of the gas explosion module of the CFD tool FLACS have been optimised – the standard version, which is released for commercial use (referred to as the *standard model*), and an in-house development version (referred to as the *development model*), for which the sub-grid models for turbulence and combustion have been updated recently. The development model arose from modelling contributions in JIP MEASURE and has fundamentally different behaviour than the standard model. The parameters that are considered for optimising the CFD tool belong to sub-grid turbulence and combustion models, cf. Paper 1 and Paper 3.

Eight parameters in the standard model are identified as candidates for optimisation. Paper 1 provides a detailed description. The development model comprises some different parameters in updated sub-grid models. In total, eleven sub-grid model parameters are subject to optimisation. The model and the corresponding parameters are described in detail in Paper 3. For each model parameter, physically allowable bounds or uncertainty intervals have been set based both on previous experience and an extensive literature review. Sensitivity analysis (Saltelli et al., 2008) is applied to determine the effect of perturbing the parameters on relevant model responses. Only the parameters with sensitivities above a certain threshold are included in the optimisation process.

2.2 Relevant model responses

Model responses must be identified as suitable targets for the optimisation process. This section revises briefly the model responses that are primarily employed in this study. Besides, model responses are introduced that in the end did not qualify to be considered in optimisation.

In Paper 2 and Paper 3, optimisation is mainly conducted for two model responses: the *maximum overpressure* and the *maximum pressure impulse* at representative monitor points. Optimising the *flame speed* has been studied additionally in Paper 2. Including the flame speed may improve the 'slope' of a pressure-time curve – more than when optimising exclusively for the maximum overpressure and pressure impulse. The term 'slope' is used to address, not the absolute pressure values of a pressure-time history, but the pressure-rise and -fall during the entire explosion.

The model responses *flame arrival time* and *time of the pressure peak* should not be employed in an optimisation process; the corresponding predictions of the CFD tool FLACS often deviate significantly from experimental data. These model responses are highly dependent on the ignition process and initial flame build up. Since the grid cell size of a simulation is often much larger than the scales on which flame initiation occurs, the initial phase of flame propagation is not resolved; a sub-grid model is used instead. In this sub-grid model, the position of the numerical flame front is corrected to agree with the expected volume and area of the region with combustion products. The model is active until the numerical flame front is 2.5 control volumes thick. This causes the deviations in the timing.

The model response *pressure rising time* has been studied additionally. The pressure rising time at a representative monitor point is defined here as the time the pressure needs to rise from 20% of the maximum overpressure to the maximum overpressure. Investigating this model response is also motivated by the possibility to optimise the slope of a pressure-time curve better. However, due to discontinuous behaviour, the model response has not been found appropriate for including in the optimisation approach, cf. Appendix A.

The optimisation of parameters should ideally be performed for the output of sub-grid models directly, e.g., the burning velocity, or at least for model outputs that are physically more closely linked to the sub-grid model parameters than overpressure. The overpressure depends significantly on the scale and the geometric configuration of the experiment. A range of different physical mechanisms contribute to the flame acceleration and the expansion of combustion products that generates overpressure; it is not straightforward to analyse these contributions separately. Quantities such as the burning velocity, a characteristic turbulence velocity fluctuation, or a measure of the flame surface area in different locations during an explosion would, therefore, be better candidates for optimisation targets. However, such measurements are difficult or impossible to obtain and are thus not available for the large-scale experiments that are relevant to the final application of the CFD tool FLACS. Most of the relevant experiments only have reliable measurements of pressure-time histories in a limited number of fixed locations, cf. Section 2.3. Therefore, the optimisation processes in this thesis are mainly limited to the targets that are connected to the overpressure.

2.3 Selecting gas explosion experiments

A key ingredient of an optimisation process is the selection of characteristic gas explosion experiments. The questions that arise are: "Which experiments can be chosen from?" and "Which experiments to combine in one optimisation process?". Both questions are addressed in the papers connected to this thesis. For a better and broader overview, important aspects are reviewed, summarised and expanded in this section; some aspects that are added to this dissertation are new and have not been included in the papers.

The experiments examined in this project are part of Gexcon's model validation database, which is organised in accordance with the model validation methodology presented by Skjold et al. (2013). That methodology focuses on identifying key physical phenomena in validation experiments. Gas explosion experiments with similar geometry layouts, scales, and fuel types are assumed to involve the same mechanisms for flame acceleration and overpressure generation. Therefore, the validation data is primarily organised according to the degree of congestion and the degree of confinement in the experimental layout. Details about the validation categories can be found in Paper 3. The methodology also includes the prioritisation of validation experiments; it takes into account the availability and quality of data, in addition to the experiment's relevance to the final model application – essential criteria when selecting experiments for parameter optimisation. In general, if optimisation was conducted on experiments which are not reliable and relevant, the optimal parameter values could not be implemented in the tool; if it was optimised for data of poor quality, the optimal parameter values are not usable. A model optimised for irrelevant experiments would possibly give good predictions for these, but most likely not for gas explosions in the final application.

2.3.1 Selecting experiments for improving modelling

Three methodologies for improving modelling of gas explosions by parameter optimisation are proposed in the following: Optimising i) for 'single phenomenon' experiments separately, ii) for several experiments separately, and iii) for various experimental campaigns simultaneously. Depending on the number and type of experiments included, the optimisation process can be used to analyse the model system or to find optimal parameter values of practical use, or both. Analysing the model system involves investigating whether the sub-grid models are able to represent the desired mechanism or whether there is a particular physical behaviour observed in the explosion that is not captured by the model. To be of *practical use* means that the parameter values that are found via an optimisation process give satisfactory results also for gas explosion scenarios that were not part of the optimisation.

The concepts are visualised in Table 2.1. The third methodology is presented in Paper 2 and employed for parameter optimisation in the CFD tool FLACS in Paper 3; discussions about and application of the first and second methodologies are added to this dissertation.

Table 2.1: Functioning of the optimisation approach.

Choice of experiments	**Use of optimisation approach**	
	find optimal parameter values of practical use	analysing sub-grid models
'single phenomenon' experiments	DIFFICULT	DIFFICULT
several experiments separately	NO	YES
various experimental campaigns together	YES	NO

'Single phenomenon' experiments

The objective of optimising 'single phenomenon' experiments is to improve the sub-grid models separately. A *'single phenomenon'* experiment denotes an experiment in which one particular phenomenon is the main driving component in (one phase of) the gas explosion. Optimisation aims at fitting one or several parameters for the sub-grid model that represents this phenomenon. This methodology is motivated by empirical model calibration processes and poses the most 'fundamental' of the three methodologies. However, in contrast to empirical model calibration, the 'single phenomenon' experiments must be relevant to the final application of the CFD tool.

In theory, this optimisation approach allows for obtaining optimal parameter values of practical use and gives insight into the predictive capabilities of the model system. In practice, however, it is challenging to find suitable 'single phenomenon' experiments, as it is extremely difficult to isolate some of the gas explosion phenomena. For example, the overpressure in explosions within a highly congested enclosure is driven by the flame folding around sub-grid obstacles; but, the turbulent burning velocity correlation has a highly important effect as well. For such experiments, several sub-grid models are active in a CFD simulation. However, optimal parameter values for one sub-grid model cannot be found if another sub-grid model with fixed non-optimal parameter values is active simultaneously. Due to the difficulties in finding 'single phenomenon' experiments, both, analysing the model system, and finding optimal parameter values of practical use is defined as "DIFFICULT" with this methodology, cf. Table 2.1.

Several experiments separately

The idea of optimising for experiments separately – even though they do not represent a single phenomenon – can still be employed to analyse the sub-grid models; however, the optimal parameter values are not of any practical use, cf. Table 2.1. Optimisation is performed for parameters of one sub-grid model for different relevant experiments or experimental campaigns separately. If the sub-grid model is able to model every essential physical aspect of the phenomenon it is intended for independently from gas explosion scenarios and geometries, the optimal parameter values from different opti-

misations will not differ significantly. Hence, comparing the optimal parameter values and optimised predictions may allow for identifying limitations of the sub-grid models and point to potential development improvements. An example of this usage of the optimisation approach is given in Section 5.4, where parameters for flame folding around obstacles are optimised.

Various experimental campaigns

If 'single phenomenon' experiments are not available for some physical phenomena, the optimisation process for the corresponding parameters or all model parameters may be employed for experiments from various validation categories together. These experiments must involve a wide range of physical phenomena. The methodology is explained and followed in Paper 2 and Paper 3. As discussed in the supplementary material of Paper 2, with this approach, analysing the optimised sub-grid models from the optimisation results becomes a difficult task; in contrast to the previous approach, varying the value of one parameter that represents a particular physical phenomenon may be compensated by variations in other parameter values. Hence, it can be concluded that analysing the sub-grid models is, in general, not possible with this methodology, cf. Table 2.1.

It should be noted that such an optimisation process compromises between the diverse experiments; it might thus not improve every single sub-grid model. However, with this approach, the overall prediction quality of the CFD tool is improved for a wide range of experiments representing the application variety. As this is the primary objective of this thesis, the work conducted in the doctoral project focuses mainly on this approach.

2.3.2 Selecting experiments for testing the optimisation approach

It is important to investigate whether the optimisation approach is applicable to gas explosion simulations; i.e., for example, whether optimising exclusively the maximum overpressure and pressure impulse can lead to a model that represents the mechanisms of gas explosions accurately, or whether the optimisation problem is adequately formulated. Furthermore, it is interesting to analyse how much the predictions can be improved by parameter optimisation. To be able to gain as much information as possible from the investigations mentioned above, it might be most convenient to optimise all parameters for one single experimental campaign or for several experimental campaigns that are assigned to the same validation category. The experiments in such a selection are assumed to involve the same mechanisms for flame acceleration and overpressure generation, and the optimisation effect is much higher than when optimising for experiments across categories. Note that this does not lead to parameter values of practical use since a single experimental campaign cannot cover a wide range of gas explosion phenomena and scenarios. Examples of the testing are given in Paper 4 and Paper 2, cf. Section 5.1. How important the testing is, becomes evident in this doctoral study; the problem formulation from Paper 4 has not been found appropriate after testing and has been changed in subsequent optimisation processes, cf. Section 2.4.

2.3.3 Experimental campaigns considered in this work

Five experimental campaigns with medium- and large-scale geometries with high priority (following the model validation methodology by Skjold et al. (2013)) are considered in this project and introduced in Paper 3:

- the project Modelling and Experimental Research into Gas Explosions (MERGE) (Mercx, 1994; Popat et al., 1996),
- the project Blast and Fire Engineering for Topside Structures (BFETS), Phase 3A (Al-Hassan and Johnson, 1998; Evans et al., 1999; Foisselon et al., 1998),
- the project BFETS, Phase 2 (Foisselon et al., 1998),
- experiments in the 64 m^3 vented explosion chamber located at the FM Global research campus (Bauwens, 2010; Chao et al., 2011), and
- the 182 m^3 vented explosion chamber experiments conducted by DNV GL, located at the Spadeadam test site (Tomlin et al., 2015).

The tests involve homogeneous fuel-air clouds, in which propane, methane, or natural gas was the combustible component, congested geometries with a low degree of confinement, and vented enclosures with and without obstacles. Some campaigns consist of much more tests than others, and the variability from one test to another is smaller. To balance the impact that each campaign has on the optimisation only the most relevant tests are selected for optimisation. In total, 37 core experiments are identified as candidates for optimisation. Additional 30 tests are used for sanity checks of the optimised model.

2.3.4 Covering a wide range of validation categories

As mentioned in Paper 3, to represent the wide application range, the optimisation should ideally have been performed on a boarder range of validation categories than covered by the five selected campaigns. However, there are no high priority experiments assigned to further categories due to lack of reliable measurements or relevance to the final applications. Two examples are added here for illustration:

- The model validation database includes small-scale experiments with detailed information about measurements as well as repetitions of tests. For example, the experimental campaign conducted by Hisken et al. (2015) comprised in total 42 propane-air gas explosion experiments in lab-scale (1.5 m $\times$ 0.3 m $\times$ 0.3 m) and medium-scale (6 m $\times$ 1.2 m $\times$ 1.2 m) vented channels with various gas concentrations. The gas explosion module of the CFD tool FLACS is designed for large-scale scenarios (Gexcon AS, 2019). Therefore, despite the high reliability of the data, these experiments are not found relevant enough to be included in the optimisation process. They may be employed for the model validation after the optimisation process.

- Another example is the large-scale balloon experiments performed by Lind and Whitson (1977). These experiments involve unconfined flame propagation through an uncongested region and are therefore highly relevant for studying phenomena such as the effect of intrinsic instabilities on flame acceleration over significant distances. Explosion experiments were performed in hemispherical balloons of 5 and 10 m radii with different fuel types premixed with air; the mixtures were ignited at the centre of the balloons. Lind and Whitson (1977) reported the flame position versus time for each test, extracted from video recordings. Several issues related to using these experiments for model validation have been identified (Skjold et al., 2017). Some of the tests were performed with obstacles placed in the hemispherical cloud; however, the investigators do not describe the obstacle configurations in detail. Furthermore, the breaking of the plastic hemisphere containing the mixture was not uniform between experiments. In some tests, the mixture was ignited in several locations inside the balloon due to flame acceleration and secondary ignition caused by an instrumentation channel. For experiments with very low pressure levels (such as those recorded in this experimental campaign), flame speeds are of primary interest. However, detailed results (such as the raw video recordings) are not available for further analysis. Since the uncertainty associated with the experimental results is likely significant, these experiments are not considered suitable for model optimisation.

Thus, the optimisation is currently limited to the campaigns listed in Section 2.3.3. Future optimisation studies, however, may include new campaigns, since the validation database is continuously extended as soon as new experimental data becomes available.

2.3.5 Experimental uncertainty

In Paper 2 and Paper 3, the experimental uncertainty is mentioned, but it is neither quantified nor further discussed. This section gives information about the experimental uncertainty in the selected campaigns and discusses its implications for optimisation and validation processes.

Measurements of physical quantities will most certainly contain errors. Since the objective of the optimisation is to minimise the fit between model responses and experimental data, the experimental uncertainty ought to be accounted for. In this doctoral study, experimental uncertainty has been indirectly accounted for in the formulation of the optimisation problem, cf. Section 2.4.3. When validating a numerical model against experimental data, however, concrete information about the experimental uncertainty can be valuable, as the model predictions cannot be expected to be more accurate than the experimental uncertainty.

For the considered experimental campaigns (Section 2.3.3), only little concrete information about the experimental uncertainty of the overpressure – the most relevant measured quantity – is reported. Thus quantifying the experimental uncertainty in terms of a single number for the deviation from the mean is not straightforward. In two experimental campaigns, efforts have been undertaken to assess the experimental uncertainty of the overpressure via the performance of nominally identical tests; the experimental uncertainty is then derived from measurements in the repetitions. As large-scale gas explosion tests are highly costly, only few repetitions were performed.

Evans et al. (1999) reported experimental uncertainty of the overpressure for the campaign BFETS Phase 3A based on two series of repeated tests: The 'Alpha' and 'Beta' series consisted of five and six nominally identical experiments, respectively. The variations in overpressure measurements are illustrated in Figure 2.1. For most of the test configurations of the FM Global 64 m^3 vented explosion chamber tests, three nomi-

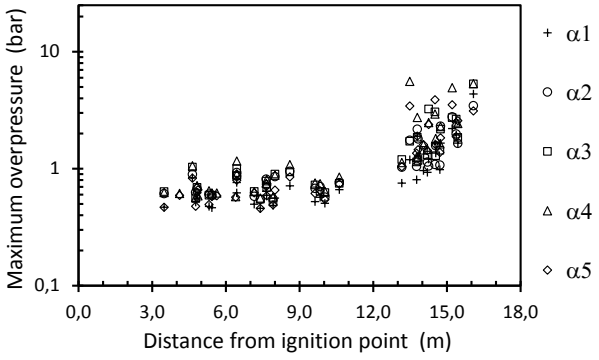

(a) 'Alpha' series

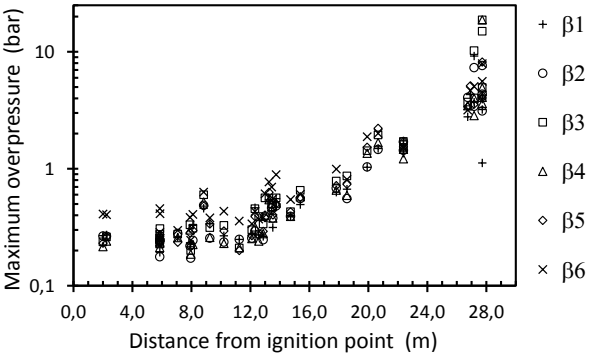

(b) 'Beta' series

Figure 2.1: Experimental variability for the repetitions of the BFETS, Phase 3A, series 'Alpha' and 'Beta'.

nally identical tests were conducted (Bauwens, 2010). The experimental uncertainty is reported as the highest deviation from the average value.

Incorporating the reported uncertainties for these two campaigns, it can be concluded on the following rough uncertainty estimation: In 90 %, the over- and underpredictions lie within a factor of 1.3, i.e., within $1/1.3$ and 1.3. It should be noted that this number is mentioned for illustrating the experimental variability in the present campaigns; it has not been derived via any sophisticated statistical method and should thus not be used for further calculations.

2.4 Assessing over- and under-predictions

Formulating the optimisation problem includes determining how to measure the agreement between model responses and experimental data. A widely applied strategy is to formulate a least-squares problem, i.e., minimising the sum of the squared (relative) errors between model predictions and experimental data (Aster et al., 2013). Paper 4 describes a least-squares problem formulation from an early stage of this doctoral project. However, as the project proceeded, this formulation did not appear to be appropriate for fitting the considered model responses; the formulation was tailored to gas explosion applications, presented in Paper 2. This formulation is briefly stated in the following section. Additionally, in Section 2.4.2, another, related problem formulation is introduced. This formulation (as well as the least-squares formulation) can be derived from a statistical point of view and has not been used in Paper 2, 3, or 4. In Section 5.3.2, it is tested for the application presented in Paper 3.

2.4.1 The validation-based problem formulation

In the problem formulation developed in Paper 2, the agreement between model responses and experimental data is measured as in model validation for gas explosions; over- and under-predictions of overpressure are assessed as multiplicative deviations instead of percentage differences as in the relative errors of the least-squares formulation.

Let ζ_i, $i \in \{1,\dots,N\}$, denote one model response at one monitor point for one experiment, and let b_i be the corresponding experimental value. Let N denote the total number of model responses taken into account. The parameter vector $\boldsymbol{k} = (k_1, k_2, \dots, k_n)$ gathers n sub-grid model parameters that are chosen for optimisation. The formulation reads:

$$\begin{aligned} &\min_{\boldsymbol{k}} \sum_{i=1}^{N} \phi\left(1 - \frac{\zeta_i(\boldsymbol{k})}{b_i}\right), \\ &\text{subject to: } k_j \in [l_j, r_j], \text{ for } j = 1,\dots,n \end{aligned} \tag{2.1}$$

with

$$\phi(t) = \begin{cases} t^2, & \text{if } t \leq 0, \\ \left(\frac{t}{1-t}\right)^2, & \text{if } 0 < t < 1. \end{cases}$$

The intervals $[l_j, r_j]$ denote the parameter's uncertainty ranges. Note that all model responses and experimental data are positive, and thus $1 - \frac{\zeta_i(\boldsymbol{k})}{b_i} < 1$ for all $\boldsymbol{k}$, such that ϕ is well defined. This formulation is here referred to as the *validation-based problem formulation*.

2.4.2 The VG formulation – minimising the geometric mean variance

An alternative to problem (2.1) is given by minimising the geometric mean variance. For model validation purposes, Hanna et al. (1993b) developed standard objective

quantitative means of evaluating the performance of a model. According to Model Evaluation Group Gas Explosions (MEGGE) (1996), for a model predicting gas explosions, the most relevant of those statistical performance measures are the geometric mean bias (MG) and geometric variance (VG). The *geometric mean bias* reports the tendency of a model to systematically over- or under-predict relevant physical properties; the *geometric mean variance* gives a measure of the spread in predictions, i.e., the degree of scatter around a mean value (Duijm and Carissimo, 2002; Hanna et al., 1993a). MG and VG for the present application are defined as

$$\mathrm{MG} = \left(\prod_{i=1}^{M} \frac{\zeta_i}{b_i}\right)^{\frac{1}{M}} = \exp\left(\frac{1}{M}\sum_{i=1}^{M} \ln\left(\frac{\zeta_i}{b_i}\right)\right) \quad \text{and} \tag{2.2}$$

$$\mathrm{VG} = \exp\left(\frac{1}{M}\sum_{i=1}^{M} \left[\ln\left(\frac{\zeta_i}{b_i}\right)\right]^2\right),$$

respectively, where M is the total number of model responses for validation.

Minimising VG leads to the following problem:

$$\min_{\boldsymbol{k}} \sum_{i=1}^{N} \ln\left(\frac{\zeta_i(\boldsymbol{k})}{b_i}\right)^2, \tag{2.3}$$
$$\text{subject to: } k_j \in [l_j, r_j], \text{ for } j = 1,\ldots,n.$$

Note that the geometric mean bias is minimised simultaneously. This formulation is referred to as the *VG problem formulation*.

2.4.3 The statistical point of view – maximum likelihood estimator

If considering the experimental data b_i as imperfect measurements that include random errors, the least-squares problem formulation, as well as the VG formulation, can be derived from a statistical point of view. One approach is the maximum likelihood estimation. Assume that the statistical characteristics of the data observations are known. Applied to parameter optimisation, this approach focuses on finding the parameter values $k_j,\ j = 1,\ldots,n$, such that the observed data points b_i most likely arise from the model given by $\zeta_i(\boldsymbol{k}),\ i = 1,\ldots,N$, cf. (Aster et al., 2013).

Assume that the experimental data include additive, normally distributed errors with 0 mean and variance σ^2

$$\zeta_i(\boldsymbol{k}) - b_i = \varepsilon_i \quad \text{with } \varepsilon_i \sim N(0,\sigma^2), \text{ for } i = 1,\ldots,N.$$

Assume furthermore, that the observations are independent of each other. Then, the maximum likelihood estimator (MLE) for the parameters $\boldsymbol{k}$ is the solution of the least-squares problem

$$\min_{\boldsymbol{k}} \sum_{i=1}^{N} (\zeta_i(\boldsymbol{k}) - b_i)^2.$$

A detailed derivation can be found in, e.g., (Aster et al., 2013).

In this study, ζ_i denotes the maximum overpressure or pressure impulse, which are always positive. In this particular case, multiplicative errors $\tilde{\varepsilon}_i$ are observed which are log-normally distributed:

$$\zeta_i(\boldsymbol{k}) = b_i \tilde{\varepsilon}_i;$$

that is

$$\ln\left(\frac{\zeta_i(\boldsymbol{k})}{b_i}\right) = \varepsilon_i \quad \text{with normally distributed errors } \varepsilon_i \sim N(0,\sigma^2), \text{ for } i = 1,\ldots,N.$$

Analogous calculations to the case with additive errors yield that the MLE for the parameters $\boldsymbol{k}$ is the solution of the VG problem formulation (2.3).

2.4.4 Relation of the VG formulation to the validation-based formulation

The objective functions of the problems (2.1) and (2.3) have the same characteristics with respect to assessing over- and under-predictions. In particular, it holds

$$\phi\left(1-\frac{\zeta_i(\boldsymbol{k})}{b_i}\right) = \begin{cases} \left(1-\frac{\zeta_i(\boldsymbol{k})}{b_i}\right)^2, & \text{if } 1 \le \frac{\zeta_i(\boldsymbol{k})}{b_i}, \\ \left(1-\frac{b_i}{\zeta_i(\boldsymbol{k})}\right)^2, & \text{if } 0 < \frac{\zeta_i(\boldsymbol{k})}{b_i} < 1. \end{cases}$$

The terms $1-\frac{\zeta_i(\boldsymbol{k})}{b_i}$ and $1-\frac{b_i}{\zeta_i(\boldsymbol{k})}$ are the first order Taylor expansions of $\ln\left(\frac{\zeta_i(\boldsymbol{k})}{b_i}\right)$ and $\ln\left(\frac{b_i}{\zeta_i(\boldsymbol{k})}\right)$ around unity, respectively, and $\ln\left(\frac{\zeta_i(\boldsymbol{k})}{b_i}\right)^2 = \ln\left(\frac{b_i}{\zeta_i(\boldsymbol{k})}\right)^2$. In this project, both problem formulations are employed for the same optimisation case to test to what extent the resulting optima differ from each other; results are presented in Section 5.3.2.

2.5 Weighting strategies and multi-objective optimisation

To prioritise certain model responses in the objective function, the sum of the errors between model responses and experimental data may be weighted accordingly. In the present doctoral study, weights in the objective function have been selected as part of each optimisation process. In the optimisation application in Paper 4, for example, several weights are tested to find a suitable problem formulation; In Paper 3 the weights are set equal to unity. The selection is based on a weighting strategy that is described in this section. How the strategy has been utilised to find the weights in Paper 3, is presented in Section 5.3.1.

Solving a weighted problem formulation can be understood as a multi-objective optimisation approach. In multi-objective optimisation approaches, a collection of objective functions is optimised simultaneously in a systematic way. In the following, some approaches are explained to introduce the present weighting strategy. A comprehensive survey of continuous non-linear multi-objective optimisation can be found in, e.g., (Marler and Arora, 2004).

In the case that preferences of the objective functions are articulated before the optimisation, one of the most intuitive and common approaches is the weighted sum method

(Marler and Arora, 2004); in a weighted sum, the different objective functions are combined to one single objective function. A reason for prioritisation of objective functions through higher weights can, for example, be higher quality or relevance of some measurements. Other reasons are discussed in Paper 4. If preferences are not known *a priori*, Pareto optimal parameter values may be generated systematically by varying the weights. A point is *Pareto optimal* if no other point improves one or more objective functions while retaining the other objective function values (Marler and Arora, 2004).

For optimising the gas explosion module of the CFD tool FLACS, no information about the relative importance of the objectives is available. However, reporting several sets of Pareto optimal parameter values to the user is both impractical and unnecessary; simulating gas explosion scenarios for several optimal parameter values results first in large running times and second in a large amount of simulation output. Finally, the user has to report a single model prediction out of the large set of simulation output; this is most probably difficult and time-consuming.

Hence, selecting weights in this doctoral study is based on a strategy that contains the following steps: Several weighted sum problems are formulated using different weights; the corresponding optimal parameter values are calculated; simulation results for all optimal parameter values are studied. In the end, the weights leading to a set of suitable optimal parameter values are selected. Note that the latter might be a subjective assessment.

To ensure that the objective functions are of similar order and thus do not naturally dominate the aggregated objective function, each is transformed before building the weighted sum – such as Marler and Arora (2010) recommend. For a weighted sum problem, Marler and Arora (2005) find the use of the *lower-bound approach* (Chen et al., 1999; Koski and Silvennoinen, 1987) beneficial: An objective function F_i is transformed to F_i^{trans}

$$F_i^{trans} = \frac{F_i}{F_i^o},$$

employing its minimum $F_i^o = \min\{F_i(\mathbf{x}) |\ \mathbf{x} \text{ in the feasable space}\}$.

2.6 Outlier robust optimisation

In this doctoral project, a strategy for handling outliers is chosen. The strategy is (intentionally) not applied in the optimisation cases presented in the papers, but in the optimisation shown in Appendix C. This section gives background on outlier-robust optimisation, the motivation for the chosen strategy, and reasons for its usage or ignorance.

For some explosion experiments and monitor points, CFD simulations significantly over- and under-predict the considered physical properties. Reasons for this may be errors in the experimental measurements or the fact that the underlying model system is not able to predict accurately the behaviour of the explosion in those scenarios, or both (Aster et al., 2013). Large over- and under-predictions produce high costs in the objective function. When including discordant observations, also called outliers, in the optimisation, the optimisation is pushed to improve especially those. To handle this problem, the objective function is modified to robust error measurements.

In literature, several ways of robust handling of outliers can be found: Errors between predictions and experimental data can, for example, be measured in the ℓ^1-norm (Aster et al., 2013). Combinations of ℓ^2- and ℓ^1-norms can lead to an error measurement function that is quadratic in the neighbourhood of zero error but grows more slowly than a quadratic beyond a threshold. With such a function, outliers will influence the optimisation only moderately (Mazet et al., 2005). A widely employed example is the Huber function for traditional least-squares problems (Guitton and Symes, 2003; Huber, 1964; Mazet et al., 2005).

In this doctoral study, two aspects speak against a (partially) linearisation of the developed transfer function ϕ from problem (2.1):

- The outliers are severe over- or under-predictions, such that it is preferred to rather exclude them totally from the optimisation than to reduce their influence. The over- and under-predictions that are not severe occur so often that they should be included in the optimisation.
- A linearisation of the developed transfer function (for over- and under-predictions with a factor larger than a certain threshold) would retract assessing over- and under-predictions as in model validation.

Hence, the strategy in this project is as follows: Model responses that are over- or under-predicted above a certain factor by the standard model are excluded from optimisation; other predictions are treated as given by the transfer function. As typically over- and under-predictions of the overpressure in gas explosions of a factor larger than 2 are not found to be acceptable, cf. Paper 3, excluding predictions above a factor between 2 and 2.7 has been found convenient.

In the study presented in Paper 2, it is not necessary to conduct special treatment of outliers. Simulations for the considered experiments result in only very few outliers; excluding outliers from optimisation does thus hardly have an effect. However, when a wider range of experiments is considered, as in the study from Appendix C, robust outlier handling is required for an unbiased optimisation, cf. Appendix C.4. For the development model in which the parameter values are set to an initial 'best guess' a large number of severe over- and under-predictions is observed. Consequently, all model responses are included in the optimisation of Paper 3. If model responses are still highly over- or under-predicted after optimisation, optimisation may be conducted a second time – excluding those model responses.

Chapter 3

Surrogate-based optimisation

Surrogate-based optimisation has been shown to be an effective approach for optimising computationally expensive models; it refers to the idea of speeding up optimisation processes by using surrogates for the objective or constraints functions (Forrester and Keane, 2009; Queipo et al., 2005). Model responses of a CFD tool can be interpreted as a function of a given set of model parameters. Those parameter-output relations can be approximated by surrogates, which then can be incorporated in the optimisation problem formulation described in Chapter 2. Surrogates, often also referred to as metamodels or response surfaces, are inexpensive to evaluate, and allow for the optimisation of problems with non-smooth or noisy responses (Queipo et al., 2005). Note that surrogate-based optimisation can only find an approximate solution.

In this project, two different types of surrogates for the output of the CFD tool FLACS have been investigated, compared, and presented in Paper 1. Paper 2, 3 and 4 present optimisation applications in which surrogates based on neural networks are employed. This chapter gives a brief overview of surrogate modelling in general as well as a motivation for the specific surrogates considered in this project.

3.1 Surrogate modelling – a general overview

Several surrogate approaches have been found to be efficient in the context of surrogate-based optimisation. Surrogate modelling started with the polynomial response surface methodology (RSM) and artificial neural networks (ANNs) and expanded in many application areas from the 1990's to a variety of approaches: radial basis functions (RBFs), support vector regression (SVR), support vector machines (SVMs), kriging, multivariate adaptive regression splines (MARS), Gaussian process (GP), to name a few. A comprehensive overview of surrogate modelling for computer-aided engineering is given by, e.g., Gorissen (2010).

A large number of comprehensive review articles present the advances in surrogate modelling in different optimisation applications. Each article gives an introduction to several surrogate modelling methods, including references to the original works and numerous examples of their applications. As a detailed description of the variety of surrogate models is out of the scope of this thesis, a selection of relevant reviews is given in the following:

- Simpson et al. (2001b) examine approximation techniques in engineering design optimisation: RSM, ANNs, inductive learning, and kriging.

- Surrogate modelling in aerospace systems is reviewed by Queipo et al. (2005). They report on RSM, RBFs, kriging, and a more general non-parametric approach called Kernel-based regression.

- In the field of electrical, chemical and aerospace engineering, and continuous-state stochastic dynamic programming, Chen et al. (2006) give a review on surrogates for computer experiments to be used in optimisation processes. They report on RSM, least interpolating polynomials, ANNs, RBFs, kriging, MARS, and regression trees.

- Forrester and Keane (2009) present the recent advances in surrogate-based optimisation of aerospace design. They examine RSM, moving least-squares that results in standard polynomial regression, interpolation and something in between the two, RBFs, SVR, and kriging.

- Razavi et al. (2012) give a review of surrogate modelling methods and applications to hydrological modelling and water resources management. According to Razavi et al. (2012), the most commonly employed surrogates (from publications in water resource journals since 2000) are ANNs and RBFs; but also RSM, SVMs, kriging, MARS, k nearest neighbours, and treed Gaussian processes can be found.

- Additionally, the review by Simpson et al. (2008) presents a historical perspective of the advancements on surrogate modelling in multidisciplinary design optimisation.

Lately, an ensemble of multiple surrogates has been used as approximation model (Goel et al., 2007; Viana, 2011). An application to the design optimisation of vehicle roof structures is shown by Pan and Zhu (2011).

In general, it is not known a priori which surrogate modelling approach to select for a specific application. Comparative studies have shown that a particular surrogate model can outperform other types depending on the problem under consideration (Queipo et al., 2005; Wang and Shan, 2006), see, e.g., (Gong et al., 2015; Razavi et al., 2012; Simpson et al., 2001a; Zhang et al., 2009).

3.2 Surrogates considered in this work

In this project, two different types of surrogates have been investigated – *polynomial response surfaces* (PRSs) and *response surfaces based on neural networks*[1] (RSNNs). The polynomial response surface approach is inspired by the work presented by Davis et al. (2004) optimising gas-phase and surface reaction kinetic models in chemical engineering; the RSNNs are based on multilayer perceptrons (MLP). Details about both

[1]The terminology is changed from surrogate to response surface throughout this section to align it with the work in Paper 1.

types of surrogates can be found in Paper 1. In the following, the motivation for the use of RSNNs is discussed.

The main motivation for employing RSNNs in this project is attributed to the universal approximation property: Leshno et al. (1993) prove that an MLP with one hidden layer can approximate any continuous function to any desired degree of accuracy if and only if the network's activation function is not polynomial. Thus, failures in applications are due to inadequate learning, a stochastic instead of deterministic input-target relation, or an inappropriate network architecture (Hornik et al., 1989). Indeed, finding an appropriate network structure in applications is the main difficulty of neural network surrogate modelling – at least for highly non-linear functions or many input parameters; for setting up an MLP most often a trial-and-error strategy is employed (Simpson et al., 2001b). Neural network surrogate modelling is widely used for function approximations and for modelling a variety of physical relationships (Chen et al., 2006; Gorissen, 2010); it has been employed successfully in optimisation processes in many industrial applications, see for example (Pan et al., 2014; Sant Anna et al., 2017). Moreover, RSNNs are smooth functions for the parameter-model relations; this allows employing gradient-based optimisation routines, cf. Section 4.1.

In surrogate-based optimisation, a reliable optimum can only be obtained if sufficiently accurate surrogates are employed. In the study presented in Paper 1, both types of surrogates have been generated and extensively tested for the model responses of the standard model: maximum overpressure and maximum pressure impulse at several monitor points for relevant experiments in the validation database. It has been observed that the RSNNs are more reliable than the PRSs; the RSNNs show a satisfactory approximation quality for the entire parameter uncertainty space. Consequently, the project has been continued with the use of neural networks as surrogates. In Appendix A.1, the validation of RSNNs for the flame speed is added.

As mentioned in Section 2.2, the pressure rising time has been investigated as an additional model response. Appendix A.2 presents the validation of an RSNN for this model response at one monitor point in the experiment MERGE B with a propane-air mixture. It is observed that for this case, the pressure rising time is a discontinuous function of the sub-grid model parameters; it cannot be approximated adequately with a neural network. Hence, the pressure rising time is not included as a target in the optimisation process.

Chapter 4

Solving the optimisation problem

This chapter addresses the solving of surrogate-based optimisation problems. To place the methodologies applied in this work in relation to other approaches, two basic concepts – gradient-free vs gradient-based optimisation and adaptive sampling vs one-shot solutions – are introduced in the first two sections. Then, the optimisation routine considered in this doctoral project is revisited briefly from Paper 2; some additional notes are given. The last section addresses why regularisation of the problem has not been required in the present applications.

4.1 Gradient-free vs gradient-based optimisation

An overview of solving surrogate-based optimisation problems is presented by Queipo et al. (2005). They distinguish between two approaches: *surrogate management framework* (SMF) and *approximation model management framework* (AMMF). The AMMF approach was earlier introduced as approximation management framework (AMF) (Alexandrov et al., 2000) and approximation model management optimisation (AMMO) (Alexandrov et al., 2001).

The SMF approach is based on gradient-free optimisation (also referred to as direct search or pattern search) and thus can be used where the objective functions are non-differentiable. Gradient-free optimisation is less likely to be trapped in non-global optima than traditional non-linear optimisation algorithms (Queipo et al., 2005). The SMF approach is applied in several engineering applications, such as, e.g., (Boto et al., 2018; Loshchilov et al., 2010; Poethke et al., 2018), and multi-objective optimisation approaches in which evolutionary methods are employed, cf., e.g., (Gong et al., 2015; Pilát and Neruda, 2013).

AMMF is typically associated with gradient-based optimisation methods. The surrogates are trusted to yield sufficiently accurate predictions of good directions of improvement for the original function. As the AMMF approach inherits convergence properties of the gradient-based method, convergence to a local solution is guaranteed. The AMMF approach is for example employed in engineering applications by Neelin et al. (2010), Davis et al. (2004) and Alexandrov et al. (2001).

In this project, the AMMF approach is chosen. Since the surrogates are smooth functions (cf. Paper 1), a gradient-based optimisation approach can guarantee convergence to a local optimum. Here, a trust region method, introduced in Section 4.3, is coupled with a one-shot solution strategy, cf. Section 4.2.

4.2 Adaptive sampling vs one-shot solution

The idea of adaptive sampling and one-shot solution approaches is briefly introduced in Paper 4. In this section, more background is given to provide a better overview of those basic concepts in surrogate-based optimisation.

Adaptive sampling refers to updating a surrogate model by including additional sample points during the optimisation process. Only if satisfactory approximation quality of a surrogate is ensured, the optimum of a surrogate-based optimisation process is a good approximation of the optimum of the original problem (Forrester and Keane, 2009). Therefore, in general, it is convenient to employ the iterative trust region optimisation approach developed by Alexandrov et al. (1998), (Forrester and Keane, 2009; Queipo et al., 2005); in each iteration, the optimisation is conducted only in a region around the current iterate in which the approximation is trusted to be a good representative to the original function (Nocedal and Wright, 2006). According to Alexandrov et al. (1998), the trust region mechanism gives a measure of how well the surrogate of the objective function predicts the improvement in the original objective function and thus suggests criteria for changing or updating the surrogate for the next iteration. Updating the surrogate by including new data points, also called infill points, can be accomplished by, for example, merit functions (Queipo et al., 2005). In a so-called efficient global optimisation approach, Jones et al. (1998) employ a merit function balancing low objective function values and uncertainty in the surrogate model; points with a high expected improvement are added to the sampling. Alternative infill criteria can be found in, e.g., (Iuliano, 2016).

If validation results let assume global accuracy of the surrogate models, the iterative procedure can be reduced to a *one-shot solution* approach, i.e., optimisation in only one single iteration with globally defined surrogates (Forrester and Keane, 2009; Queipo et al., 2005).

In the present project, a one-shot solution approach is applied for the following two reasons: (i) Up to 37 experiments can be considered in an optimisation process, cf. Section 2.3. Including new data points for the surrogate generation, requires running CFD simulations during the optimisation process. Due to simulation execution times of up to several hours, an optimisation process incorporating adaptive sampling would exceed any practical time frame. (ii) The considered surrogates based on neural networks generated for sufficiently large samplings are found to give satisfactory global approximation quality of the selected model responses, cf. Paper 1 and Appendix A.

4.3 Trust region optimisation with a multi-start strategy

The surrogate-based optimisation problem is solved with a trust region optimisation algorithm combined with a multi-start strategy for a global search. The trust region algorithm is provided by a MATLAB® routine called *lsqnonlin* (The MathWorks Inc., 2017), which is briefly described in Paper 2 and in more detail in Appendix B.

The routine *lsqnonlin* is tailored to solve non-linear least-squares problems. Hence, when applying it to the validation-based optimisation problem described in Section 2.4, it is crucial to investigate whether convergence to an optimum is achieved, i.e., whether the first order necessary conditions are satisfied at the limit point of a converging se-

quence of points generated by the algorithm. A convergence proof can be found in Paper 2.

A few words are added here about Hessian approximations in the routine. The routine exploits the specific structure of least-squares problems; computational time is saved by neglecting the second term in the Hessian, cf. Equation (B.5) in Appendix B. The Hessian of the validation-based objective function differs from the one of the least-squares problem. However, the term that corresponds to the first term of the least-squares' Hessian also dominates over the others. Thus, the truncation of the Hessian is equally appropriate for the validation-based problem formulation.

4.4 Regularisation

Ill-posed problems require stabilisation, also called regularisation, to obtain meaningful solutions. To discuss whether regularisation of the presented optimisation problem is necessary, we introduce the notion of *inverse problems*. A non-linear discrete inverse problem considers finding a parameter vector $\boldsymbol{m}$ such that a non-linear continuous model function G evaluated at the parameter vector models the experimental data vector $\boldsymbol{d}$,

$$G(\boldsymbol{m}) = \boldsymbol{d}. \tag{4.1}$$

An inverse problem is called ill-posed if noise in the data results in a significant change in the estimated solution (Aster et al., 2013). A formal definition is for example given by Rieder (2003): A problem is locally ill-posed for a solution $\boldsymbol{m}^*$ of (4.1)

- if $\boldsymbol{m}^*$ is not an isolated solution, i.e., in all neighbourhoods of $\boldsymbol{m}^*$, $B_r(\boldsymbol{m}^*)$, for $r > 0$, there exists another $\boldsymbol{m}^r$ with $G(\boldsymbol{m}^r) = \boldsymbol{d}$
- or if $\boldsymbol{m}^*$ is not continuously dependent on the data $\boldsymbol{d}$.

In a regularisation process, the original problem is replaced by a closely related problem that can be solved in a stable way. Regularisation methods comprise amongst others the Tikhonov regularisation and iterative methods, cf., e.g., (Aster et al., 2013; Rieder, 2003). Discrete inverse problems are often derived by discretising ill-posed continuous inverse problems, in which m and d are functions and G is an operator. Typically, the discrete problem becomes ill-posed if the number of points of discretisation increases (Aster et al., 2013). In the presented model parameter optimisation, however, the number of parameters is relatively small (in the order of 10), such that effects of ill-posedness are not expected to arise in practice. The studied optimisation problems in Paper 2 and Paper 3 have been tested, and the solutions are found to be stable with respect to small changes in the experimental data. Thus, it can be concluded that regularisation of these optimisation problems is not required.

Chapter 5

Application to the CFD tool FLACS

In the present project, the optimisation approach has been applied to the gas explosion module of the CFD tool FLACS. This chapter summarises briefly and expands on the applications presented in Paper 2 and Paper 3. Two additional application cases are presented in this dissertation in sections 5.2, 5.4 and appendices C, D.

As described in Section 2.1, different versions of the CFD model have been considered: the released standard model and an in-house development model. As part of a continuous model development process, the development model has been optimised several times at different development stages throughout the doctoral project. However, to avoid repetition, results are only presented for one version.

Optimisation has been conducted for experiments within a single validation category to investigate the applicability of the approach. To obtain optimal parameter values that can be implemented in the CFD tool, the optimisation approach has been employed for several experiments across a wider range of validation categories. Moreover, optimisation has been conducted for different experimental campaigns separately to gain information about particular sub-grid models.

5.1 Optimising the standard model within a single validation category

In Paper 2, the applicability of the parameter optimisation approach to the standard model is tested, cf. Section 2.3.2. It is investigated to what extent optimisation can improve the selected model responses maximum overpressure and pressure impulse. Therefore, the optimisation is first conducted for a single test series involving similar physical phenomena. The results show that the optimised model predicts the maximum overpressure significantly better than the standard model. Second, two other test series from the same validation category are added to the previous optimisation case, yielding an optimised model with satisfactory predictions. In a third optimisation, the flame speed is added as optimisation target to the first optimisation case. Although the results indicate that including the flame speed can improve the performance of the optimised model, it is not included in subsequent optimisation processes when optimising for several campaigns together. This is due to a lack of reliable flame speed data for the considered experiments (cf. Section 2.3.3) aside from the campaign MERGE. Including the flame speed only for one experimental campaign can result in an undesired biased optimisation.

5.2 Optimising the standard model across validation categories

An optimisation for several campaigns within a single validation category was conducted successfully in Paper 2, cf. Section 5.1. The study can be seen as a proof of concept, but the optimal parameter values are not of any practical use.

Finding optimal parameter values for the standard model by optimising for numerous experiments across validation categories, cf. Section 2.3.1, is investigated additionally; detailed results are included in Appendix C. It is observed that for most of the campaigns the considered predictions after the overall optimisation show less deviation from the experimental data. As expected, the effect of optimisation is not significant.

This study and the study in Paper 2 show that the laminar burning velocity is often optimised towards the edge of its uncertainty range. To ensure that optimising the laminar burning velocity does not compensate for insufficient representation of physical phenomena that are not covered by the selected parameters, it was decided to exclude the laminar burning velocity from subsequent optimisation (despite the uncertainty connected with its value).

5.3 Optimising the development model across validation categories

Paper 3 reports on the application of the optimisation approach to the development model. The optimisation is conducted for a wide range of gas explosion experiments across validation categories, cf. Section 2.3.1. Analysing the optimised model shows that the optimisation improves the predictions of the maximum overpressure and maximum pressure impulse significantly and that the physical mechanisms of gas explosions are represented by the optimised model. The optimisation process has been very efficient; manual searching for good parameter values does in general not lead to optimal ones and can take several weeks or months. Furthermore, the optimisation is an important support in the modelling process. Analysing the predictions of the optimised model suggests updated user guidelines and to exclude the quasi-laminar burning velocity from optimisation, cf. Paper 3. Such conclusions for the recently updated model have not been possible to draw before model parameter optimisation. It is important to note that an extensive model validation against experimental data is required to decide whether the development model can confidently be used for process safety; this is, however, outside the scope of this dissertation.

Two aspects that have not been addressed in the paper are discussed in the following: motivation for the choice of setting the weights in the objective function equal to unity, and a comparison of optimising the validation-based and the VG problem formulation. The comparison suggests that both problem formulations are applicable with similar final results.

5.3.1 Testing different weights in the objective function

To motivate the equal weighting of all contributions in the objective function, the weighting strategy from Section 2.5 is employed. Results are provided in the following.

The objective function can be understood as a weighted sum of two objective functions; let F_{pmax} denote the objective function associated with the maximum overpres-

sure, which is given by the sum over the transferred relative errors for all experiments and monitor points, cf. Section 2.4. Similarly, let F_{pimpmax} denote the sum over the transferred relative errors of the maximum pressure impulse. Note that here, the surrogates are employed instead of the original model responses from the CFD tool. The weighted sum of the two objective functions is transformed with the lower-bound approach (cf. Section 2.5) such that the aggregated objective function reads

$$w_{\text{pmax}} \frac{F_{\text{pmax}}}{F^o_{\text{pmax}}} + w_{\text{pimpmax}} \frac{F_{\text{pimpmax}}}{F^o_{\text{pimpmax}}} \tag{5.1}$$

with

$$\begin{aligned} F^o_{\text{pmax}} &= \min\{F_{\text{pmax}}(\mathbf{x}) |\ \mathbf{x} \text{ in the feasable parameter space}\} \text{ and} \\ F^o_{\text{pimpmax}} &= \min\{F_{\text{pimpmax}}(\mathbf{x}) |\ \mathbf{x} \text{ in the feasable parameter space}\}. \end{aligned}$$

It can be assumed that F^o_{pmax} and F^o_{pimpmax} are both non-zero, as it is improbable that there exists a set of parameter values such that the model responses coincide with the experimental data.

Since preferences for F_{pmax} and F_{pimpmax} are not known *a priori*, the Pareto optimal parameter values are found by varying the weights w_{pmax} and w_{pimpmax} in the optimisation process. Table 5.1 shows the two objective functions evaluated at default parameter values, as well as at optimal parameter values for weights between 0 and 1. Note that the parameter values are reported as the transformed values in the reference interval $[-1,1]$. By setting one of the weights to zero, optimisation is exclusively conducted for the maximum overpressure or the maximum pressure impulse. Setting both weights to 0.5 reflects the same importance of both objective functions. The weights $w_{\text{pmax}} = 0.866$ and $w_{\text{pimpmax}} = 0.134$ are chosen, as minimising (5.1) is then equivalent to minimising

$$F_{\text{pmax}} + F_{\text{pimpmax}},$$

where the weights of the untransformed formulation are equal to unity; this corresponds to the optimisation case presented in Paper 3. For comparison, the opposite weighting, $w_{\text{pmax}} = 0.134$ and $w_{\text{pimpmax}} = 0.866$, is also analysed.

Table 5.1 visualises that the optimal parameter values, as well as the evaluated objective functions F_{pmax} and F_{pimpmax}, change continuously when varying the weights from 'more weight to the maximum overpressure' to 'more weight to the maximum pressure impulse'. The changes are not significant as long as the contribution of the maximum overpressure in the weighted sum (5.1) is sufficiently large, i.e., here $w_{\text{pmax}} > 0.134$.

Figure 5.1 shows pressure-time histories of simulations for experiment MERGE E with a propane-air mixture in the middle of the rig. The plot comprises simulations with the different optimised models as well as experimental data. The experimental data is filtered using a suitable Savitzky–Golay filter (Savitzky and Golay, 1964). The plot illustrates that the pressure-time histories for different weights do not differ significantly from each other.

In total, it seems possible that the maximum overpressure and the maximum pressure impulse are so closely linked that they are optimised simultaneously, not highly

Table 5.1: Optimal parameter values of the development model for different weights in the aggregated objective function (5.1).

before optimisation	objective function evaluation		default parameter values, chosen as zero
	F_{pmax}	F_{pimpmax}	
	15733.176	321,380	

weights		objective function evaluation		optimal parameter values				
w_{pmax}	w_{pimpmax}	F_{pmax}	F_{pimpmax}	$C_{\alpha,ma}$	C_{gs}	C_{λ}	a	...
1.0	0.0	153.897	28.706	0.1219	-1.0	0.8465	1.0	...
0.866	0.134	154.315	27.792	0.1269	-1.0	1.0	1.0	...
0.5	0.5	160.462	25.835	0.1270	-1.0	1.0	1.0	...
0.134	0.866	185.324	24.286	0.0864	-0.997	1.0	1.0	...
0.0	1.0	238.617	23.774	0.0993	-1.0	1.0	1.0	...

weights		optimal parameter values					
w_{pmax}	w_{pimpmax}	...	C_{ql}	K_q	C_o	γ_t	$C_{tp,lim}$
1.0	0.0	...	-0.2676	0.7329	-0.7399	-0.6231	1.0
0.866	0.134	...	-0.2811	0.6502	-0.7770	-0.6108	1.0
0.5	0.5	...	-0.3137	0.5317	-0.8709	-0.5595	1.0
0.134	0.866	...	-0.3591	0.3521	-0.9312	-0.4904	1.0
0.0	1.0	...	-0.4041	0.2544	-1.0	-0.6098	1.0

dependent on the choice of the weights. The question that arises is: "Which weights shall be chosen in the parameter optimisation process?". Following the study above, the conclusion may be to set the weights w_{pmax} and w_{pimpmax} in the transformed formulation equally. However, similar studies with a different splitting of the objective function could lead to different weighs. Alternative multiple objective functions could be defined, for example, as the sum over all model responses for each experimental campaign, or at specific places in the rig relative to the ignition source. As no *a priori* preferences of any of those multiple objectives are known in the present application, the weights in the respective transformed formulations might also be set to equal values. However, these formulations would most likely differ from the one studied in this section due to different minima F_*^o. Consequently, the weights for each error between model response and experimental data (in the original objective function) would differ for different multi-objective studies. Thus, it has been found appropriate to set the weights to unity in the original (untransformed) problem formulation.

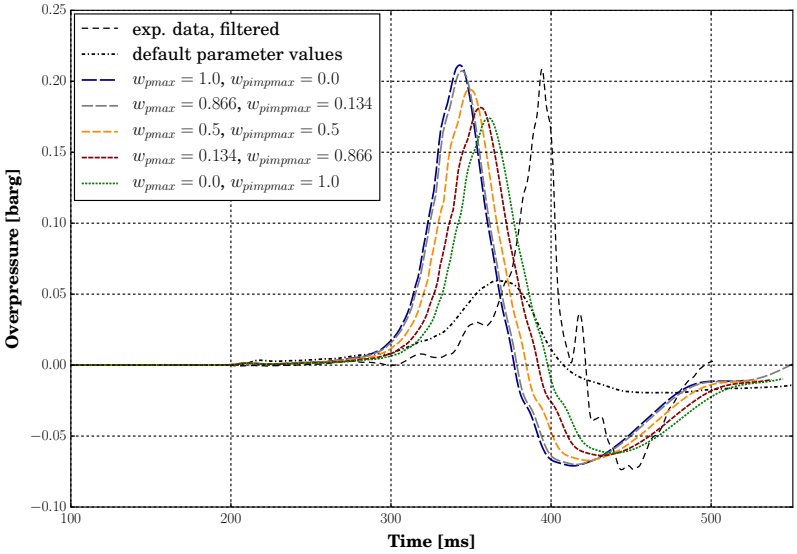

Figure 5.1: Overpressure-time histories for MERGE E with a propane-air mixture in the middle of the rig simulated with a default development model and optimised models for different weighted sums.

5.3.2 Testing the VG problem formulation

In this section, the VG problem formulation (2.2) is tested for optimising the development model; results are compared to the optimisation with the validation-based formulation presented in Paper 3. Note that surrogates are employed for both formulations, and that optimisation includes all selected experiments.

Table 5.2 presents the optimal parameter values for both formulations. The most striking differences in the values can be found for the factor in the correlation of the quasi-laminar burning velocity, C_{ql}, the quenching limit for the turbulent burning velocity, K_q, and the parameter accounting for turbulence production from sub-grid obstacles, C_o. Figure 5.2 shows scatter and parabola plots for the validation of the optimised

Table 5.2: Optimal parameter values for the development model for different problem formulations.

Formulation	$C_{\alpha,ma}$	C_{gs}	C_λ	a	C_{ql}	K_q	C_o	γ_t	$C_{tp,lim}$
VG	0.1018	-0.9422	1.0	1.0	-0.5015	0.3984	-0.8406	-0.6232	1.0
validation-based	0.1269	-1.0	1.0	1.0	-0.2811	0.6502	-0.7770	-0.6108	1.0

model for the VG formulation. Analogous plots for the validation-based formulation can be found in Figure 4 of Paper 3. Both optimised models give excellent overall predictions; the predictions of the maximum pressure impulse are nearly the same. The VG formulation leads to slightly more under-prediction of the maximum overpressure

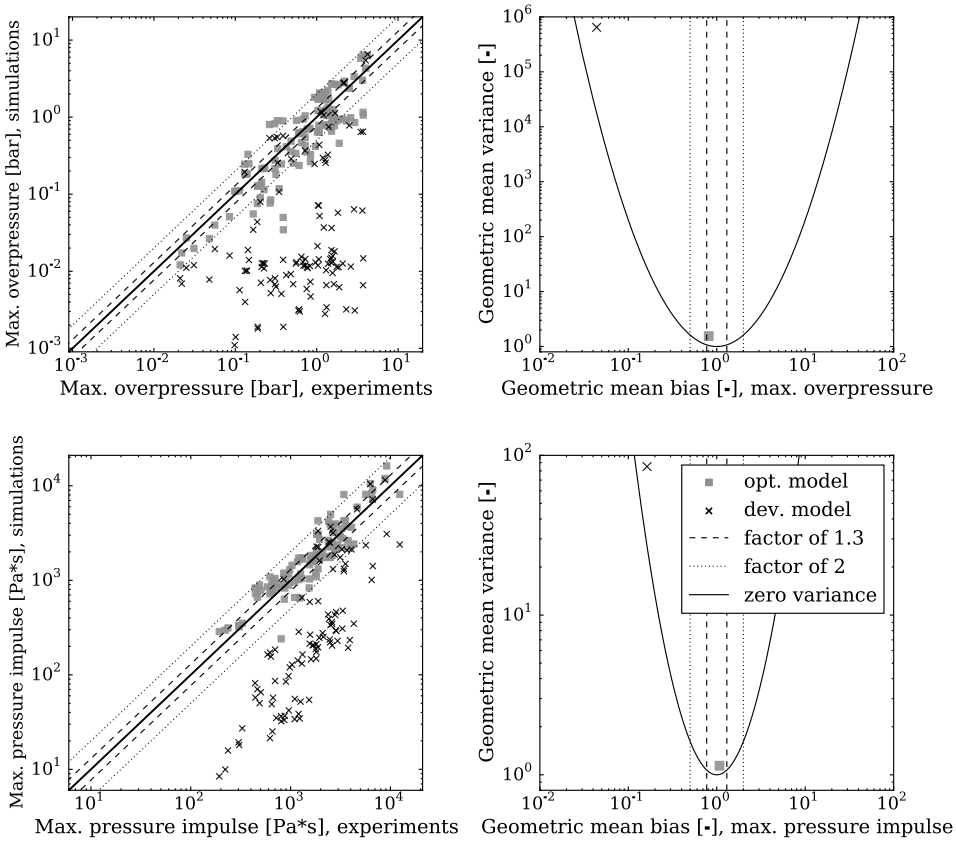

Figure 5.2: Maximum overpressure (upper panel) and maximum pressure impulse (lower panel) simulated with the development and optimised model vs. experimental data for all selected experiments (left) and corresponding values of the geometric mean bias and variance (right). The model is optimised via the VG formulation.

than the validation-based formulation. However, as the differences in the predictions of the optimised models are minimal, it can be concluded that both problem formulations are appropriate for optimisation.

Different optimised predictions of the maximum overpressure are mainly observed for the FM Global 64 m^3 vented chamber experiments with overpressures below 0.1 barg, cf. upper left scatter plots of Figure 5.2 and Figure 4 of Paper 3. These overpressures are very sensitive to changes in C_{ql}. Thus, the low value of C_{ql} for the VG problem formulation most likely causes the slightly more under-prediction for the FM Global 64 m^3 vented chamber experiments – without changing the other predictions appreciably; in the other experiments, the different optimal parameter values seem to compensate for each other such that the predictions from both optimisations are almost the same. This finding supports the discussion in Paper 3 about excluding the quasi-laminar burning velocity from subsequent optimisation.

5.4 Optimisation for analysing the flame folding model

As presented in Section 2.3.1, the optimisation approach can additionally be utilised to analyse modelling strengths of sub-grid models individually. In this thesis, this usage of the optimisation method is tested for a model accounting for flame folding around sub-grid obstacles. The objective is to optimise parameters in the flame folding model to gain information about how well the model represents flame folding in different gas explosion scenarios. The CFD model that is considered in this study is a development version of FLACS, similar to the development model examined in Paper 3, but contains changes to some sub-grid models. The flame folding model, however, remains unchanged; a description of the model and its parameters can be found in Paper 3.

Selected for optimisation are 15 tests in the DNV GL 182 m^3 explosion vessel (see Paper 3) and 4 tests from the Gaps project (see Appendix D.1). In those tests, the gas explosions are mainly driven through the flame folding around sub-grid obstacles as well as the turbulent burning velocity; the tests are thus not 'single phenomenon' experiments for flame folding. When optimising for the flame folding model, the optimal parameter values depend on the fixed parameter values in the turbulent burning velocity correlation. The latter are set to the values found in an overall optimisation of the present development model. Therefore, optimal parameter values resulting from this study should not be implemented in the tool.

The maximum overpressure and pressure impulse at relevant monitor points are optimised with respect to two flame folding parameters with high sensitivities. Details about the sensitivity analysis can be found in Appendix D.2. The optimisation approach is employed for three cases: the selected tests of the DNV GL 182 m^3 vented enclosure, the selected tests of the Gaps project and for all selected tests together. The optimal parameter values, as well as validation results of the overall optimised model, can be found in Appendix D.3

The optimal parameter values for all cases are very similar. This indicates that the flame folding model is able to predict the basic aspects of flame folding around sub-grid obstacles independently from the gas explosion scenario and geometry. If the optimal parameter values diverged, the gas explosions in the DNV GL 182 m^3 vented enclosure would be predicted best with a flame folding model that is different from the one that is best for the Gaps project tests (due to different parameter values). This would point out that different parameter values try to compensate for mechanisms in the flame folding that are not captured by the model.

Chapter 6

Concluding remarks and future work

The goal of this doctoral study was to improve the predictive capabilities of a CFD model by parameter optimisation. The model predicts the consequences of industrial-scale gas explosions. The parameters are contained in sub-grid models for turbulence and combustion; their values were optimised to improve the agreement between relevant experimental data and the corresponding predictions of the simulation tool. This chapter summarises shortly the main results from the doctoral study and gives an outlook for future work.

This thesis proposes a surrogate-based optimisation approach, in which the problem was formulated to account for assessing under- and over-predictions as in model validation processes. This validation-based problem formulation has been tailored to the specific output in gas explosion simulations, and is shown to be more appropriate than a least-squares problem formulation. It was shown that the validation-based formulation is closely connected to another formulation for which the solution is the maximum likelihood estimator in the case of log-normally distributed errors in the measurements. Three model responses amongst several candidates were found suitable as optimisation targets for the present application. Different methodologies for selecting gas explosion experiments to be included in an optimisation process were developed. Surrogates were employed for a fast evaluation of the model parameter-output relations. Surrogates based on neural networks were compared to polynomial response surfaces. A satisfactory approximation quality of the neural networks for the entire parameter space was shown; thus, these surrogates were employed for subsequent optimisations. Because of the smoothness and global approximation quality of the surrogates, a trust region multi-start algorithm was used for solving the surrogate-based optimisation problem in a one-shot solution technique. As the optimisation routine has been originally intended for non-linear least-squares problems, not covering the validation-based formulation, its convergence for this optimisation problem with respect to the first order necessary optimality conditions has been proven.

The methodologies for selecting gas explosion experiments for one optimisation process were developed to serve two different purposes: first, obtaining optimal parameter values that can be implemented in the tool, and second, analysing the predictive capabilities of sub-grid models after optimisation and gain information about possible improvements. The following paragraph elaborates on how the methodologies were employed in this thesis.

1. To serve the first purpose – obtaining optimal parameter values of practical use – the quality of the predictions was improved directly via parameter optimisation. Since it has not been straightforward to find 'single phenomenon' experiments, which isolate single phenomena in gas explosions, this doctoral study focused on optimising all sub-grid models together for various experiments that represent a wide range of explosion phenomena. The optimisation was tested and applied successfully to several versions of the CFD tool FLACS in different stages of the development process; the standard model released for commercial use and an in-house development model:

   (a) The standard model was mainly utilised to investigate the applicability of the optimisation approach. For this purpose, optimisation was tested for experiments from one validation category first. Results demonstrate that on the one hand, the approach is able to improve the predictions notably and on the other hand that the characteristic physical mechanisms of gas explosions are represented by the optimised model. Second, an overall optimisation for experiments comprising a wide range of scenarios was conducted, resulting in a model with improved and satisfactorily predictive capabilities for all considered experimental test series. Due to already good model performance before optimisation, the improvement was just moderately. In the end, it was concluded that the approach is applicable to gas explosion simulations.

   (b) To support modelling efforts, optimisation was also performed on a development model, in which sub-grid models had been updated, and parameter values had been set to an initial 'best guess'. The optimisation was conducted for various experiments representing a wide range of physical phenomena; the improvement of the predictions was significant. The optimisation process has been very efficient and important as support in the modelling process; manual searching for good parameter values does in general not lead to optimal ones and can take several weeks or months. Furthermore, analysing predictions of the optimised model suggested updated user guidelines and enabled the discussion on how to progress with the development of the physical models. Such conclusions for the recently updated model would not have been possible to draw before model parameter optimisation. It is important to note that an extensive model validation against experimental data is required to decide whether the development model can confidently be used for process safety; this is, however, outside the scope of this dissertation. Nevertheless, optimisation results were analysed carefully in sanity checks; by analysing pressure-time histories, it was shown that the physical mechanisms of gas explosions are represented by the optimised model.

2. The second purpose – analysing sub-grid models to improve predictions – was served by applying the optimisation approach to just one single sub-grid model. A model accounting for flame folding around sub-grid obstacles was optimised for two relevant experimental campaigns separately, and for both together. Since the optimal parameter values for the three cases did hardly differ, it was concluded that the flame folding model is able to predict the basic aspects of flame folding

around sub-grid obstacles independently from the specific gas explosion scenario and geometry.

It is important to emphasise that the optimisation process cannot compensate for models that do not capture the physical mechanisms of gas explosions. Thus, optimisation processes do not replace further efforts in CFD modelling.

The research presented in this thesis opens up different directions for future work. In the following, two potential continuations are discussed.

Improving the predictive capabilities of a CFD tool is not finalised after the optimisation process. The steady progress towards models that predict the physics of gas explosions better than the existing ones is addressed by many researchers in various research projects. In particular, the results from new high-quality experiments may give new insights into the physical behaviour of gas explosions. With the help of the optimisation approach, the predictive capability of a novel sub-grid model incorporated in a CFD tool can be investigated in a quick and efficient way, and manual parameter tuning is circumvented. Moreover, future experimental studies on gas explosions could comprise 'single phenomenon' tests for a more fundamental optimisation of sub-grid models.

Another topic for future work is research into including uncertainties in consequence modelling. Aven (2014) highlights, for example, the importance of including uncertainties in risk assessments. Traditionally, a CFD tool predicts the quantity of interest with a single deterministic value, such as a certain maximum overpressure in a gas explosion. The question is: "How uncertain is the model's prediction?".

Uncertainties arise on the one hand from uncertain input parameters, e.g., the leakage rate of combustible gas in accidental gas explosions; on the other hand, the model itself is uncertain. Quantifying how good the predictions of a model are (with given input parameters) requires considering the experimental uncertainty of both the input parameters as well as the quantity of interest (McGrattan and Toman, 2011).

To a certain extent, information about the quality of model output is given through the model validation process. For example, it may be reported that the predictions are within a particular factor of experimental measurements. Even more information and confidence would be given to the user through a probability distribution of the quantity of interest (McGrattan and Toman, 2011). In risk assessment, such a probability distribution may be calculated by propagating entire probability distributions of input parameters through the model (Coffey et al., 2019; Cordero et al., 2007). Alternatively, uncertainties in the model, incorporating uncertainties in experimental measurements, may be estimated and propagated. A relatively simple method to express model uncertainties for complex numerical models such as CFD codes is for example given by McGrattan and Toman (2011).

When model and experimental uncertainties are accounted for in the validation process, results from the optimisation of model parameters can be quantified accordingly. Additionally, it can be investigated to what extent model uncertainty might be reduced by parameter optimisation.

Appendices

This chapter contains four appendices. They either comprise background information to the thesis or support studies from the thesis by presenting detailed results. An overview is given in the following:

- In Appendix A, plots present the approximation quality of response surfaces based on neural networks for two model responses of the standard model: flame speed and pressure rising time. The plots provide a basis for the decision that the flame speed may be included in the optimisation, but not the pressure rising time, cf. 2.2, 3.2, and 4.2.
- Appendix B describes the basic idea of the trust region routine called *lsqnonlin* from MATLAB. Thus, it provides background information to the introduction of the routine from Paper 2 and Section 4.3.
- Appendix C provides detailed results from the optimisation case summarised in Section 5.2; it presents the application of the optimisation approach to the standard model for experiments from a wide range of validation categories. Furthermore, Section 2.6 refers to this Appendix for the work on including outliers in the optimisation.
- Appendix D supports the analysis from Section 5.4; it provides plots and tables presenting the results from optimising the sub-grid model for flame folding around obstacles.

Appendix A

Approximation quality of surrogates

In this section, the approximation quality of response surfaces based on neural networks, RSNNs, is analysed for two model responses of the standard model: flame speed and pressure rising time. For illustration, the experiment MERGE B with a propane-air mixture is considered. The neural networks are generated based on a Latin hypercube sampling (McKay et al., 1979) of the parameter uncertainty space with 400 points. The approximation quality is visualised via scatter plots comparing RSNNs evaluations to the corresponding simulation output for a different Latin hypercube sampling of 250 points. In a perfect fit, the plotted points would all lay on the diagonal line.

A.1 Flame speed

The scatter plots of Figure A.1 visualise the ability of RSNNs to approximate the flame speed predictions. The flame speed is calculated from flame arrival times between monitor points 1–2, 2–3, 4–5, 5–6 across the rig and outside the congested region. Due to the small scatter between the simulated flame speeds and the surrogate evaluations, the flame speed is found appropriate to be approximated by RSNNs.

A.2 Pressure rising time

The scatter plot of Figure A.2 shows the validation result of an RSNN for the pressure rising time, cf. 2.2, for the experiment MERGE B with a propane-air mixture at monitor point 6. The approximation quality of the RSNN is not satisfactory. In particular, the gap between the dots in the plot visualises that the pressure rising time prediction for this experiment is a discontinuous function of the sub-grid model parameters. To explain the discontinuity, Figure A.3 a) illustrates simulated pressure-time histories for different model parameter values. The curves consist of two nearby pressure peaks. There exist parameter values inside the uncertainty range such that the first peak is the higher peak resulting in a short pressure rising time, cf. Figure A.3 b), and others such that the second peak dominates resulting in a longer pressure rising time, cf. Figure A.3 c). It is observed that the pressure-time histories change only slightly with small parameter perturbations. However, the pressure rising time will change significantly, if a small parameter perturbation causes a switch in the highest pressure peak. This results in a severe discontinuity in the pressure rising time-parameter relation such

that it cannot be approximated with satisfactory quality. Therefore, the pressure rising time is not included in the optimisation process.

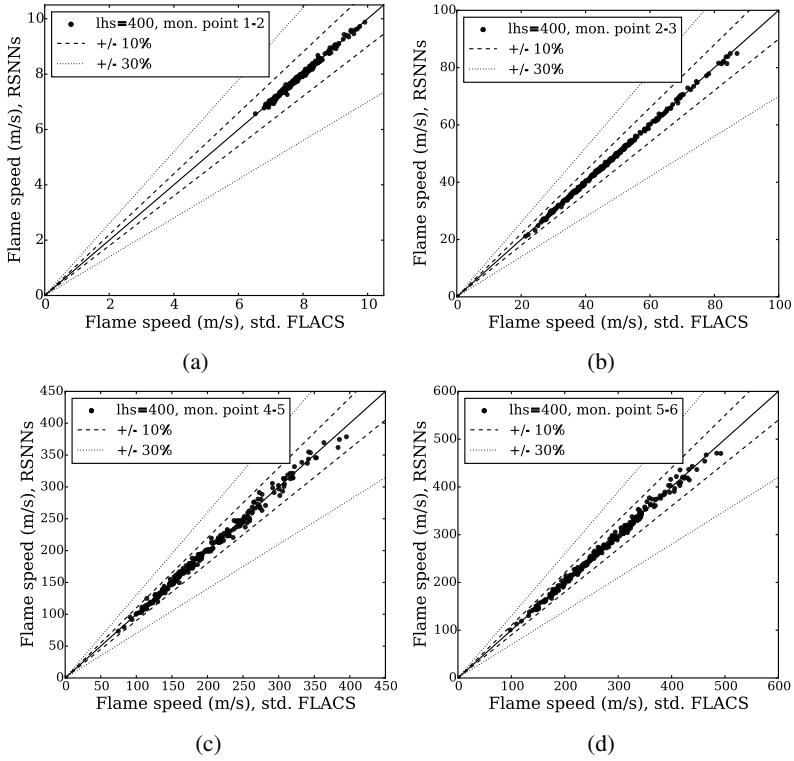

Figure A.1: Validation of RSNNs for the flame speed of experiment MERGE B with propane-air, monitor point (a) 1–2 , (b) 2–3, (c) 4–5, (d) 5–6.

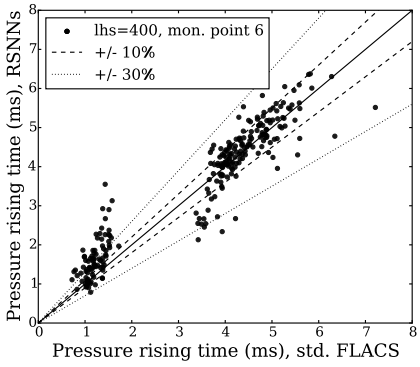

Figure A.2: Validation of an RSNN for the pressure rising time of experiment MERGE B with propane-air, monitor point 6.

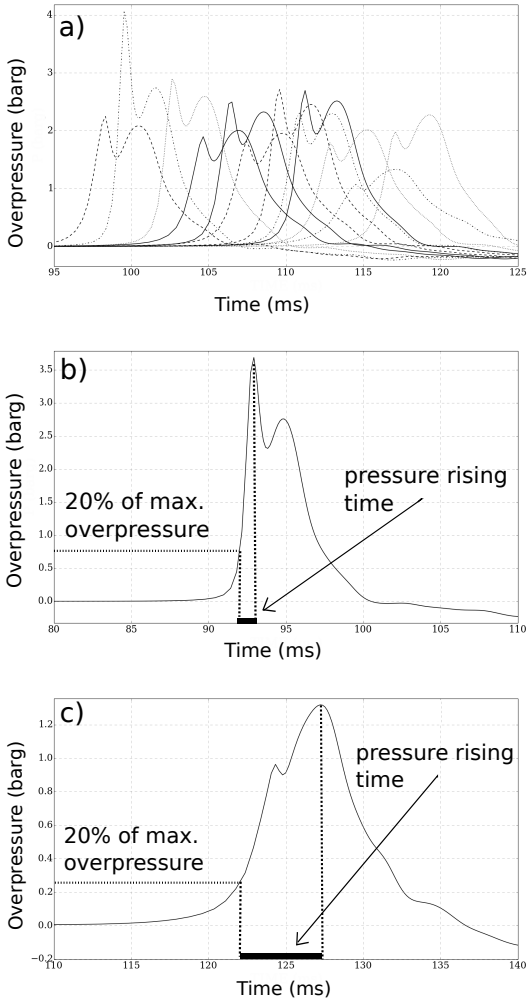

Figure A.3: Switch in the strength of the pressure peaks: a) for varying parameter values from the uncertainty space, b) and c) for two specific sets of parameter values, for MERGE B with propane-air, monitor point 6.

Appendix B

Trust region algorithm

In this section, the basic idea of the trust region routine called *lsqnonlin* from MATLAB is described (The MathWorks Inc., 2017). The routine is an iterative method and employs a two-dimensional subspace trust region method on a transformed, unconstrained problem given by Coleman and Li (1996b). To obtain 'sufficient decrease' in a step of a subproblem iteration, a reflective path is followed as described in (Coleman and Li, 1996a).

The algorithm is described for the following general form of a minimisation of a function f on $\mathbb{R}^n$ subject to lower and upper bounds l_i and u_i, respectively:

$$\begin{aligned} &\min_{\mathbf{x}\in\mathbb{R}^n} f(\mathbf{x}), \\ &\text{subject to: } l_i \leq x_i \leq u_i, \quad \text{for } i = 1,\ldots,n. \end{aligned} \tag{B.1}$$

B.1 Without box constraints

Assume that no bound constraints are present. In each iteration of a trust region method, a quadratic approximation to the objective function is minimised on a so-called trust region with radius Δ_k (Nocedal and Wright, 2006). The trust region subproblem in the kth iteration reads

$$\begin{aligned} &\text{minimise: } m_k(\mathbf{p}) = \frac{1}{2}\mathbf{p}^\top \mathbf{B}_k \mathbf{p} + \mathbf{g}_k^\top \mathbf{p}, \\ &\text{subject to: } \|\mathbf{p}\| \leq \Delta_k, \end{aligned} \tag{B.2}$$

where $\mathbf{B}_k$ is an approximation to the Hessian and $\mathbf{g}_k$ the exact gradient of f evaluated at the iterate $\mathbf{x}_k$. $\|\cdot\|$ denotes the Euclidean norm. Let $\mathbf{p}_k$ denote the approximate solution of (B.2). If the step is accepted (with respect to certain criteria), the new iterate is set to $\mathbf{x}_{k+1} = \mathbf{x}_k + \mathbf{p}_k$, otherwise, the trust region is updated. In the following, subscripts indicating the current iteration are omitted to simplify the notation.

According to Nocedal and Wright (2006), the subproblem (B.2) may be solved with an iterative method based on the following theorem by Moré and Sorensen (1983).

Theorem 1 *The vector* $\mathbf{p}^*$ *is a global solution of the problem* (B.2)*, if and only if it is feasible (*$\|\mathbf{p}^*\| \leq \Delta$*), and there exists a scalar* $\lambda \geq 0$ *such that*

$$(\mathbf{B} + \lambda \mathbf{I})\mathbf{p}^* = -\mathbf{g}, \tag{B.3a}$$

$$\lambda(\Delta - \|\mathbf{p}^*\|) = 0, \tag{B.3b}$$

$$(\mathbf{B} + \lambda \mathbf{I}) \textit{ is positive semidefinite}. \tag{B.3c}$$

The iterative method finds an approximation to $\mathbf{p}^*$ and λ that are satisfying conditions (B.3a)–(B.3c). If the initial guess $(\lambda_0 = 0, \mathbf{p}_0)$ satisfies (B.3c), (B.3a) and $\mathbf{p}_0$ is feasible, the global solution is found. Otherwise, Newton's method is applied to the function of λ:

$$\frac{1}{\Delta} - \frac{1}{\| - (\mathbf{B} + \lambda \mathbf{I})^{-1}\mathbf{g}\|}.$$

The inverse of the matrix $(\mathbf{B} + \lambda \mathbf{I})$ is not calculated explicitly such that the main work in each iteration lies in a Cholesky factorisation of the matrix. Since practical versions of this method typically find an approximation to λ after 2 or 3 iterations, the iterative method requires in total 2–3 matrix factorisations, which are costly in high dimensions (Nocedal and Wright, 2006).

The trust region routine *lsqnonlin* employs therefore a two-dimensional subspace method, which solves the subproblem (B.2) on a two-dimensional subspace S. The subspace is spanned by $\mathbf{g}$ and $\mathbf{s}$ either satisfying the Newton system $\mathbf{Bs} = \mathbf{g}$ or, if encountered, a direction of negative curvature, i.e.,

$$S = \text{span}[\mathbf{g}, \mathbf{s}], \quad \text{with } \mathbf{Bs} = \mathbf{g} \text{ or } \mathbf{s}^\top \mathbf{Bs} < 0. \tag{B.4}$$

Then, the restricted subproblem is solved by the iterative method described above, which is not costly due to the low dimension. Thus, the main work is reduced to solving one large linear equation, $\mathbf{Bs} = \mathbf{g}$.

Moreover, the routine exploits the special structure of the least-squares objective function:

$$f(\mathbf{x}) = \frac{1}{2}\sum_{i=1}^{m} r_i(\mathbf{x})^2.$$

The gradient $\mathbf{g}$ and the Hessian $\mathbf{H}$ of f are given by

$$\mathbf{g}(\mathbf{x}) = \mathbf{J}(\mathbf{x})^\top \mathbf{r}(\mathbf{x}) \text{ and } \mathbf{H}(\mathbf{x}) = \mathbf{J}(\mathbf{x})^\top \mathbf{J}(\mathbf{x}) + \sum_{i=1}^{m} r_i(\mathbf{x}) \nabla^2 r_i(\mathbf{x}) \tag{B.5}$$

with $\mathbf{r}(\mathbf{x}) = (r_1(\mathbf{x}), \cdots, r_m(\mathbf{x}))^\top$ and $\mathbf{J}$ is the Jacobian of $\mathbf{r}$. Near the solution the second term of the Hessian is typically small, as typically $r_i(\mathbf{x})$ are either small or close to affine and thus $\nabla^2 r_i(\mathbf{x})$ are small. Finally, the subspace S is defined via the Gauss–Newton direction $\mathbf{s}$ by

$$S = \text{span}[\mathbf{J}(\mathbf{x})^\top \mathbf{r}(\mathbf{x}), \mathbf{s}], \quad \text{with } \mathbf{J}(\mathbf{x})^\top \mathbf{J}(\mathbf{x})\mathbf{s} = \mathbf{J}(\mathbf{x})^\top \mathbf{r}(\mathbf{x}) \text{ or } \mathbf{s}^\top \mathbf{J}(\mathbf{x})^\top \mathbf{J}(\mathbf{x})\mathbf{s} < 0.$$

The large linear systems are solved using the method of preconditioned conjugate gradients.

B.2 With box constraints

In the presence of finite bounds on $\mathbf{x}$ as given by the problem (B.1), the inequality restrictions may be added to the quadratic subproblem (B.2). Instead, in this routine, the subproblem is transformed by scaling as described in the interior-reflective Newton method by Coleman and Li (1996a,b). The scaling strategy arises from examining the first order necessary optimality conditions. Let the vector $\mathbf{v}(\mathbf{x}) = (v_1(\mathbf{x}), \ldots, v_n(\mathbf{x}))$ be defined by

$$v_i(\mathbf{x}) = \begin{cases} x_i - u_i & \text{if } g_i < 0 \text{ and } u_i < \infty, \\ -1 & \text{if } g_i < 0 \text{ and } u_i = \infty, \\ x_i - l_i & \text{if } g_i \geq 0 \text{ and } l_i > -\infty, \\ 1 & \text{if } g_i \geq 0 \text{ and } l_i = -\infty, \end{cases} \qquad \text{for } i = 1, \ldots, n.$$

The diagonal scaling matrix $\mathbf{D}(\mathbf{x})$ is based on the distance to the boundary of the feasible region. Its entries are given by

$$|v_i(\mathbf{x})|^{-1/2}, \qquad \text{for } i = 1, \ldots, n.$$

Then, the first order necessary conditions for $\mathbf{x}^*$ to be a local minimiser of problem (B.1) are equivalent to

$$\mathbf{D}(\mathbf{x}^*)^{-2}\mathbf{g}(\mathbf{x}^*) = 0. \tag{B.6}$$

Let $\mathbf{x}_k$ denote a point in the interior of the feasible set $\mathcal{F} = \{\boldsymbol{x} \in \mathbb{R}^n \mid l_i \leq x_i \leq u_i, \text{ for } i = 1, \ldots, n\}$. When approximating the Hessian of f at $\mathbf{x}_k$ with $\mathbf{B}_k$, an inexact Newton step to (B.6) is given by

$$(\mathbf{D}_k^{-2}\mathbf{B}_k + \mathbf{diag}(\mathbf{g}_k)\mathbf{J}_k^v)\mathbf{d}_k = -\mathbf{D}_k^{-2}\mathbf{g}_k, \tag{B.7}$$

where $\mathbf{D}_k = \mathbf{D}(\mathbf{x}_k)$ and $\mathbf{J}_k^v$ is the Jacobian matrix of $|\mathbf{v}_k|$ whenever it is differentiable and 0 otherwise, cf. Coleman and Li (1996b). Then, a subproblem similar to (B.2) is formulated employing $\mathbf{D}_k$ and $\mathbf{J}_k^v$ such that in the neighbourhood of a local minimiser, its solution is given by the Newton step from Equation (B.7). The subproblem reads

$$\begin{aligned} &\text{minimise: } \tilde{m}_k(\mathbf{p}) = \frac{1}{2}\mathbf{p}^\top(\mathbf{D}_k^{-1}\mathbf{B}_k\mathbf{D}_k^{-1} + \mathbf{diag}(\mathbf{g}_k)\mathbf{J}_k^v)\mathbf{p} + \mathbf{g}_k^\top\mathbf{D}_k^{-1}\mathbf{p}, \\ &\text{subject to: } \|\mathbf{p}\| \leq \Delta_k. \end{aligned} \tag{B.8}$$

The scaled subproblem (B.8) is solved analogously as described in Appendix B.1; in particular the Newton system in Equation (B.4) is replaced by a scaled modified Newton system. After the scaled subproblem is solved, the solution, if necessary, simply needs to be truncated into the interior of the feasible set $\mathcal{F}$. Details about the truncation, when to accept a step in the trust region method, and how to update the trust region radius can be found in Coleman and Li (1996b).

Appendix C

Optimisation of the standard model for a wide range of experiments

In this section, the optimisation approach is applied to the standard model, FLACS v10.7, for experiments from a wide range of validation categories. The experiments that are considered for optimisation and validation belong to the selected campaigns from Gexcon's validation database listed in Section 2.3.3 – MERGE A, B, C, C*, D, and E experiments for methane and propane mixed with air; BFETS Phase 3A tests 1, 4, 16, 17, 24 ('Alpha'), and 39 ('Beta'); BFETS Phase 2 tests 6, 7, 13, 18, and 22; eight FM Global 64 m^3 vented chamber experiments with and without obstacles; and DNV GL 182 m^3 vented enclosure tests 4, 12, 14, 22, 26, and 38. Details on the experiments can be found in Paper 3, in which a similar optimisation and analysis is studied for another version of the CFD tool FLACS. The optimisation is conducted for the maximum overpressure and pressure impulse at key monitor points. For an unbiased optimisation, all cases that are over- or under-predicted by the unoptimised standard model with a factor larger than 2.7 (so-called outliers) are excluded from the optimisation process, cf. Section 2.6. However, they are included in the validation process. For comparison, results of an optimisation including outliers are presented in Section C.4.

First, the optimisation approach is applied to two validation categories separately. As discussed in Section 2.3.2, the resulting sets of optimal parameter values are not of any practical use. Therefore, optimisation is also conducted for all experiments together (referred to as the overall optimisation). Separate optimisation processes give inherently better results than the overall optimisation since the latter needs to compromise between the two separate cases. The separate optimisation can be utilised as a reference; one criterion for the optimisation to be applicable across validation categories is that the optimised model's predictive capabilities should be close to the reference case.

As part of each optimisation process, the optimised models are analysed in a sanity check. Scatter plots visualise the deviation from the predictions of models to the experimental data. In parabola-plots, the corresponding geometric mean bias, MG, and geometric variance, VG, are plotted, cf. Equation (2.2). To ensure that the optimisation is not a blind fit of the selected model responses, plots for the maximum overpressure at several distances across the explosion module, as well as pressure-time histories, are analysed.

C.1 Optimisation within validation categories

Optimisation is conducted for the selected experiments from two validation categories separately – (i) category 1B with the MERGE and BFETS Phase 3A experiments and (ii) category 3B with the experiments from BFETS Phase 2, the FM Global 64 m^3 vented chamber experiments with obstacles, as well as the DNV GL 182 m^3 vented enclosure tests. Table C.1 presents both sets of optimal parameter values. The separate optimisations result in two optimised models with different optimal parameter values implemented. For simulating cases in categories 1B and 3B the respective model is employed. In the following, for the sake of brevity, the 'optimised model' refers to the two models interpreted as one. The FM Global 64 m^3 vented chamber experiments without obstacles are assigned to category 3A. For this category, optimisation is not conducted separately, as only four experiments are available in this study, and a larger number of experiments is necessary to obtain appropriate optimal parameter values. Those tests are thus excluded from optimisation and validation in this section.

Figure C.1 visualises the performance of the unoptimised standard model and the optimised CFD model. The left-hand side of Figure C.1 shows scatter plots; on the

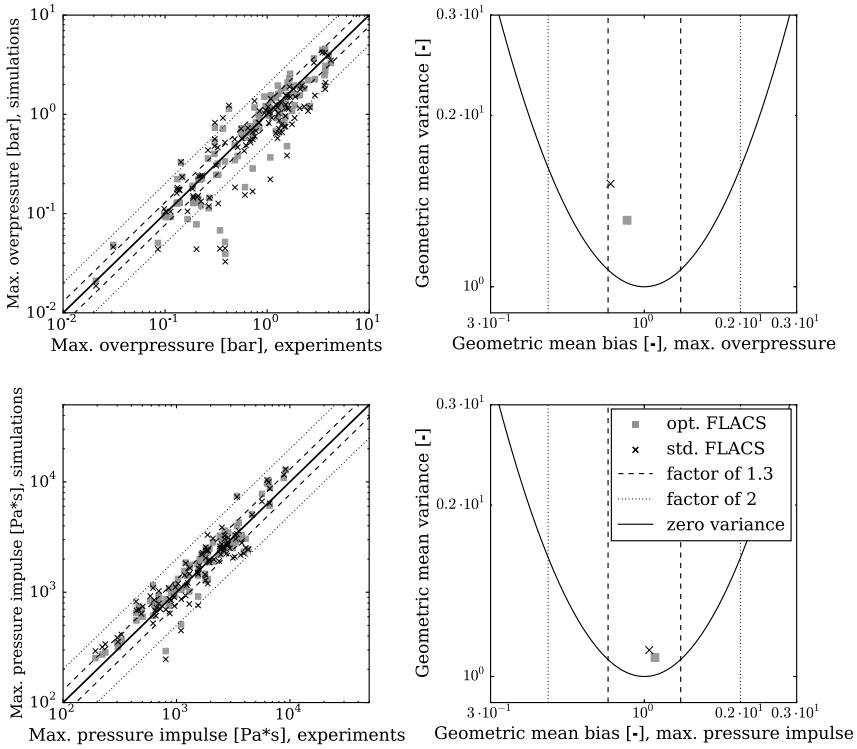

Figure C.1: Maximum overpressure (upper panel) and maximum pressure impulse (lower panel) simulated with the standard and the optimised model vs experimental data for all selected experiments from category 1B and 3B (left) and corresponding values of the geometric mean bias and variance (right). Optimisation is conducted for selected experiments in validation categories 1B and 3B separately.

upper and lower panel, the measured maximum overpressure and pressure impulse, respectively, for the selected experiments at several monitor points are plotted against the simulation output. On the right-hand side of Figure C.1, the corresponding geometric mean bias and variance of the differences between simulation output and experimental data are plotted. Note that both the scatter and parabola plots comprise results for simulations with the standard and the optimised model simultaneously. The experimental data throughout this study is filtered using a suitable Savitzky–Golay filter (Savitzky and Golay, 1964).

The plots show that the predictions with the optimised model are overall better than with the standard model, which even holds for predictions at monitor points that are excluded from optimisation due to a deviation larger than a factor of 2.7 before optimisation. The predictions of the optimised model are less biased towards underpredictions and contain less scatter around the mean bias. The improvement is more significant for the maximum overpressure than for the maximum pressure impulse.

C.2 Optimisation for experiments across validation categories

To obtain optimal parameter values of practical use, cf. Section 2.3.1, optimisation is conducted and analysed for experiments across validation categories. Table C.1 presents the optimal parameter values; Figure C.2 visualises the optimisation results. The geometric mean bias for the predictions of the maximum overpressure and pressure impulse for the overall optimisation differs only slightly from those for optimising the categories 1B and 3B separately, cf. Figure C.1. However, the optimisation for all experiments together leads to a slightly larger scatter of both model outputs. In the following sections, a more detailed analysis of the overall optimised predictions is presented.

Validation of surrogates at the optimal parameter values

Although the surrogates for the selected output of the CFD tool have been tested extensively in Paper 1, it should be further investigated whether the optimum found using the surrogate-based optimisation approach can be trusted to represent the optimum of the original problem. In Figure C.3 the predictions of the optimised model are compared to the surrogates (RSNNs) evaluated at the optimal parameter values. The small differences between surrogate evaluations and model responses are found acceptable.

Separate validation of the overall optimised model

In this section, we investigate to what extent the overall optimisation improves the predictions of the maximum overpressure and pressure impulse for each campaign. Figure C.4 presents the validation results. Test cases that have not been employed for optimisation are included in the validation to provide an impression of how the optimised model performs on ‘new’ scenarios.

The optimised model predicts the maximum overpressure and pressure impulse with less scatter than the standard model for all campaigns except for the FM Global 64 m^3 vented chamber experiments. For most of the campaigns, optimisation leads to over-

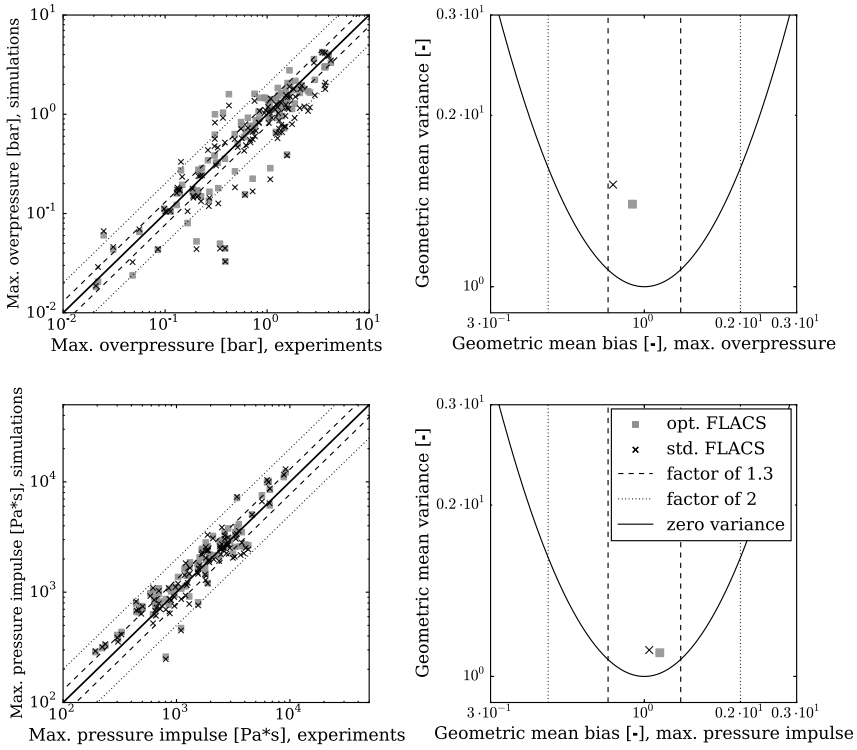

Figure C.2: Maximum overpressure (upper panel) and maximum pressure impulse (lower panel) simulated with the standard and the optimised model vs experimental data for all selected experiments (left) and corresponding values of the geometric mean bias and variance (right). Optimisation is conducted for all selected experiments together.

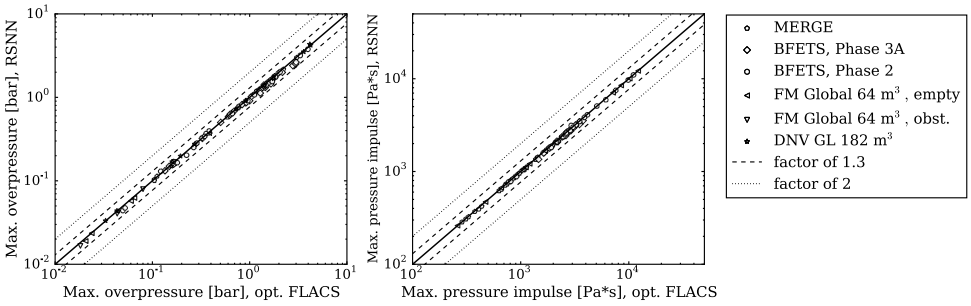

Figure C.3: Maximum overpressure (left) and maximum pressure impulse (right) simulated with the optimised model vs evaluation of the surrogates at the optimal parameter set.

rather than under-predictions, which may be preferred in the field of safety. The predictions of the maximum overpressure for the campaign MERGE are improved the most with respect to bias and scatter, see Figure C.4(a). The maximum pressure impulse is over-predicted with a factor of less than 1.3. For the BFETS Phase 3A experiments, the overall optimisation reduces slightly the scatter of the deviations from simulation

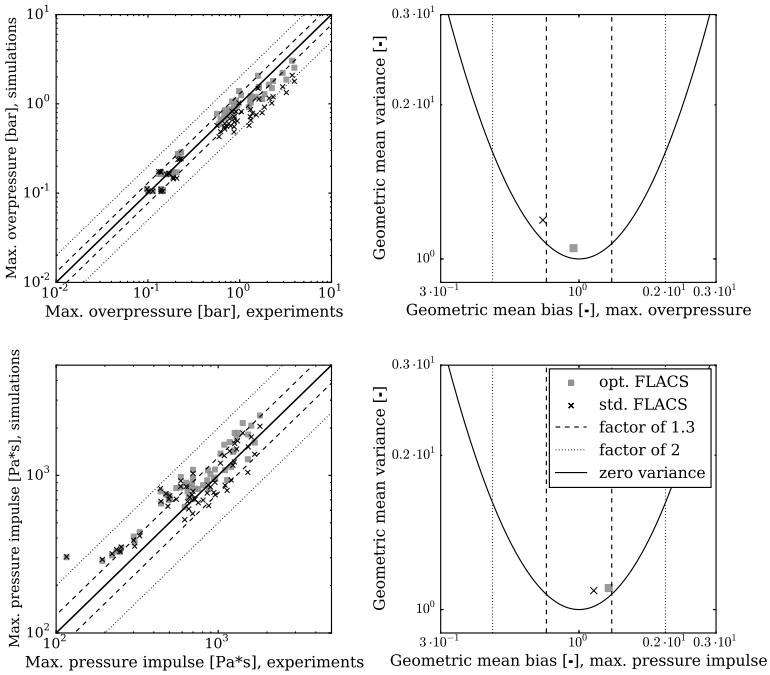

(a) MERGE

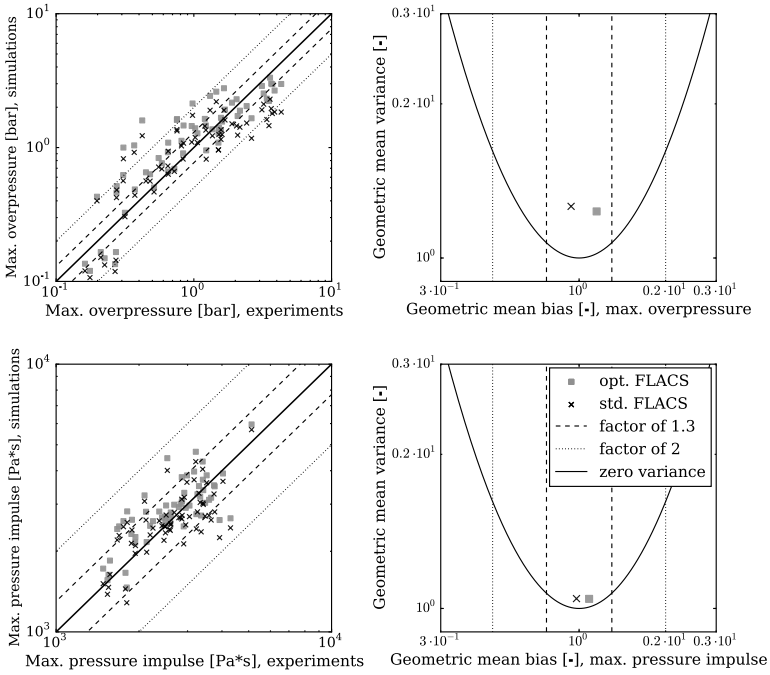

(b) BFETS Phase 3A

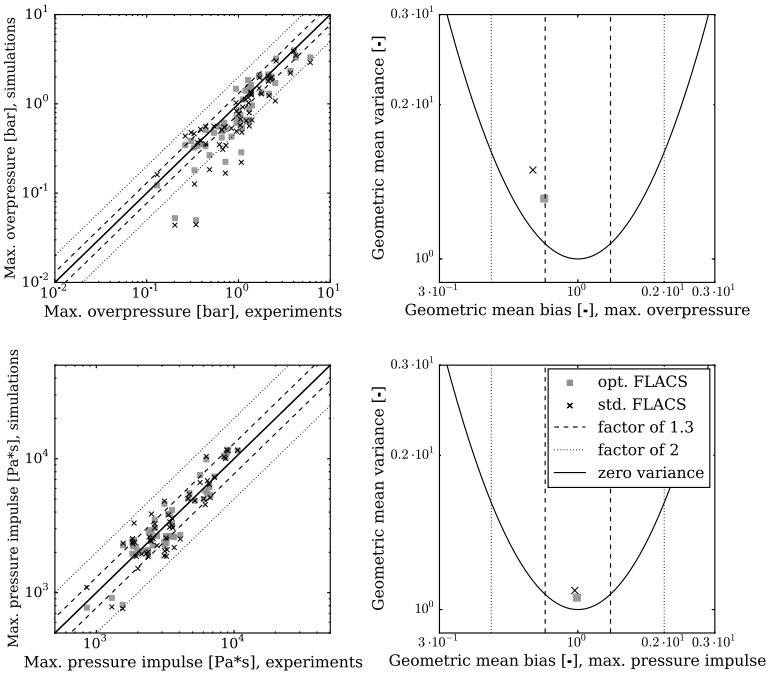

(c) BFETS Phase 2

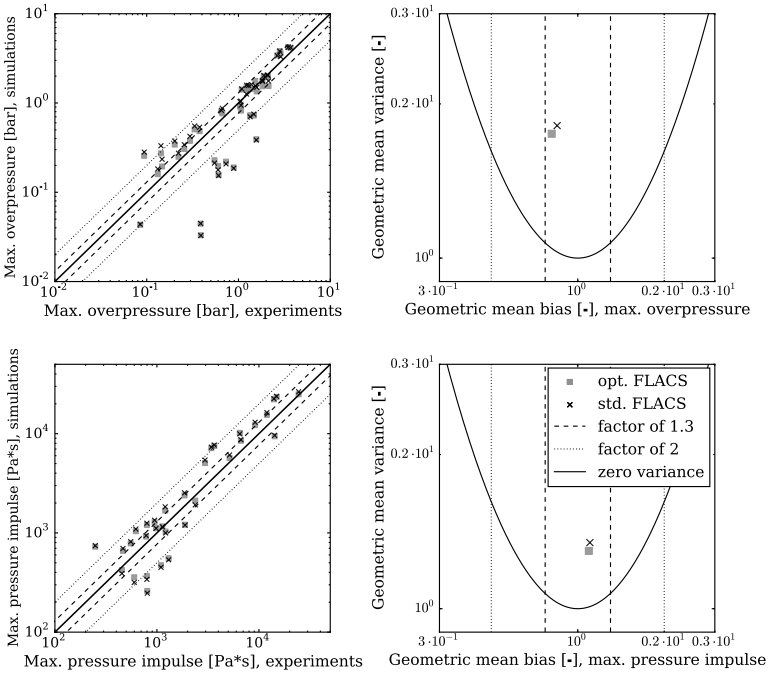

(d) DNV GL 182 m^3 vented enclosure

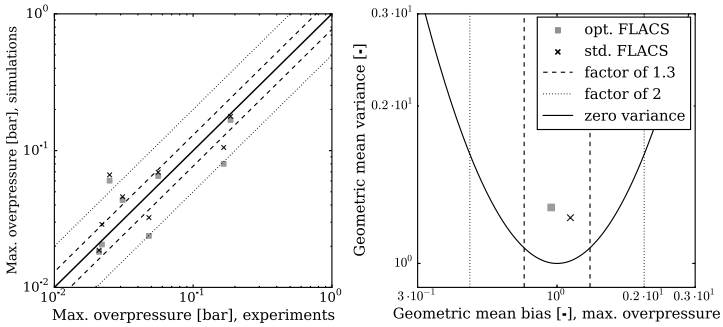

(e) FM Global 64 m^3 vented chamber

Figure C.4: Maximum overpressure (upper panel) and maximum pressure impulse (lower panel) simulated with the standard and overall optimised model vs experimental data for all experiments of the respective campaign (left) and corresponding values of the geometric mean bias and variance (right).

output to experimental data, see Figure C.4(b); the simulation output is over- instead of under-predicted. Figure C.4(c) presents the results for the BFETS Phase 2 experiments; the value of MG improves only slightly, whereas VG is reduced significantly. Figure C.4(d) visualises that the predictions for the DNV GL 182 m^3 vented enclosure tests improve only slightly through the optimisation process. The FM Global 64 m^3 vented chamber experiments pose the only campaign where the predictions deteriorate after optimisation, see Figure C.4(e).

Maximum overpressure at several monitor points across the rig

To make sure that the predicted overpressure at monitor points excluded from optimisation is not artificially high or low for the optimised model, it is analysed for several points across the module. Figures C.5(a)–(e) show the maximum overpressure for BFETS Phase 2 experiments at the lower deck for several distances from the front side. Ignition in all tests, except Test 13, occurred in the front side of the rig; in Test 13 the gas mixture was ignited in the centre. Optimisation is conducted for the monitor points at the front side, in the middle and opposite end of the rig, i.e., 25 m from the front side. The monitor points in between are neither included in the optimisation nor in the previous validation. With the optimised model, the behaviour of the maximum overpressure at several distances from the front side is captured reasonably well or even better than with the standard model for all tests, except Test 13, which is over-predicted, cf. Figure C.5(c). For Test 18 the optimised maximum overpressure is much lower than the experimental data through the rig and increases at the end, cf. Figure C.5(d). Even if optimisation is conducted exclusively for the experiments from BFETS Phase 2, the trend of the experimental data cannot be captured, cf. Figure C.5(f).

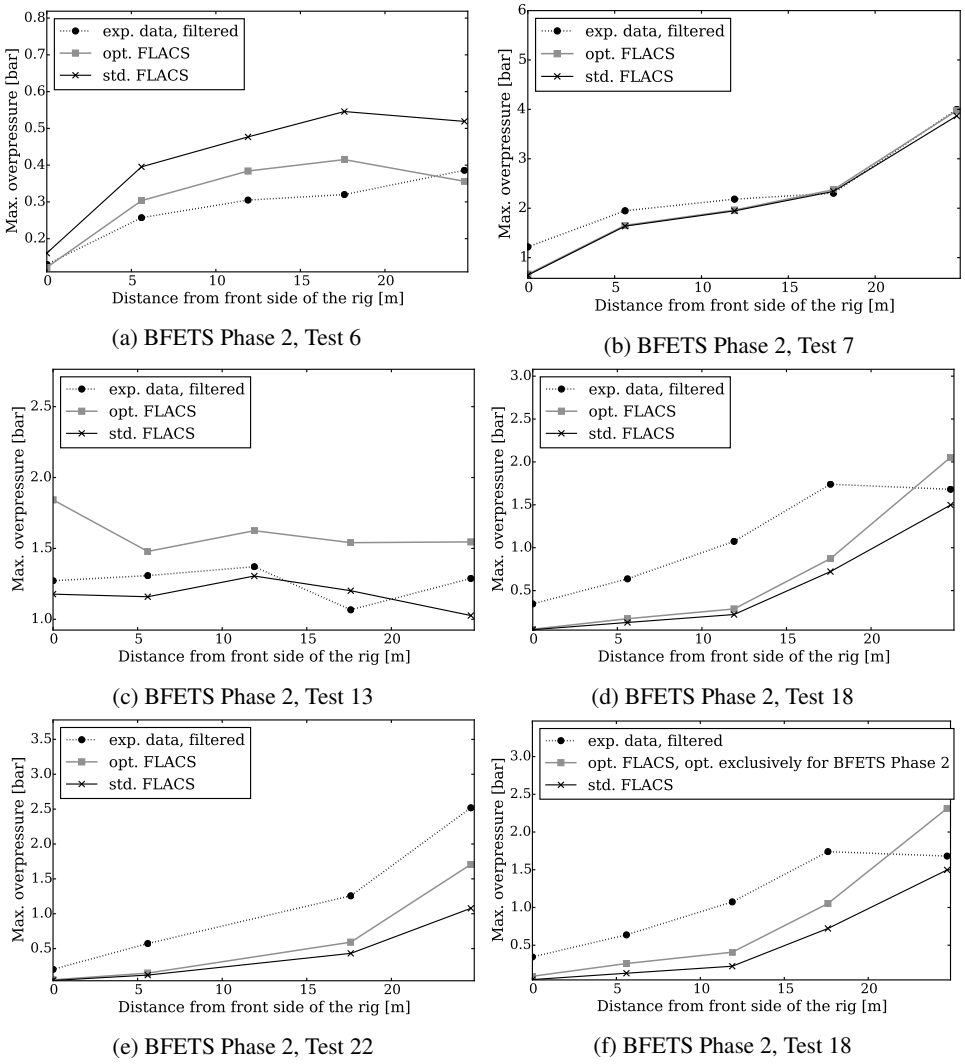

(a) BFETS Phase 2, Test 6

(b) BFETS Phase 2, Test 7

(c) BFETS Phase 2, Test 13

(d) BFETS Phase 2, Test 18

(e) BFETS Phase 2, Test 22

(f) BFETS Phase 2, Test 18

Figure C.5: Maximum overpressure at several distances from the front side of the rig for selected tests of the campaign BFETS Phase 2 simulated with the standard and overall optimised model and experimental data.

Pressure-time histories

Analysing pressure-time histories simulated with the optimised model forms a crucial part of the optimisation approach. The plots in Figure C.6 show the overpressure over time for tests of the campaign BFETS Phase 2 at monitor points 2 (black lines) and 10 (grey lines) for the standard model (solid lines), the overall optimised model (dashed lines) as well as the filtered experimental data (dotted lines). Monitor point 2 and 10 are located at the front side and the middle of the rig, respectively. Even if the pressure over time for Test 13 and Test 18 is over- and under-predicted, respectively, the shapes

of the optimised curves are reasonable. In total, the pressure-time histories of all tests are represented satisfactorily by the optimised model.

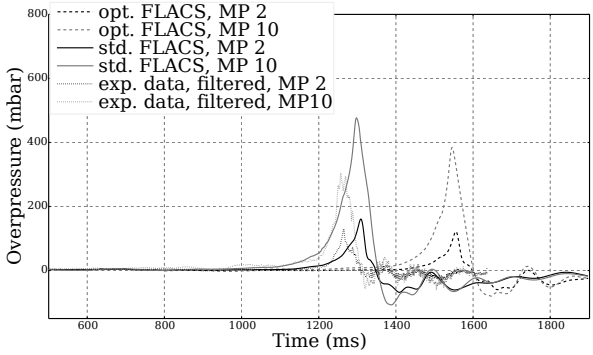

(a) BFETS Phase 2, Test 6

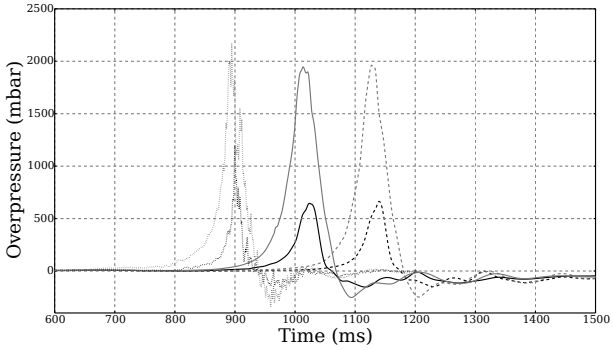

(b) BFETS Phase 2, Test 7

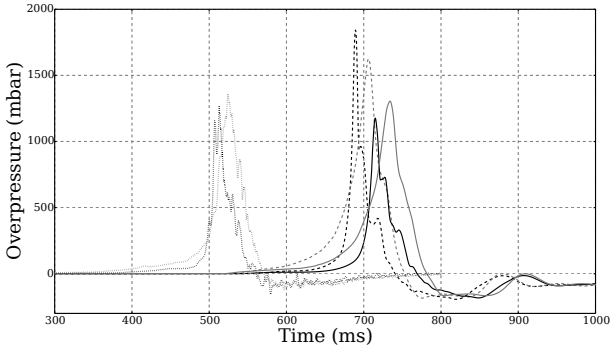

(c) BFETS Phase 2, Test 13

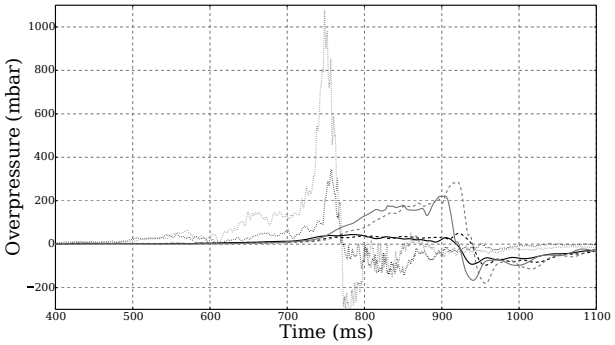

(d) BFETS Phase 2, Test 18

Figure C.6: Overpressure-time histories for selected BFETS Phase 2 experiments at monitor points 2 (black lines) and 10 (grey lines), simulated with the standard model, overall optimised model and experimental data.

C.3 The optimal parameter values

The optimal parameter values obtained from the different optimisation cases are shown in Table C.1. The parameters are named as in Paper 2. The optimal values differ significantly from each other. During the present doctoral study, it has been observed that different parameter values give similar good optimisation results. This indicates that one parameter value may be compensated by variations in other parameter values. Therefore, it is difficult to analyse the optimal parameter values to gain additional information about the model.

Table C.1: Optimal parameter values for different optimisation cases for the standard model.

Optim. case	C_o	u_l	C_{ql}	a	α	β	K_q	C_{fl}
Category 1B	0.2717	$k_0 - 0.02^*$	$0.5k_0{}^*$	0.5^{**}	1.0684	-0,373	1.2303	8.6103
Category 3B	0.3609	$k_0 + 0.02^*$	$1.1758k_0{}^*$	0.5^{**}	1.1304	-0,4	1.0^{**}	6.4779
Overall optim.	0.4278	$k_0 + 0.02^*$	$1.0731k_0{}^*$	0.5^{**}	0.9722	-0,4	1.6202	7.3738

* k_0 denotes the respective nominal, unoptimised value and is scenario-dependent.

** Parameter excluded from optimisation due to small sensitivities, default value shown.

C.4 Including outliers in the optimisation

Figure C.7 presents results for the overall optimisation including all outliers. As the outliers comprise here mainly severe under-predictions, the optimisation process is pushed to increase those model predictions – resulting in an overall over-prediction.

Figures C.7 and C.2 illustrate that the predictive capability of the optimised model is significantly worse when including the outliers in the optimisation process.

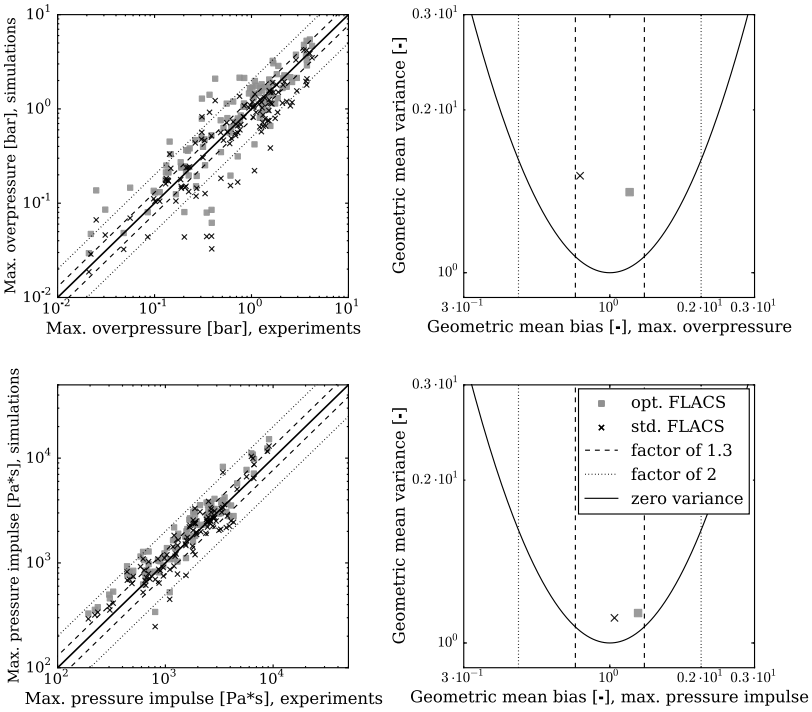

Figure C.7: Maximum overpressure (upper panel) and maximum pressure impulse (lower panel) simulated with the standard and the optimised model vs experimental data for all selected experiments (left) and corresponding values of the geometric mean bias and variance (right). Optimisation is conducted for all selected experiments together including outliers.

C.5 Conclusion

The model parameter optimisation was first conducted for selected gas explosion experiments from campaigns within certain validation categories separately. For the final application of the CFD tool, however, it is highly impractical if there exists an optimal version for each validation category. Therefore, the optimisation was second conducted for all campaigns together. Both optimisation cases result in models with a similar, satisfactory overall predictive capability, which is better than for the standard model. Thus, a detailed analysis was conducted for the overall optimised model only. Note that this analysis served exclusively checking the parameter optimisation; it is not a model validation process that is crucial to ensure that a gas explosion simulation tool can confidently be used for process safety.

For most of the campaigns, the predictions of the maximum overpressure and the pressure impulse after the overall optimisation show less deviation from the experimental data measured in terms of the geometric mean bias and variance. The analysis

comprised tests that optimisation was conducted for as well as additional tests. For the BFETS Phase 2 experiments, it was shown that the maximum overpressure at several points across the module was predicted satisfactorily after optimisation. Furthermore, the optimised model predicted pressure-time histories at relevant monitor points well – showing that the optimisation in this study is not a blind fit of the maximum overpressure and pressure impulse, but that the characteristic physical mechanisms of gas explosions are represented by the optimised model.

In total, it can be concluded that the optimisation approach can be applied to gas explosion experiments across validation categories with satisfactory results.

Appendix D

Optimising the flame folding model

This section presents detailed results from analysing a sub-grid model for flame folding around obstacles, cf. Section 5.4. In the following, the Gaps project is introduced, and results from a sensitivity analysis and the optimisation processes are presented.

D.1 The Gaps project

The Gaps project investigated so-called separation distances between two congested regions. If two regions of congestion are located close to each other, a gas explosion starting in one region may result in the same severe overpressure that is observed in a combined large congestion region. If, however, the two regions are separated by a sufficiently large gap, the overpressure of the explosion may not exceed the overpressure of a single region of congestion. To design safe process plants with congested regions, it is crucial to know about the recommended minimum distance between the regions that prevents enhanced overpressures in the case of an accidental explosion.

The Gaps project was performed within the framework of JIP MEASURE (Skjold et al., 2017). The tests were conducted by GL Noble Denton at the Spadeadam Test site in Cumbria, UK on behalf of Shell Projects and Technology. The tests involved large scale congested rigs of arrays of pipes (as the ones in the MERGE experiments, cf. Paper 3) comprising different geometric configurations with varying obstacle size, pitch between obstacles, and rig dimensions. Tests were conducted for two separated rigs as well as for single rigs. In all cases, the congested region(s) were located within a large polythene enclosure which was filled with a methane- or propane-air mixture. For the present optimisation case, only tests with a single rig (5 m $\times$ 5 m $\times$ 2.5 m) have been included. The ignition was either at the edge of the congestion or in the gas cloud outside the congestion (far field ignition). Table D.1 summarises the experimental conditions.

It is important to note that the project was performed with sponsors, and thus most of the experimental data is confidential.

D.2 Sensitivity analysis

Three parameters are connected to the flame folding model: C_{gs}, $C_{eq,lim}$, and $C_{fl,o}$; see Paper 3 for more details. First order local sensitivities $\tilde{s}_i$, cf. Paper 1, are calculated

Table D.1: Experimental configurations for selected tests of the Gaps project.

Module	Geometric layout	Fuel type	Ignition position
Rig 7	16 × 16 × 8 pipes with 76 mm diameter and 342 mm pitch	methane	at the edge of the congested region, far field ignition
Rig 8	8 × 8 × 4 pipes with 168 mm diameter and 655 mm pitch	propane	

for the maximum overpressure and maximum pressure impulse at relevant monitor points. Three out of the five selected monitor points for the Gaps project tests lie inside the rig, one at the edge, and one outside of the congested region. The positioning of the monitor points for the DNV GL 182 m^3 vented enclosure tests are described in Paper 3. Figures D.1 and D.2 show sensitivities at relevant monitor points for the DNV GL 182 m^3 vented enclosure tests with different vent opening sizes and for the selected Gaps experiments, respectively. The active parameters for the DNV GL 182 m^3 vented enclosure tests are identified as C_{gs} and $C_{eq,lim}$. Although $C_{eq,lim}$ is not active for the Gaps experiments, both parameters are optimised for all tests.

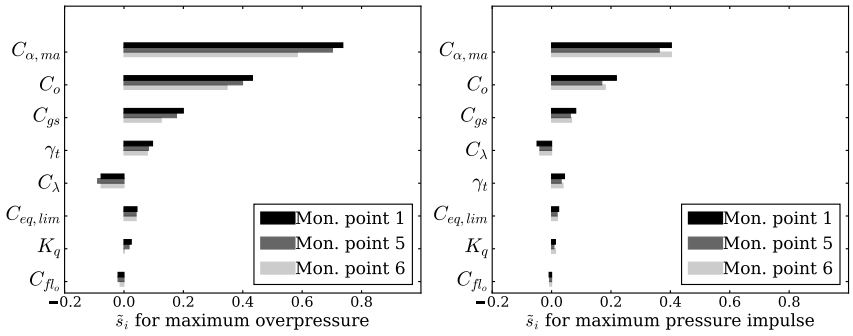

(a) Test 4

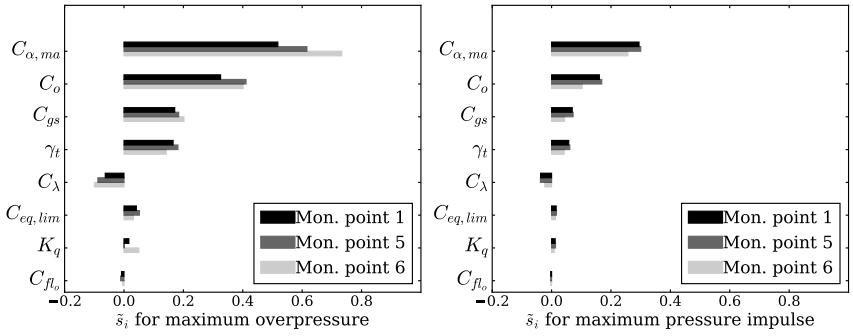

(b) Test 17

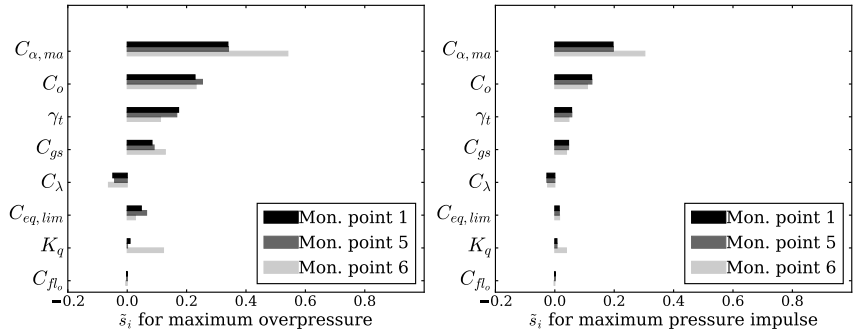

(c) Test 26

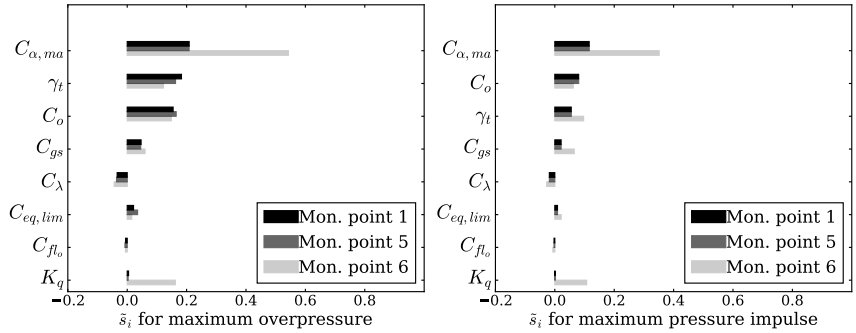

(d) Test 32

Figure D.1: First order local sensitivities of maximum overpressure (left) and maximum pressure impulse (right) for DNV GL 182 m^3 vented enclosure tests.

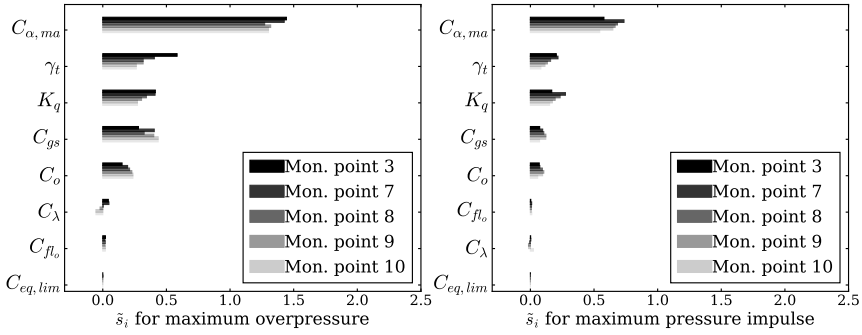

(a) Rig 7, ignition at the edge of the congested region

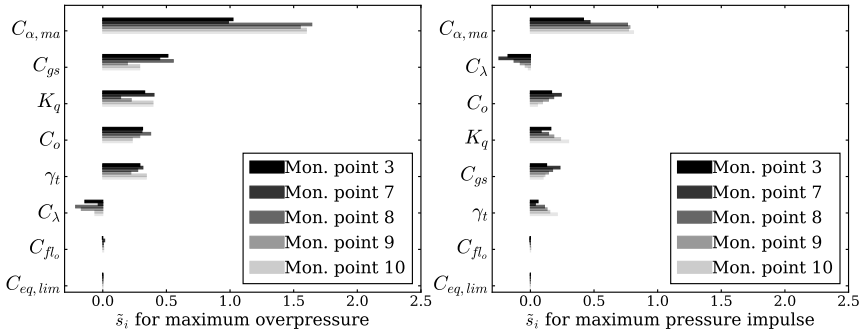

(b) Rig 7, far field ignition

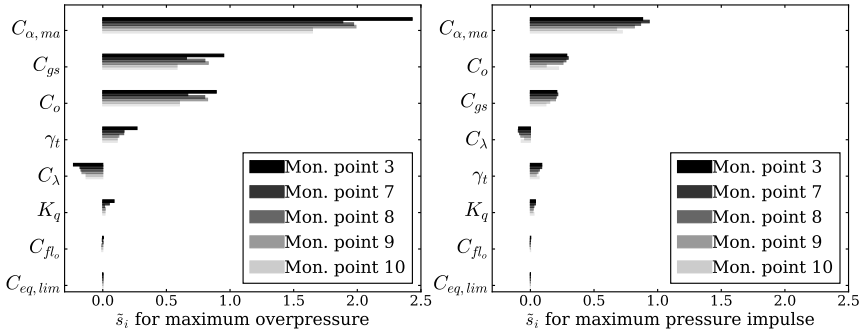

(c) Rig 8, ignition at the edge of the congested region1

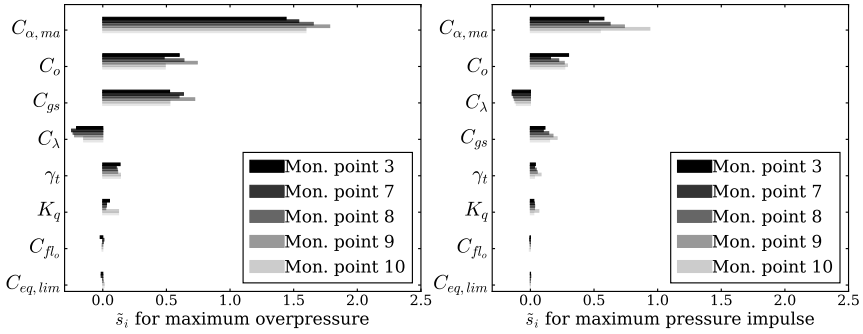

(d) Rig 8, far field ignition

Figure D.2: First order local sensitivities of maximum overpressure (left) and maximum pressure impulse (right) for Gaps project tests.

D.3 Optimal parameter values and validation results

The optimisation is conducted for the maximum overpressure and pressure impulse at the selected monitor points with respect to the active flame folding parameters. Surrogates based on neural networks are generated on the basis of 150 Latin hypercube sample points in the two-dimensional uncertainty space. Three optimisation cases are

considered: one for each campaign separately, and one for both together. The corresponding optimal parameter values, as well as the initial values, are shown in Table D.2. Note that the uncertainty ranges are transformed to the range $[-1, 1]$.

Table D.2: Optimal parameter values for different optimisation cases.

Optimisation case	C_{gs}	$C_{eq,lim}$
DNV GL 182 m^3	0.1988	-0.9711
Gaps project	0.1717	-0.9570
all tests together	0.1830	-0.9597
initial values	-1.000	-0.7154

Due to the small differences in the optimal parameter values, the predictions of the optimised models do hardly differ form each other. Figures D.3 and D.4 present validation results for the DNV GL 182 m^3 vented enclosure tests and the Gaps project tests, respectively. The dots represent the selected tests and relevant monitor points. Please note that due to confidentiality in the Gaps project, the axis values in the scatter plot of Figure D.4 are removed. Optimisation improves the predictions for both campaigns.

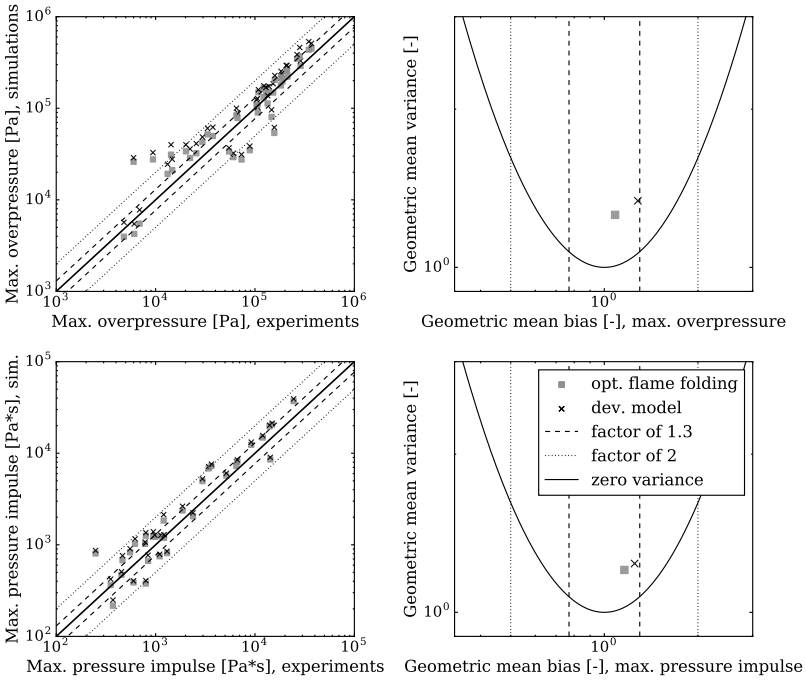

Figure D.3: DNV GL 182 m^3 vented enclosure experiments: maximum overpressure (upper panel) and maximum pressure impulse (lower panel) simulated with the dev. model and optimised model for flame folding vs experimental data (left) and corresponding values of the geometric mean bias and variance (right).

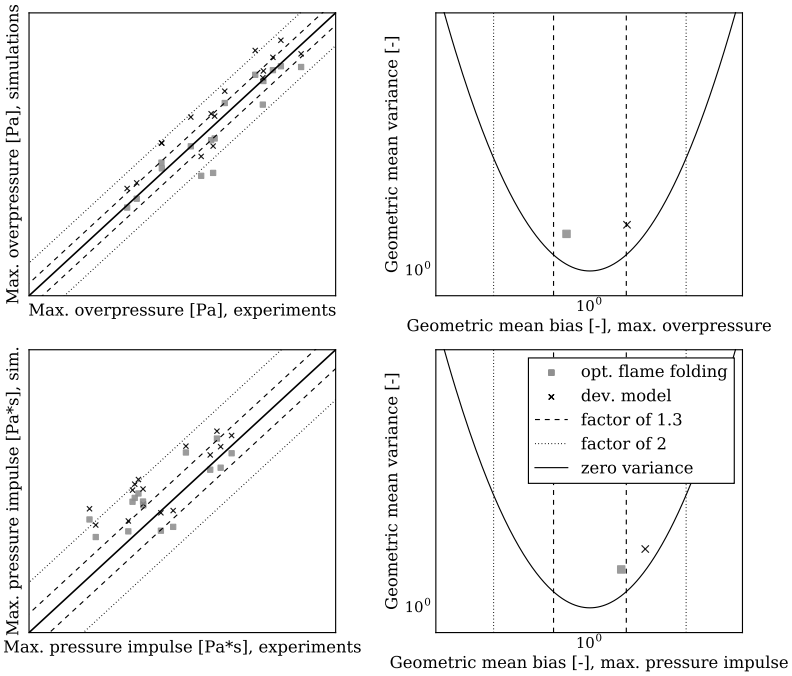

Figure D.4: Gaps project experiments: maximum overpressure (upper panel) and maximum pressure impulse (lower panel) simulated with the dev. model and optimised model for flame folding vs experimental data (left) and corresponding values of the geometric mean bias and variance (right).

Bibliography

Al-Hassan, T. and Johnson, D. M. (1998). Gas explosions in large scale offshore module geometries: overpressures, mitigation and repeatability. In *Seventeenth International Conference on Offshore Mechanics and Arctic Engineering (OMAE)*, Lisbon. 2.3.3

Alexandrov, N. M., Dennis, J. E., Lewis, R. M., and Torczon, V. (1998). A trust-region framework for managing the use of approximation models in optimization. *Structural optimization*, 15(1):16–23. 4.2

Alexandrov, N. M., Lewis, R. M., Gumbert, C. R., Green, L. L., and Newman, P. A. (2000). Optimization with variable-fidelity models applied to wing design. *38th Aerospace Sciences Meeting and Exhibit, Aerospace Sciences Meetings*. 4.1

Alexandrov, N. M., Lewis, R. M., Gumbert, C. R., Green, L. L., and Newman, P. A. (2001). Approximation and model management in aerodynamic optimization with variable-fidelity models. *Journal of Aircraft*, 38(6):1093–1101. 4.1

Aster, R. C., Borchers, B., and Thurber, C. H. (2013). *Parameter Estimation and Inverse Problems (Second Edition)*. Academic Press, Boston. 2.4, 2.4.3, 2.6, 4.4

Aven, T. (2014). *Risk, Surprises and Black Swans*. Routledge, London. 6

Bauwens, C. R. (2010). Effect of ignition location, vent size, and obstacles on vented explosion overpressures in propane-air mixtures. *Combustion Science and Technology*, 182(11–12):1915–1932. 2.3.3, 2.3.5

Boto, F., Manjarres, D., and Landa-Torres, I. (2018). Metaheuristic optimization of natural resources in thermal cracking process. In *Proceedings 6th International Conference on Engineering Optimization (EngOpt 2018)*, pages 1409–1419. Springer International Publishing. 4.1

Bradley, D., Lawes, M., Liu, K., and Mansour, M. S. (2013). Measurements and correlations of turbulent burning velocities over wide ranges of fuels and elevated pressures. *Proceedings of the Combustion Institute*, 34(1):1519–1526. 1.2, 1.3

Bradley, D., Lawes, M., and Mansour, M. S. (2011a). Measurement of turbulent burning velocities in implosions at high pressures. *Proceedings of the Combustion Institute*, 33(1):1269–1275. 1.2, 1.3

Bradley, D., Lawes, M., and Mansour, M. S. (2011b). The problems of the turbulent burning velocity. *Flow, Turbulence and Combustion*, 87(2):191–204. 1.3

Cant, R. S., Dawes, W. N., and Savill, A. M. (2004). Advanced CFD and modeling of accidental explosions. *Annual Review of Fluid Mechanics*, 36(1):97–119. 1.1, 1.2, 1.4

Castelletti, A., Pianosi, F., Soncini-Sessa, R., and Antenucci, J. P. (2010). A multiobjective response surface approach for improved water quality planning in lakes and reservoirs. *Water Resources Research*, 46(6). 16 pages. 1.4

Chao, J., Bauwens, C. R., and Dorofeev, S. B. (2011). An analysis of peak overpressures in vented gaseous explosions. *Proceedings of the Combustion Institute*, 33(2):2367–2374. 2.3.3

Chen, V. C. P., Tsui, K.-L., Barton, R. R., and Meckesheimer, M. (2006). A review on design, modeling and applications of computer experiments. *IIE Transactions*, 38(4):273–291. 3.1, 3.2

Chen, W., Wiecek, M. M., and Zhang, J. (1999). Quality utility – a compromise programming approach to robust design. *Journal of Mechanical Design*, 121:179–187. 2.5

Ciccarelli, G. and Dorofeev, S. (2008). Flame acceleration and transition to detonation in ducts. *Progress in Energy and Combustion Science*, 34(4):499–550. 1.3

Coffey, C., Gibson, R., and Christon, M. (2019). Uncertainty in explosion risk assessment. *Accepted for Hazards29 conference in Birmingham, UK, 2019*. 6

Coleman, T. and Li, Y. (1996a). A reflective newton method for minimizing a quadratic function subject to bounds on some of the variables. *SIAM Journal on Optimization*, 6(4):1040–1058. B, B.2

Coleman, T. F. and Li, Y. (1996b). An interior trust region approach for nonlinear minimization subject to bounds. *SIAM Journal on Optimization*, 6:418–445. 1.5, B, B.2, B.2, B.2

Cordero, R. R., Seckmeyer, G., and Labbe, F. (2007). Evaluating the uncertainties of data rendered by computational models. *Metrologia*, 44(3):L23–L30. 6

Davis, S. D., Mhadeshwar, A. B., Vlachos, D. G., and Wang, H. (2004). A new approach to response surface development for detailed gas-phase and surface reaction kinetic model optimization. *International Journal of Chemical Kinetics*, 36:94–106. 3.2, 4.1

Duijm, N. J. and Carissimo, B. (2002). Evaluation methodologies for dense gas dispersion models. In Fingas, M., editor, *The handbook of hazardous materials spills technology*. McGraw-Hill. 2.4.2

Edeling, W., Cinnella, P., Dwight, R., and Bijl, H. (2014). Bayesian estimates of parameter variability in the k–ε turbulence model. *Journal of Computational Physics*, 258:73–94. 1.4

Evans, J. A., Exon, R., and Johnson, D. M. (1999). *The Repeatability of Large Scale Explosion Experiments*. Offshore technology report. Great Britain, Health and Safety Executive. Available at www.hse.gov.uk/research/otopdf/1999/oto99042.pdf, accessed 04 April 2019. 2.3.3, 2.3.5

Feyen, L., Vrugt, J. A., Nualláin, B. O., van der Knijff, J., and De Roo, A. (2007). Parameter optimisation and uncertainty assessment for large-scale streamflow simulation with the lisflood model. *Journal of Hydrology*, 332(3):276–289. 1.4

Foisselon, P., Hansen, O. R., and van Wingerden, K. (1998). Detailed analysis of FLACS performance in comparison to full-scale experiments. CMR report no. CMR-98-F30058, Chr. Michelsen Research, Bergen, Norway. 2.3.3

Forrester, A. I. J., Bressloff, N. W., and Keane, A. J. (2006). Optimization using surrogate models and partially converged computational fluid dynamics simulations. *Proceedings of the Royal Society of London A: Mathematical, Physical and Engineering Sciences*, 462(2071):2177–2204. 1.4

Forrester, A. I. J. and Keane, A. J. (2009). Recent advances in surrogate-based optimization. *Progress in Aerospace Sciences*, 45(1–3):50–79. 3, 3.1, 4.2

Gexcon AS (2019). FLACS v10.9 User's Manual. Technical report, Gexcon AS, Bergen, Norway. Information at www.flacs.com. 1.1, 2.3.4

Goel, T., Haftka, R. T., Shyy, W., and Queipo, N. V. (2007). Ensemble of surrogates. *Structural and Multidisciplinary Optimization*, 33(3):199–216. 3.1

Gong, W., Duan, Q., Li, J., Wang, C., Di, Z., Dai, Y., Ye, A., and Miao, C. (2015). Multi-objective parameter optimization of common land model using adaptive surrogate modeling. *Hydrology and Earth System Sciences*, 19(5):2409–2425. 3.1, 4.1

Gorissen, D. (2010). *Grid-enabled adaptive surrogate modeling for computer aided engineering*. PhD thesis, Ghent University (Belgium). AAI3416412. 3.1, 3.2

Guillas, S., Glover, N., and Malki-Epshtein, L. (2014). Bayesian calibration of the constants of the k–ε turbulence model for a CFD model of street canyon flow. *Computer Methods in Applied Mechanics and Engineering*, 279:536–553. 1.4

Guitton, A. and Symes, W. W. (2003). Robust inversion of seismic data using the huber norm. *Geophysics*, 68(4):1310–1319. 2.6

Hanna, S. R., Chang, J. C., and Strimaitis, D. G. (1993a). Hazardous gas model evaluation with field observations. *Atmospheric Environment. Part A. General Topics*, 27(15):2265–2285. 2.4.2

Hanna, S. R., Strimaitis, D. G., and Chang, J. C. (1993b). Hazard response modeling uncertainty (a quantitative method). Volume 2. Evaluation of commonly used hazardous gas dispersion models. Technical report. 2.4.2

Hisken, H., Enstad, G., Middha, P., and van Wingerden, K. (2015). Investigation of concentration effects on the flame acceleration in vented channels. *Journal of Loss Prevention in the Process Industries*, 36:447–459. 2.3.4

Hjertager, B. H. (1984). Influence of turbulence on gas explosions. *Journal of Hazardous Materials*, 9(3):315–346. 1.1

Hjertager, B. H. (1986). Three-dimensional modeling of flow, heat transfer, and combustion. In *Handbook of Heat and Mass Transfer*, chapter 41, pages 1303–1350. Gulf Publishing, Houston. 1.1

Hornik, K., Stinchcombe, M., and White, H. (1989). Multilayer feedforward networks are universal approximators. *Neural Networks*, 2(5):359–366. 3.2

Huang, N. and Li, Z. (2018). Hydraulic design and optimization of a lng hydraulic turbine runner. In *Proceedings 6th International Conference on Engineering Optimization (EngOpt 2018)*, pages 115–121. Springer International Publishing. 1.4

Huber, P. J. (1964). Robust estimation of a location parameter. *The Annals of Mathematical Statistics*, 35(1):73–101. 2.6

Iuliano, E. (2016). Adaptive sampling strategies for surrogate-based aerodynamic optimization. In Iuliano, E. and Pérez, E. A., editors, *Application of Surrogate-based Global Optimization to Aerodynamic Design*, pages 25–46. Springer International Publishing, Cham. 4.2

Jones, D. R., Schonlau, M., and Welch, W. J. (1998). Efficient global optimization of expensive black-box functions. *Journal of Global Optimization*, 13(4):455–492. 4.2

Kennedy, M. C. and O'Hagan, A. (2001). Bayesian calibration of computer models. *Journal of the Royal Statistical Society B*, 63:425–464. 1.4

Koski, J. and Silvennoinen, R. (1987). Norm methods and partial weighting in multicriterion optimization of structures. *International Journl for Numererical Methods in Engineering*, 24:1101–1121. 2.5

Leshno, M., Lin, V. Y., Pinkus, A., and Schocken, S. (1993). Multilayer feedforward networks with a nonpolynomial activation function can approximate any function. *Neural Networks*, 6(6):861–867. 3.2

Lind, C. D. and Whitson, J. C. (1977). Explosion hazards associated with spills of large quantities of hazardous materials: Phase 2. Technical report. Report No. CG-D-85-77. 2.3.4

Loshchilov, I., Schoenauer, M., and Sebag, M. (2010). Comparison-based optimizers need comparison-based surrogates. In *Proceedings of the 11th International Conference on Parallel Problem Solving from Nature: Part I*, PPSN'10, pages 364–373, Berlin, Heidelberg. Springer-Verlag. 4.1

Marler, R. T. and Arora, J. S. (2004). Survey of multi-objective optimization methods for engineering. *Structural and Multidisciplinary Optimization*, 26:369–395. 2.5

Marler, R. T. and Arora, J. S. (2005). Function-transformation methods for multi-objective optimization. *Engineering Optimization*, 37(6):551–570. 2.5

Marler, R. T. and Arora, J. S. (2010). The weighted sum method for multi-objective optimization: new insights. *Structural and Multidisciplinary Optimization*, 41(6):853–862. 2.5

Mazet, V., Carteret, C., Brie, D., Idier, J., and Humbert, B. (2005). Background removal from spectra by designing and minimising a non-quadratic cost function. *Chemometrics and Intelligent Laboratory Systems*, 76(2):121–133. 2.6

McGrattan, K. and Toman, B. (2011). Quantifying the predictive uncertainty of complex numerical models. *Metrologia*, 48(3):173–180. 6

McKay, M. D., Beckman, R. J., and Conover, W. J. (1979). A comparison of three methods for selecting values of input variables in the analysis of output from a computer code. *Technometrics*, 21(2):239–245. A

Mercx, W. P. M. (1994). Modelling and Experimental Research into Gas Explosions. Overall final report for the MERGE project. CEC contract STEP-CT-0111 (SMA). 2.3.3

Model Evaluation Group Gas Explosions (MEGGE) (1996). Gas explosion model evaluation protocol. Technical report, version 1, EuropeanCommunities, Directorate-General XII, Science Research and Development. 2.4.2

Moré, J. J. and Sorensen, D. C. (1983). Computing a trust region step. *SIAM Journal on Scientific and Statistical Computing*, 4:553–572. B.1

Morgut, M. and Nobile, E. (2012). Numerical predictions of cavitating flow around model scale propellers by CFD and advanced model calibration. *International Journal of Rotating Machinery*. 11 pages. 1.4

Neelin, J. D., Bracco, A., Luo, H., McWilliams, J. C., and Meyerson, J. E. (2010). Considerations for parameter optimization and sensitivity in climate models. *Proceedings of the National Academy of Sciences*, 107(50):21349–21354. 4.1

Nocedal, J. and Wright, S. J. (2006). *Numerical Optimization*. Springer, New York, 2nd edition. 4.2, B.1, B.1, B.1

Pan, F. and Zhu, P. (2011). Design optimisation of vehicle roof structures: benefits of using multiple surrogates. *International Journal of Crashworthiness*, 16(1):85–95. 3.1

Pan, I., Babaei, M., Korre, A., and Durucan, S. (2014). Artificial neural network based surrogate modelling for multi- objective optimisation of geological CO_2 storage operations. *Energy Procedia*, 63:3483–3491. 3.2

Patankar, S. V. and Spalding, D. B. (1974). A calculation procedure for the transient and steady-state behavior of shell-and-tube heat exchangers. In Afgan, N. F. and Schlunder, E. U., editors, *Heat Exchangers: Design and Theory Sourcebook*, pages 155–176. McGraw-Hill, New York. 1.1

Pilát, M. and Neruda, R. (2013). Surrogate model selection for evolutionary multiobjective optimization. In *2013 IEEE Congress on Evolutionary Computation*, pages 1860–1867. 4.1

Poethke, B., Völker, S., and Vogeler, K. (2018). Aerodynamic optimization of turbine airfoils using multi-fidelity surrogate models. In *Proceedings 6th International Conference on Engineering Optimization (EngOpt 2018)*, pages 556–568. Springer International Publishing. 4.1

Popat, N. R., Catlin, C. A., Arntzen, B. J., Lindstedt, R. P., Hjertager, B. H., Solberg, T., Saeter, O., and Van den Berg, A. C. (1996). Investigations to improve and assess the accuracy of computational fluid dynamic based explosion models. *Journal of Hazardous Materials*, 45(1):1–25. 2.3.3

Queipo, N. V., Haftka, R. T., Shyy, W., Goel, T., Vaidyanathan, R., and Tucker, P. K. (2005). Surrogate-based analysis and optimization. *Progress in aerospace sciences*, 41(1):1–28. 1.4, 3, 3.1, 4.1, 4.2

Razavi, S., Tolson, B. A., and Burn, D. H. (2012). Review of surrogate modeling in water resources. *Water Resour. Res.*, 48,W7401. 3.1

Rieder, A. (2003). *Keine Probleme mit Inversen Problemen*. Vieweg, Wiesbaden. 4.4

Saltelli, A., Ratto, M., Andres, T., Campolongo, F., Cariboni, J., Gatelli, D., Saisana, M., and Tarantola, S. (2008). *Global Sensitivity Analysis. The Primer*. John Wiley & Sons, Ltd. 2.1

Sant Anna, H. R., Barreto, A. G., Tavares, F. W., and de Souza, M. B. (2017). Machine learning model and optimization of a PSA unit for methane-nitrogen separation. *Computers & Chemical Engineering*, 104:377–391. 3.2

Savitzky, A. and Golay, M. J. E. (1964). Smoothing and differentiation of data by simplified least squares procedures. *Analytical Chemistry*, 36(8):1627–1639. 5.3.1, C.1

Sha, W. T., Yang, C. I., Kao, T. T., and Cho, S. M. (1982). Multidimensional numerical modeling of heat exchangers. *Journal of Heat Transfer*, 104(3):417–425. 1.1

Simpson, T., Toropov, V., Balabanov, V., and Viana, F. (2008). Design and analysis of computer experiments in multidisciplinary design optimization: A review of how far we have come – or not. In *12th AIAA/ISSMO Multidisciplinary Analysis and Optimization Conference, Multidisciplinary Analysis Optimization Conferences*, Victoria, British Columbia Canada. 22 pages. 3.1

Simpson, T. W., Mauery, T. M., Korte, J. J., and Mistree, F. (2001a). Kriging models for global approximation in simulation-based multidisciplinary design optimization. *AIAA Journal*, 39(12):2233–2241. 3.1

Simpson, T. W., Poplinski, J. D., Koch, N. P., and Allen, J. K. (2001b). Metamodels for computer-based engineering design: Survey and recommendations. *Engineering with Computers*, 17(2):129–150. 3.1, 3.2

Skjold, T., Hisken, H., Atanga, G., Narasimhamurthy, V. D., Lakshmipathy, S., Storvik, I. E., Pesch, L., and Braatz, A.-L. (2017). Modelling Escalating Accident Scenarios and the Use of Risk-reducing technology for Explosion safety (MEASURE), final report. Confidential. Technical report, Gexcon AS, Bergen, Norway. 2.3.4, D.1

Skjold, T., Pedersen, H. H., Bernard, L., Ichard, M., Middha, P., Narasimhamurthy, V. D., Landvik, T., Lea, T., and Pesch, L. (2013). A matter of life and death: validating, qualifying and documenting models for simulating flow-related accident scenarios in the process industry. *Chemical Engineering Transactions*, 31:187–192. 2.3, 2.3.3

Skjold, T., Pedersen, H. H., Narasimhamurthy, V. D., Lakshmipathy, S., Pesch, L., Atanga, G. F., Folusiak, M., Bernard, L., Siccama, D., and Storvik, I. E. (2014). Pragmatic modelling of industrial explosions in complex geometries: review of the state-of-the-art and prospects for the future. In Borisov, A. A. and Frolov, S. M., editors, *Zel'dovich Memorial: Accomplishments in the combustion Science in the last decade*, volume 1, pages 70–74. Torus Press, Moscow. 1.1

Skjold, T., Souprayen, C., and Dorofeev, S. (2018). Fires and explosions. *Progress in Energy and Combustion Science*, 64:2–3. 1.1

The MathWorks, Inc. (2015). MATLAB 2015b, Natick. 1.5

The MathWorks Inc. (2017). *MATLAB Optimization Toolbox: User's Guide*. The MathWorks, Natick, MA. Available at http://se.mathworks.com/help/pdf_ doc/optim/optim_ tb.pdf, accessed 04 April 2019. 4.3, B

Tomlin, G., Johnson, D. M., Cronin, P., Phylaktou, H. N., and Andrews, G. E. (2015). The effect of vent size and congestion in large-scale vented natural gas/air explosions. *Journal of Loss Prevention in the Process Industries*, 35:169–181. 2.3.3

Viana, F. A. C. (2011). *Multiple surrogates for prediction and optimization*. PhD thesis, University of Florida. 3.1

Wang, G. G. and Shan, S. (2006). Review of metamodeling techniques in support of engineering design optimization. *Journal of Mechanical Design*, 129(4):370–380. 3.1

Warnatz, J., Maas, U., and Dibble, R. W. (1996). *Combustion: physical and chemical fundamentals, modelling and simulation, experiments, pollutant formation*. Springer, Berlin. 1.1

Zhang, X., Srinivasan, R., and Van Liew, M. (2009). Approximating SWAT model using artificial neural network and support vector machine. *Journal of the American Water Resources Association (JAWRA)*, 45(2):460–474. 3.1

Papers

This chapter contains the four papers of this dissertation.

Paper 1

Response Surfaces for Advanced Consequence Models: Two Approaches

Braatz, A.-L. & Hisken, H.

Journal of Loss Prevention in the Process Industries, **49**, Part B: 683–699. (2017).

Journal of Loss Prevention in the Process Industries 49 (2017) 683–699

Contents lists available at ScienceDirect

Journal of Loss Prevention in the Process Industries

journal homepage: www.elsevier.com/locate/jlp

Response surfaces for advanced consequence models: Two approaches

Anna-Lena Braatz [a, b, *], Helene Hisken [a, c]

[a] Gexcon AS, R&D, P.O. Box 6015, 5892 Bergen, Norway
[b] Department of Informatics, University of Bergen, P.O. Box 7803, 5020 Bergen, Norway
[c] Department of Physics and Technology, University of Bergen, Allgaten 55, 5007 Bergen, Norway

ARTICLE INFO

Article history:
Received 28 October 2016
Received in revised form
19 January 2017
Accepted 12 February 2017
Available online 16 February 2017

Keywords:
Response surfaces
Neural networks
Sensitivities
CFD modelling
Gas explosions
Optimisation

ABSTRACT

This paper reports the approximation quality of response surfaces as metamodels for key results from computational fluid dynamics (CFD) gas explosion simulations. The response surfaces constitute smooth approximations to variations in the CFD output with respect to perturbing empirically determined sub-grid model parameters. Two response surface approaches are tested – polynomial response surfaces (PRSs) created from Taylor polynomials via finite differences of the model output, and response surfaces based on neural networks (RSNNs) generated on the basis of Latin hypercube samplings. First, results for selected examples of medium- and large-scale gas explosions are presented in detail. It was found that in order to achieve the same approximation quality with RSNNs as with PRSs, a higher number of simulations may be required. However, in contrast to the polynomial approach, the number of simulations required for an RSNN can be adapted to the non-linearity of the model output. For the scenarios for which a PRS approximates the model output poorly, an RSNN built from an increased number of simulations is found to yield a significantly more reliable approximation. Second, the paper investigates the general applicability of the RSNNs for industrial-scale gas explosion simulations. Based on the results from the detailed analysis, the extended analysis is only conducted for the RSNN approach, including 37 experiments from 5 experimental campaigns commonly used for model validation.

1. Introduction

Accidental gas explosions pose a severe hazard in industry – 11 of the 20 largest accidents in the hydrocarbon industries from 1972 to 2013 involved gas and vapour cloud explosions (Marsh, 2014). The process industries undertake considerable efforts to manage the risk of accidental explosions, and consequence analysis of accident scenarios is part of the overall risk analysis (Aven and Vinnem, 2007). To predict the consequences of an explosion, a computational fluid dynamics (CFD) simulation tool that solves the time-dependent averaged Navier-Stokes equations for compressible fluid flow is often used. Due to limitations in practical simulation time and memory storage, the grid resolution needs to be significantly larger than the scales on which chemical reactions interact with the flow. Turbulence, as well as other governing physical phenomena on scales smaller than grid cell size are inherently under-resolved. The success of CFD tools for estimating explosion loads in large-scale geometries consequently relies on the implementation of sub-grid models to ensure representative solutions (Skjold et al., 2014). Sub-grid models are less fundamental than the Navier-Stokes equations and contain model parameters estimated through theoretical or, more frequently, experimental studies. Consequently, uncertainty is associated with the values of the parameters.

The output of a CFD tool, referred to as the model response, can be seen as a function of a given parameter set, which may consist of user-defined input or model parameters. Even for coarse grids, CFD simulations typically require a (single-core) CPU time ranging from a few minutes up to several hours. Hence, model response evaluation via direct simulation is time consuming. For some applications it is therefore convenient not to work with the model directly, but to approximate the model response by an explicit function of the parameter set, called a response surface. Evaluation of such a function is cheap (order of seconds or less) and if appropriate, sufficiently accurate.

In engineering in general, response surfaces as metamodels, i.e.

* Corresponding author. Gexcon AS, R&D, P.O. Box 6015, 5892 Bergen, Norway.
E-mail address: anna-lena.braatz@gexcon.com (A.-L. Braatz).

http://dx.doi.org/10.1016/j.jlp.2017.02.007
0950-4230/

models of models, find application in various fields like optimisation, uncertainty quantification, reliability analysis and model-based prediction (Rutherford et al., 2006). The response surface approaches comprise amongst others Gaussian processes and kriging, radial basis functions, non-parametric regression, multivariate adaptive regression splines, polynomial response surfaces and neural networks (Rutherford et al., 2006; Simpson et al., 2004). Response surface approaches are widely used in the field of risk analysis. Response surfaces may constitute the functional relationship between the size of a flammable gas cloud and the most important dependent user-defined inputs, e.g. leak rate or wind direction. In risk analysis, when performing Monte Carlo simulations with millions of scenarios, the use of a response surface instead of the model response obtained from simulations directly significantly reduces computational cost (Huser and Kvernvold, 2000; Ferreira and Vianna, 2014). Vianna and Cant (2012) employ response surfaces in a conceptual engineering design phase for a fast evaluation of the maximum explosion pressure as function of explosive cloud size and ignition location.

The present study constitutes the starting point for optimisation of sub-grid model parameters to improve the predictive capabilities of the CFD tool FLACS for simulating gas explosions (Gexcon AS, 2015). The optimisation problem can be formulated as a least-squares problem to find the best fit between certain model responses and corresponding experimental values. Optimising this problem directly requires numerous CFD simulations. In contrast, if the model responses have been replaced by response surfaces, no simulations are needed during optimisation, accelerating the evaluation of the least-squares function and hence the optimisation process significantly (Braatz et al., 2016).

In this work, response surfaces to model responses of gas explosions with respect to empirically determined sub-grid model parameters are generated and validated against the CFD model. Sensitivity analysis is applied to determine which model parameters have the greatest influence on the model output (Saltelli et al., 2008). This allows for reducing the amount of parameters the response surfaces depend on. Two response surface approaches are tested – (i) polynomial response surfaces (PRSs) created from Taylor polynomials via finite differences of the model output and (ii) response surfaces based on artificial neural networks (RSNNs) generated on the basis of Latin hypercube samplings. The analysis of the resulting approximations of both approaches is twofold. First, the response surfaces are validated in detail against two experimental campaigns with medium- and large-scale geometries – the projects Modelling and Experimental Research into Gas Explosions (MERGE) (Mercx, 1994; Popat et al., 1996), and Blast and Fire Engineering for Topside Structures (BFETS), Phase 3A (Al-Hassan and Johnson, 1998; Evans et al., 1999; Foisselon et al., 1998). Results are evaluated with respect to approximation quality and computational costs, i.e. the amount of simulations required to generate the response surfaces. Second, an extended analysis is conducted for the RSNN approach, as the approximation quality of the RSNNs is found to outperform the one of the PRSs in the detailed analysis. The general applicability of the RSNNs for industrial-scale explosions is investigated by validation for 37 experiments from 5 experimental campaigns providing highly relevant validation data for premixed combustion modelling.

It is important to note that in the present study, response surfaces are generated for parameters that affect the way physical phenomena are represented by the model. To our knowledge, response surfaces for CFD output as a function of model parameter perturbations have not yet been studied for industrial-scale gas explosions.

The paper is structured as follows. In Section 2, key sub-grid model parameters are introduced. In Section 3, sensitivity analysis, the polynomial response surface (PRS) approach and response surfaces based on neural networks (RSNN) are formulated. In Section 4, the experimental campaigns used to validate the response surfaces are described. Validation results for the detailed and extended analysis are presented in Section 5. Finally, concluding remarks are given in Section 6.

2. Model system and parameters

2.1. General overview

The CFD tool FLACS (Gexcon AS, 2015) solves the three-dimensional Favre-averaged conservation equations for mass, momentum, enthalpy h, mass-fraction of fuel Y_f, mixture-fraction ξ, turbulent kinetic energy k, and rate of dissipation of turbulent kinetic energy ε on a structured Cartesian grid. Turbulence is modelled by the 'standard' $k-\varepsilon$ model for turbulence (Launder and Spalding, 1974). The equations are closed by invoking the ideal gas equation of state. Boundary layers are not resolved, instead wall-functions are used to compute turbulence production and drag forces for objects that are on-grid, i.e. larger than the size of a computational cell. Each three-dimensional grid cell represents a control volume with volume V_{cv} and surface area A_{cv}. Geometry is represented on the computational grid using the porosity/distributed resistance (PDR) concept (Patankar and Spalding, 1974; Sha and Launder, 1979; Sha et al., 1982; Hjertager, 1986). A volume porosity β_v, denoting the ratio of open volume to the total volume of each computational cell, is computed prior to the simulation. Similarly, the area porosity β_j is defined as the ratio of the projected unoccupied area between two neighbouring cell centres to the total area of the respective control volume face in the jth direction. In the following, β_j is excluded from the Einstein summation convention in the partial differential equations.

Using the finite volume approach, the conservation equation for a general variable Φ (representing either 1, u_j, h, k, ε, Y_f or ξ) is integrated over the porous part of the control volume. The flux terms in the conservation equation for Φ are weighted with the area porosity β_j. The general equation on integral form reads

$$\int_{V_{cv}} \frac{\partial}{\partial t}(\beta_v \rho \Phi) dV + \int_{A_{cv}} n_j \left(\beta_j \rho \Phi u_j\right) dA = \int_{A_{cv}} n_j \left(\beta_j \Gamma_\Phi \frac{\partial \Phi}{\partial x_j}\right) + \int_{V_{cv}} \beta_v (S_\Phi + R_\Phi) dV, \quad (1)$$

where ρ is the fluid density, u_j is the fluid velocity in the jth direction, n_j is the vector normal to the control volume surface pointing outwards in the jth direction, Γ_Φ is the effective turbulence diffusion coefficient, S_Φ is the source term for Φ, and R_Φ represents additional resistance, additional mixing and/or additional heat transfer caused by solid obstructions in the flow. Sub-grid models are applied for modelling the terms S_Φ and R_Φ (cf. Hjertager, 1982, 1986).

Table 1 summarises the sub-grid model parameters investigated in the present study. The parameters are related to turbulence generation and premixed combustion. The table includes brief descriptions of the sub-grid model process, references to the sub-grid models associated with the parameters and the parameters' uncertainty intervals within which the parameter values may vary. A detailed description of the parameters and the corresponding sub-grid models can be found in Appendix A. The uncertainty intervals of the parameters are based both on previous experience and an extensive literature review. Although the sub-grid model

Table 1
Model parameters investigated for model responses of gas explosion simulations.

Parameter	Description of the model process	Reference	Uncertainty range
C_o	Turbulence production from sub-grid objects	Eq. (A.4)	[0.25, 1.0]
u_l	Laminar burning velocity	Appendix A.3	$[0.905k_0, 1.095k_0]$[a]
C_{ql}	Quasi-laminar burning velocity	Eq. (A.6)	$[0.5k_0, 1.5k_0]$[a]
a		Eq. (A.6)	[0.25, 0.75]
α	Turbulent burning velocity	Eq. (A.7)	[0.58, 1.31]
β		Eq. (A.7)	[−0.39, −0.23]
K_q	Quenching limit of turbulent burning velocity	Appendix A.5	[0.5, 2.0]
C_{fl}	Flame folding due to sub-grid geometry	Eq. (A.8)	[3.0, 12.0]

[a] k_0 denotes the respective nominal, unperturbed value and is scenario dependent.

parameters represent specific physical processes or chemical properties, the determination of their uncertainty ranges is not straightforward. As physical phenomena involved in industrial-scale gas explosions are inherently under-resolved in typical CFD simulations (Skjold et al., 2014), sub-grid models often represent a lumped effect of many un-resolved processes. However, the uncertainty intervals in Table 1 are assumed appropriate for investigating the applicability of the response surface approaches.

The model system employed in the present work is a development version of the standard release of FLACS v10.4r1 (Gexcon AS, 2015), in which the nominal values of the studied parameters are modified, i.e. set to the centre of the respective uncertainty ranges, to facilitate sensitivity analysis and response surface generation. Furthermore, some of the sub-grid model settings in the present version differ from those in the standard release FLACS v10.4r1.

3. Methods

3.1. Parameter transformation and sensitivity analysis

To assure that different scales of model parameter values do not affect the approximation quality of the response surfaces, it is convenient to transform each uncertainty range to a reference interval. Then, the transformed parameter x_i denotes the deviation of the model parameter k_i from its nominal, unperturbed value $k_{i,0}$, with respect to its uncertainty range $[k_{i,0} - R_i, k_{i,0} + R]_i$. In the present study, the linear transformation

$$x_i = \frac{k_i - k_{i,0}}{R_i}, \quad i = 1, \ldots, n \tag{2}$$

is employed (Box and Draper, 2006). According to Equation (2), the parameter x_i is 0 if the corresponding parameter k_i is unperturbed, and x_i equals −1 and 1 at the lower or upper boundary of the uncertainty range, respectively. The parameter set of all vectors $\mathbf{x} = (x_1, x_2, \ldots, x_n)$ therefore forms an uncertainty hypercube in n dimensions, where each side is of length 2.

Sensitivity analysis investigates the effect of perturbing input parameters on the output of a model (Turányi, 1997). Knowing this effect is especially important when parameters are poorly defined or feature a large range of variability (Gant et al., 2013). Performing sensitivity analysis is useful for any system for which the number of parameters involved, combined with the complex behaviour of the system, hinders the understanding of how certain parameters influence the results of interest. The Navier-Stokes equations coupled with sub-grid models as considered in Section 2 constitute such a complex system. Local sensitivity analysis quantifies the influence a single input parameter has on a model response. The local, relative, first order sensitivity s_i of a model response ζ to a parameter k_i can be expressed as

$$s_i = \frac{\partial \ln(\zeta)}{\partial \ln(k_i)}\bigg|_{k_{i,0}} = \frac{\partial \zeta}{\partial k_i}\bigg|_{k_{i,0}} \frac{k_{i,0}}{\zeta(k_{i,0})}, \quad i = 1, \ldots, n,$$

where n is the total number of parameters. As the local relative sensitivities s_i do not account for the different uncertainty ranges, in the present study, modified sensitivities $\bar{s}_i$ are calculated via

$$\bar{s}_i = s_i \frac{R_i}{k_{i,0}} = \frac{\partial \zeta}{\partial x_i}\bigg|_0 \frac{1}{\zeta(\mathbf{x} = 0)}, \quad i = 1, \ldots, n. \tag{3}$$

If $\bar{s}_i$ exceeds a threshold value, which is set depending on the situation, the corresponding parameter k_i is called active in the process that generates ζ. When generating response surfaces, taking only active parameters into account reduces the dimensionality of the parameter space and hence the amount of simulations required.

3.2. Polynomial response surface

The *polynomial response surface* (PRS) approach is inspired by the work presented by Davis et al. (2004). They employed polynomial response surfaces in the development and optimisation of gas-phase and surface reaction kinetic models in chemical engineering. The model response, understood as a function of a set of model parameters, can be written in terms of its multivariate Taylor series around the nominal values. Truncating after terms of a certain order and approximating derivatives with central finite differences leads to the polynomial approximation of the model response applied in the present study.

The truncated Taylor series of the model response ζ, called the Taylor polynomial η, is an explicit function in the parameters $\mathbf{x}$ and reads e.g. for third order

$$\begin{aligned}\eta(\mathbf{x}) = \zeta(0) &+ \sum_{i=1}^{n} \frac{\partial \zeta}{\partial x_i}\bigg|_0 x_i + \frac{1}{2}\sum_{i=1}^{n} \frac{\partial^2 \zeta}{\partial x_i^2}\bigg|_0 x_i^2 \\ &+ \sum_{i=1}^{n}\sum_{\substack{j=1 \\ j>i}}^{n} \frac{\partial^2 \zeta}{\partial x_i \partial x_j}\bigg|_0 x_i x_j + \frac{1}{6}\sum_{i=1}^{n} \frac{\partial^3 \zeta}{\partial x_i^3}\bigg|_0 x_i^3 \\ &+ \frac{1}{2}\sum_{i=1}^{n}\sum_{\substack{j=1 \\ j\neq i}}^{n} \frac{\partial^3 \zeta}{\partial x_i^2 \partial x_j}\bigg|_0 x_i^2 x_j + \sum_{i=1}^{n}\sum_{\substack{j=1 \\ j>i}}^{n}\sum_{\substack{k=1 \\ k>j}}^{n} \frac{\partial^3 \zeta}{\partial x_i \partial x_j \partial x_k}\bigg|_0 x_i x_j x_k.\end{aligned} \tag{4}$$

The coefficients are denoted by $a_0, a_i, a_{i,j}$ and $a_{i,j,k}$, respectively. If the curvature of η is too large to be described by Equation (4), a

response surface based on the logarithmic model response $\ln(\zeta)$ may be more suitable (Davis et al., 2004).

The zeroth order coefficient in Equation (4) is the nominal response value $a_0 = \zeta(0)$. Using central finite differences, the first order coefficients may be expressed as

$$a_i = \frac{\zeta[\mathbf{x}(+\tau)_i] - \zeta[\mathbf{x}(-\tau)_i]}{2\tau}, \quad i = 1, \ldots, n, \tag{5}$$

where $\mathbf{x}(\pm\tau)_i$ is a vector of parameters, whose elements are all 0 except for the ith parameter, which is perturbed by $\pm\tau$. Approximations to higher order coefficients can be found by applying central finite differences (several times) to the first order derivative approximations from Equation (5). Hence, calculating the second order coefficients and the third order coefficients, $a_{i,i,i}$ and $a_{i,i,j}$, requires additional simulations for perturbed parameters $\mathbf{x}(\pm\tau, \pm\tau)_{i,j}$ and $\mathbf{x}(\pm 2\tau)_i$, respectively, using analogous notation. To keep the computational costs low, the third order coefficients $a_{i,j,k}$ with $i \neq j \neq k \neq i$, which require a larger amount of additional simulations, are treated separately later. In total, computing the coefficients of a polynomial up to partial third order, including $a_{i,i,i}$ and $a_{i,i,j}$, requires $2n^2 + 2n + 1$ simulations for n parameters. Fig. 1 illustrates the case $n = 2$ in which the model response has to be simulated for a set of 13 parameter values.

In order to include higher order dependencies between parameters, a partial fourth order polynomial can be constructed. With an additional amount of $\binom{n}{3}2^3$ simulations the third order coefficients $a_{i,j,k}$ with $i \neq j \neq k \neq i$, and the fourth order coefficients $a_{i,i,i,i}$, $a_{i,i,j,j}$ and $a_{i,i,j,k}$, with analogous notation as before, are determined via central finite differences. Polynomials of an order higher than partial fourth are not considered in this study, since higher order terms are likely to be of the same magnitude as the errors made by applying central finite differences, resulting in no significant increase of accuracy.

3.3. Neural networks

Artificial neural networks, commonly called *neural networks* (NNs), are computational models inspired by the architecture of the human brain and the way it performs tasks. Consequently, learning processes, also called training, in NNs are loosely based on how a nervous system develops to adapt to its surrounding environment (Haykin, 1998).

A variety of designs of an NN and of learning algorithms find application in such diverse fields as model building, time series analysis, signal processing, pattern recognition and classification and control (Haykin, 1999; Hudson and Postma, 1995). However, the focus of this work lies on the ability of an NN to represent a nonlinear function from a set of inputs and desired responses (targets). For this purpose, most commonly, the multilayer feed-forward network with supervised learning, also referred to as *multilayer perceptron* (MLP), is chosen (Haupt et al., 2008).

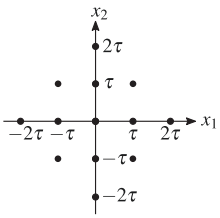

Fig. 1. Parameter set to be simulated to generate a partial third order polynomial response surface for $n = 2$.

3.3.1. General overview

A multilayer perceptron is often presented as a set of information-processing units, called nodes or neurons, which are arranged in an input layer, one or more hidden layers and a final output layer. The nodes are connected through directed lines feeding signals from input to output. The lines hold numerical weights symbolising each connection's strength. The structure of an MLP with n input nodes, one hidden layer with m nodes and k output nodes is shown in Fig. 2. To illustrate the basic operation of an MLP, we consider one specific output node as shown in Fig. 3. According to Haupt et al. (2008), each output node can be described mathematically by an explicit function of the signals x_i of input nodes and the weights $w_{i,j}$ and v_j of the connection of input node i and hidden layer node j and the hidden layer node j with the output node, respectively. The so called transfer functions ϕ and ψ evaluated at weighted linear combination of signals build the core of the function, which reads

$$y(\mathbf{x}, \mathbf{W}, \mathbf{v}) = \psi\left(\sum_{j=1}^{m} v_j \phi\left(\sum_{i=1}^{n} w_{i,j} x_i - b_j\right) - b\right).$$

Adding the biases b_j and b has the effect of increasing or lowering the net input to the transfer function (Haykin, 1998). A popular choice for ϕ is a symmetric sigmoid function, e.g. the logistic function $\phi(x) = \frac{1}{(1+e^{-ax})}$ with slope parameter $a \in \mathbb{R}$, or the hyperbolic tangent function $\phi(x) = \tanh(x)$, whereas ψ commonly is chosen as identity function. Training constitutes the process, where weights and biases are adjusted in order to minimise the difference of output of the network for given input data and the provided target values (Masters, 1993). In an MLP, training usually is performed with a back-propagation algorithm.

The performance of the NN, i.e. generalisation beyond data used in the generation process, can be improved by partitioning the set of known input-target pairs for learning into three sets – training, validation and test set. Training iterations are performed on the training set. Between each iteration, the generalisation ability is measured using the validation set. To avoid overfitting, this set may additionally be used to stop the training as soon as generalisation stops improving (Haykin, 1998). Finally, the performance of the generated network is measured independently on the test set.

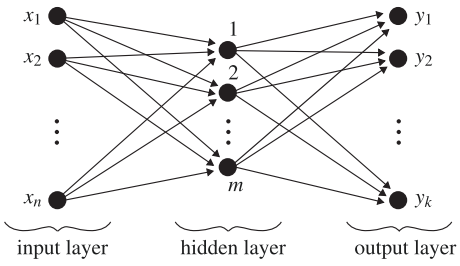

Fig. 2. Structure of a neural network with n input nodes, one hidden layer with m nodes and k output nodes.

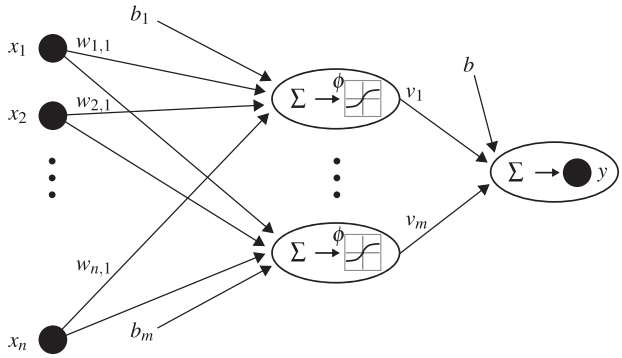

Fig. 3. Visualisation of the operation of a neural network with one output node and transfer function ϕ.

Well-developed recommendations for how to generate an NN most suitable for a respective application do not exist. Validation of generated networks may be used to identify a suitable structure of the NN with an appropriate amount of hidden layers and nodes, connectivity of nodes, transfer functions and training algorithms.

3.3.2. Neural network generation in this study

In the present study, multilayer perceptrons are applied to approximate the model response to model parameter perturbations. The output of an MLP is written in terms of a non-linear, smooth function which is in the following referred to as the *response surface based on a neural network* (RSNN). The MLPs are constructed with the Neural Network Toolbox ™ from MATLAB® (2015b, The MathWorks Inc.). They are generated on the basis of a *maximin Latin hypercube sampling* (McKay et al., 1979) of the transformed uncertainty space and the corresponding model responses. The advantage of the maximin Latin hypercube sampling, for which the minimum distance between points is maximised, is that no value of a parameter is repeated. Due to the transformation of uncertainty ranges, further normalising of the input data (Haykin, 1999) is not necessary. The MLPs are structured in one input layer with 5 or 6 nodes, representing the active parameters, one hidden layer with 10 nodes and one node in the output layer, representing the model response. The logistic function is chosen as transfer function. Back-propagation with a Levenberg-Marquardt optimisation routine is used as training algorithm, as suggested by MATLAB's Neural Network Toolbox User's Guide (Beale et al., 2015). The set of known input-target pairs for learning is divided into training, validation and test sets with 70%, 15% and 15% of the data, respectively. As some of the experiments let assume that the selected model responses are highly non-linear functions of the parameters, 20 hidden layer nodes are used in the overall analysis and the data is divided into 80%, 10% and 10%.

4. Experiments

In the present study, the response surfaces described in the previous section are applied to gas explosion experiments with homogeneous fuel-air clouds, with near-stoichiometric mixtures, where either methane, propane or natural gas was the flammable component. The experiments are part of Gexcon's model validation database, organised in accordance with the model validation methodology presented by Skjold et al. (2013). This methodology focuses on identifying the key physical phenomena in the validation experiments, and assessing how the model represents each of these phenomena. Hence, for gas explosions, the organisation of validation data is primarily according to the degree of congestion, the degree of confinement and the spatial scale of the experiments.

For the detailed analysis of the response surfaces, cf. Section 5.1, experiments from two experimental campaigns with medium- and large-scale geometries are employed, MERGE and BFETS Phase 3A, involving congested geometries with a low degree of confinement. Both campaigns are highly relevant for realistic accident scenarios in complex geometries and provide key validation data for premixed combustion modelling in FLACS (van Wingerden, 2013). For the extended analysis, cf. Section 5.2, experiments from three additional experimental campaigns involving medium- and large-scale vented enclosures are included.

4.1. Modelling and experimental research into gas explosions (MERGE)

The experiments of the project Modelling and Experimental Research into Gas Explosions (MERGE) (Mercx, 1994; Popat et al., 1996) involved a single array of pipes contained in a homogeneous gas cloud, enclosed in a polythene tent. Fig. 4a) illustrates the geometry layout. The flammable mixture was ignited in the centre of the rig, at ground level. The present study is limited to four medium-scale (4 m × 4 m × 2 m) and two large-scale (8 m × 8 m × 4 m) experiments of the campaign, comprising six different geometric configurations with varying obstacle size, pitch between obstacles, rig dimensions, volume blockage and fuel reactivity. In this paper, response surfaces are analysed in detail for the experiment MERGE C* with a propane-air mixture. The geometry of this experiment consists of pipes with diameter of 82 mm and 384 mm spacing between pipe centres in each orthogonal direction, leading to a 10% volume blockage. The model responses selected for the detailed analysis were recorded by pressure transducers 2, 5 and 6 located inside the gas cloud 0.8, 3.1 and 4 m from the ignition point in the centre of the congested region, respectively. Pressure transducer 6 is located just outside of the congested region.

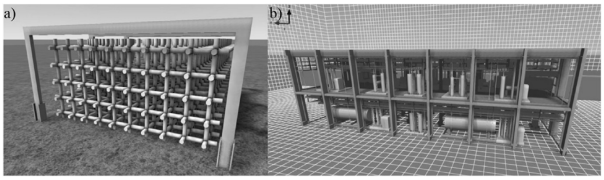

Fig. 4. a) A MERGE geometry, b) the module used in BFETS Phase 3A, Test 4.

4.2. Blast and fire engineering for topside structures (BFETS), Phase 3 A

The second campaign, the project Blast and Fire Engineering for Topside Structures (BFETS), Phase 3A (sponsored by the Health and Safety Executive, HSE), included 45 experiments with natural gas in offshore modules of dimensions 28 m × 12 m × 8 m (Al-Hassan and Johnson, 1998; Evans et al., 1999; Foisselon et al., 1998). The investigated parameters include the degree of congestion (equipment density), degree of confinement (vent area), ignition location, repeatability, and the effect of various water deluge layouts. Fig. 4b) illustrates the congestion and confinement type of Test 4, for which response surfaces are analysed in detail in the present study. Test 4 comprises a relatively densely congested geometry with a fully confined roof and fully open walls, representing a realistic offshore module. The present study includes in total 6 tests (none involving water deluge). Initial turbulence was assumed present in the fuel-air cloud, and the low hill located nearby the module has been included in the simulations (Hansen and Johnson, 2014). The ignition point is located close to one end of the module, allowing the flame to propagate through the full length of the rig. The model responses selected for the detailed analysis were recorded by pressure transducers 6, 8 and 10 located inside the gas cloud 0.5, 14 and 27.5 m from the ignition point on the lower deck, respectively.

4.3. Additional experiments

The BFETS Phase 2 project comprises 27 tests with natural gas performed in offshore modules of dimensions 25.6 m × 8 m × 8 m or 28 m × 12 m × 8 m (Foisselon et al., 1998). The investigated parameters included equipment density, vent area, ignition location, gas concentration, and the presence of water deluge. The present study focuses on 5 experiments from BFETS Phase 2, all performed in the smaller module, without water deluge. Fig. 5a) shows the geometry for a representative test.

Bauwens (2010) and Chao et al. (2011) describe explosion experiments involving stoichiometric methane- and propane-air mixtures, performed in a vented explosion chamber of dimensions 4.6 m × 4.6 m × 3.0 m, located at the FM Global research campus. Bauwens (2010) and Chao et al. (2011) investigated the effect on explosion overpressures from varying the vent size, ignition position, and inserting 8 square obstructions spanning the vertical direction of the explosion chamber, see Fig. 5b). The present study focuses on four experiments, all with a vent area of 5.4 m^2, where ignition occurred either in the centre of the chamber or at the back wall, opposite of the vent opening.

Tomlin et al. (2015) describe a series of large-scale experiments conducted by DNV GL in a 182 m^3 vented explosion chamber, located at the Spadeadam test site (cf. Fig. 5c)). The campaign comprised 38 stoichiometric natural gas-air explosions with varying vent area and degree of congestion. The congestion level was varied by placing 180 mm diameter polyethylene pipes within the explosion chamber, providing different volume- and cross-sectional area blockages. In the present study, 6 tests with different congestion levels are included.

5. Results and discussion

The methods introduced in Section 3 are applied to relevant model responses from simulations of the experimental campaigns described in Section 4. The simulations are performed with the CFD tool FLACS. Relevant model responses are the maximum overpressure ζ_{pmax} and the maximum pressure impulse $\zeta_{pimpmax}$ at representative monitor points. The pressure impulse is the integral of the pressure-time curve and hence a function of both the duration of the overpressure peak/peaks and its/their magnitude, and may therefore respond differently to parameter perturbations than the maximum overpressure. In a simulation, monitor points are defined spacial points for which physical properties are saved and correspond to pressure transducers in the experiments.

In order to quantify the approximation quality of a response surface, i.e. how accurately the response surface reproduces the model response of the CFD tool, the response surface is validated for a large amount of simulations, *M*, with parameters varying in their uncertainty ranges, cf. Table 1. For the detailed analysis of response surfaces for MERGE and BFETS Phase 3A campaigns in Section 5.1, several thousand simulations are included. Due to limitations in practical simulation time, only 250 simulations are included in the analysis of the general applicability of the response surfaces based on neural networks in Section 5.2. It is worth to note, that in some applications, it may not be convenient to perform a large amount of simulations to validate the response surfaces. However, in order to get an adequate impression of the

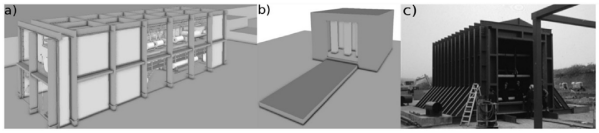

Fig. 5. a) The BFETS Phase 2 module, b) the FM Global 64 m^3 vented explosion chamber, c) the DNV GL 182 m^3 vented explosion chamber (courtesy of DNV GL).

approximation quality, validation can be performed for the simulations used to generate the response surfaces. In the RSNN approach it is therefore crucial to divide the learning data in a training and a testing set.

The approximation quality is visualised by scatter plots comparing response surface evaluations with the corresponding model responses from simulations. Furthermore, the geometric mean bias and the corresponding geometric mean variance are plotted to quantify systematic bias and to provide a measure of the consistency of over/under-prediction, respectively, cf. (Model Evaluation Group Gas Explosions (MEGGE, 1996). In the present context, the geometric mean bias (MG) and variance (VG) of the differences between a response surface η and a model response ζ for parameter variations $\mathbf{x}^i$, $i = 1, \ldots, M$, are defined as

$$\mathrm{MG} = \exp\left(\frac{1}{M}\sum_{i=1}^{M}\ln\left(\frac{\eta(\mathbf{x}^i)}{\zeta(\mathbf{x}^i)}\right)\right),\ \mathrm{VG} = \exp\left(\frac{1}{M}\sum_{i=1}^{M}\ln\left(\frac{\eta(\mathbf{x}^i)}{\zeta(\mathbf{x}^i)}\right)^2\right), \tag{6}$$

respectively. Values of MG and VG are presented in log-log plots together with a zero variance curve denoting a zero arithmetic variance. The geometric mean bias and variance are only defined for positive values. However, both approximation approaches may return negative values for certain parameter combinations. As negative values for the maximum overpressure and pressure impulse should not occur in the studied explosion scenarios, it is convenient to set negative approximation output to a fixed small positive value and use the resulting truncated approximation in the respective application. This methodology is employed in the present paper.

To provide a more complete picture of the accuracy of the RSNNs in the extended analysis, the approximation quality is measured by several metrics. In addition to MG and VG, the normalised root mean square error (NRMSE) given by

$$\mathrm{NRMSE} = \sqrt{\frac{\frac{1}{M}\sum_{i=1}^{M}\left(\eta(\mathbf{x}^i) - \zeta(\mathbf{x}^i)\right)^2}{\frac{1}{M}\sum_{i=1}^{M}\zeta(\mathbf{x}^i)}} \tag{7}$$

and the maximum normalised error (NEmax)

$$\mathrm{NEmax} = \frac{\max\{|\eta(\mathbf{x}^i) - \zeta(\mathbf{x}^i)|,\ i = 1, \ldots, M\}}{\frac{1}{M}\sum_{i=1}^{M}\zeta(\mathbf{x}^i)} \tag{8}$$

are calculated.

The definition of a satisfactory response surface depends on the respective application. It should be noted that in this paper, the approximation quality of the response surfaces is analysed with respect to parameter optimisation.

5.1. Detailed analysis of response surfaces

In this section, results from the sensitivity analysis and response surface validation are shown in detail for the experiment MERGE C* with propane-air and Test 4 in BFETS Phase 3A.

5.1.1. Sensitivity analysis

In order to facilitate the response surface approaches, each parameter's uncertainty range, cf. Table 1, is transformed to the reference interval $[-1, 1]$ via Equation (2). Sensitivity analysis is conducted as described by Equation (3).

Fig. 6 shows the local sensitivities $\bar{s}_i$ of ζ_{pmax} (left) and ζ_{pimpmax} (right) for the experiment MERGE C* with propane-air in three monitor points. The monitor points in the simulations are located in accordance with the pressure transducers of the experiments. Although the sensitivities are somewhat higher for the maximum overpressure than for the maximum pressure impulse, they occur in similar order when ranked according to size. Fig. 7 shows the local sensitivities $\bar{s}_i$ of ζ_{pmax} (left) and ζ_{pimpmax} (right) for Test 4 in BFETS Phase 3A in three different monitor points.

In both tests, due to the low degree of confinement, the overpressure is mainly generated by the acceleration of the flame front through the turbulent boundary layers and unsteady wakes of the obstructions. As the flow in both experiments becomes turbulent relatively shortly after ignition, some of the parameters governing the turbulent burning velocity, α, u_l, together with the parameter C_{fl} accounting for flame folding around sub-grid objects produce high sensitivities for the maximum overpressure. The sensitivities for C_o in Test 4, BFETS Phase 3A, indicate that flame acceleration is in addition effectively enhanced by promoting the sub-grid turbulence production.

According to the sensitivities obtained for experiments in the MERGE and BFETS Phase 3A campaigns, the active parameters in the detailed analysis, and thus the ones included in the response surface approaches, are chosen to be α, β, C_{fl}, K_q, u_l and C_o. However, the parameters a and C_{ql} produce higher values of sensitivities for other geometries in particular for explosions in empty vented enclosures, cf. Section 5.2.

5.1.2. Validation of polynomial response surfaces

Polynomial response surfaces of second, partial third and partial fourth order are constructed according to the approach defined in Section 3.2. The width of the central finite differences as e.g. used in Equation (5) is characterised by τ, chosen as either 0.25, 0.5 or 0.75. Generating partial third and partial fourth order polynomials for 6

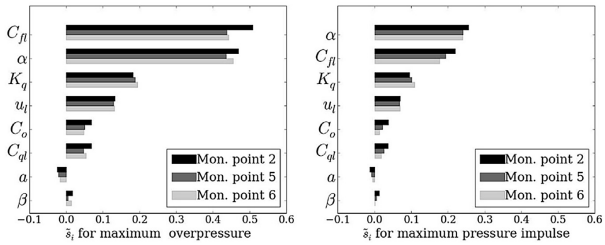

Fig. 6. First order local sensitivities of maximum overpressure (left) and maximum pressure impulse (right) for MERGE C*, propane-air, in monitor points 2, 5 and 6.

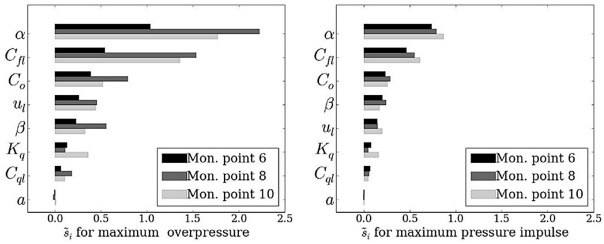

Fig. 7. First order local sensitivities of maximum overpressure (left) and maximum pressure impulse (right) for BFETS Phase 3A, Test 4, in monitor points 6, 8 and 10.

parameters requires 85 and 245 simulations, respectively. Due to inaccuracy of the Taylor series further away from the value which it is derived from, the PRSs can only be trusted in a smaller region. Hence, validation of the PRSs is performed for a reduced uncertainty space spanned by narrower ranges than the assigned uncertainty intervals. In the following, the reduced uncertainty space denotes the hypercube spanned by $[-0.6, 0.6]$ in all directions. Scatter plots and values of MG and VG are based on 3072 parameter perturbations within the reduced uncertainty space.

Testing several MERGE and BFETS Phase 3A experiments shows that, in general, PRSs generated for $\tau = 0.5$ or $\tau = 0.75$ show better approximation quality than those for $\tau = 0.25$. Furthermore, the approximation quality increases with increasing order of the polynomials. The model responses for the MERGE experiments can be approximated in a satisfactory way with partial third order polynomials, whereas the model responses for some of the experiments in the BFETS Phase 3A campaign cannot be reproduced with a PRS with satisfactory accuracy. Results for the experiments MERGE C* with propane-air and Test 4 in BFETS Phase 3A are presented in the following.

Fig. 8 visualises the ability of the PRSs to approximate ζ_{pmax} at monitor point 2 for the experiment MERGE C* with propane-air predicted by FLACS. The PRSs of second and partial third order predict the model response well when calculating finite differences with $\tau = 0.5$ or $\tau = 0.75$ and their approximation quality is similar. It is worth mentioning that when evaluating the PRSs at points

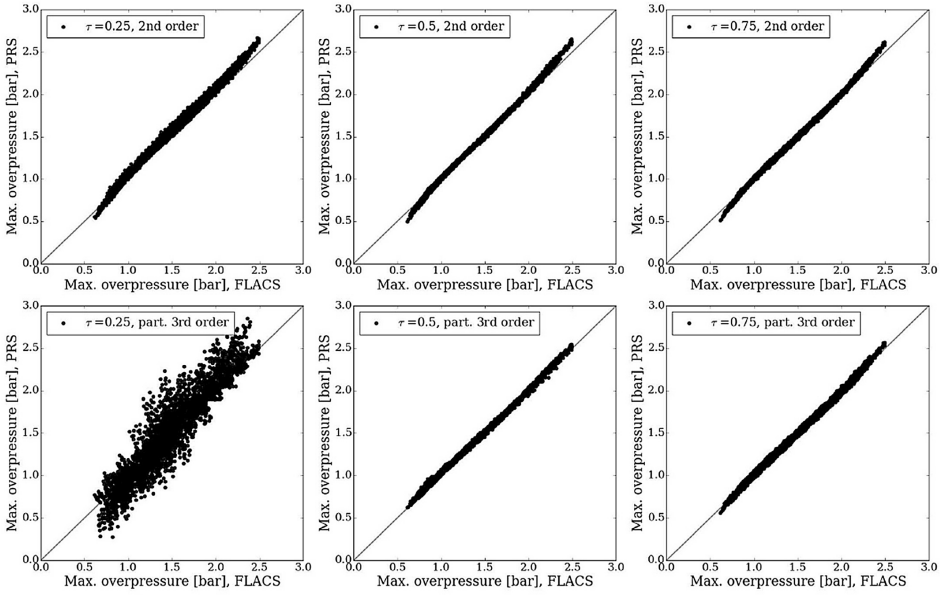

Fig. 8. PRSs for maximum overpressure vs. FLACS for MERGE C* with propane-air, for $\tau = 0.25,\ 0.5$ and 0.75, validated for the reduced uncertainty space. The upper and the lower panel show the second and the partial third order PRS, respectively.

further away from the expansion point of the Taylor polynomial, the approximation quality of higher order PRSs may become worse, as for the partial third order PRS with $\tau = 0.25$ in Fig. 8 (left). The partial fourth order PRSs do not produce better results but require 160 additional simulations and are therefore not shown here. Similar results are obtained for ζ_{pimpmax}.

For Test 4 of the campaign BFETS Phase 3A the PRSs approximate the model responses ζ_{pmax} and ζ_{pimpmax} in the reduced uncertainty space best when generated for $\tau = 0.75$ and $\tau = 0.5$, respectively. The validation of the PRSs for monitor point 6 with second, partial third and partial fourth order, as well as of those based on the logarithmic model response are shown in Figs. 9 and 10. Fig. 11 presents the corresponding values of MG and VG for ζ_{pmax} (left) and ζ_{pimpmax} (right). As mentioned, truncated response surfaces without negative output are taken into account. In model validation, Test 4 constitutes a challenging test case and is therefore chosen for the detailed analysis. The response surfaces for Test 4 show the largest scatter to the corresponding model responses for the investigated campaigns. The maximum overpressure is best reproduced by a PRS of partial fourth order. The scatter plots in Fig. 10 might give the impression that the maximum pressure impulse is as well best represented by the PRS of partial fourth order for the original model response. However, the partial fourth order PRS based on the logarithmic model response shows a higher approximation quality in terms of MG and VG. This is due to the fact that the geometric mean normalises the ranges being averaged, such that it is affected by relative and not absolute changes of the model response.

Fig. 12 shows further validation of the PRSs approximating maximum overpressure for points within the entire uncertainty space, i.e. 1449 additional points in $([-1.0, -0.6] \cup [0.6, 1.0])^6$. As all of the polynomials show poor approximation quality, the PRSs can only be trusted inside the reduced uncertainty space spanned by $[-0.6, 0.6]$ in all directions.

5.1.3. Validation of response surfaces based on neural networks

Response surfaces based on neural networks are generated according to the approach described in Section 3.3. While the order of the PRSs determines the amount of simulations used for construction, the number of simulations required to generate a sufficiently accurate RSNN has to be investigated by numerical experiments. If the RSNN is not evaluated at the entire uncertainty space, it is convenient to generate it for a reduced uncertainty space, as a given number of points fill a smaller space more densely. This leads in general to better generalisation of the RSNN (inside the reduced space). For evaluation at the entire uncertainty space, the networks are constructed for Latin hypercube samplings distributed over the entire uncertainty range, since RSNNs show poor extrapolation properties. The concept is visualised in Fig. 13.

Validating RSNNs generated for experiments of the campaigns MERGE and BFETS Phase 3A shows that the approximation quality increases with increased amount of Latin hypercube sampling points, as expected. In general, ζ_{pmax} and ζ_{pimpmax} of the MERGE experiments and ζ_{pimpmax} of the BFETS Phase 3A experiments can be approximated in a satisfactory way when generated from around 150 sampling points. To represent ζ_{pmax} accurately enough for the BFETS Phase 3A experiments, around 400 sampling points are required. Results for the experiments MERGE C* with propane-air and Test 4 in BFETS Phase 3A are presented in the following.

For the experiment MERGE C* with a propane-air mixture the RSNNs for ζ_{pmax} and ζ_{pimpmax} are constructed from different amounts of Latin hypercube sampling points, $\text{lhs} = 100, 150$ and 250, distributed over both the reduced and the entire uncertainty space. Validation is performed for 3072 points in the reduced uncertainty space. As expected, the RSNN for the maximum overpressure generated from a certain amount of sampling points distributed in the reduced uncertainty space shows a better approximation quality than the RSNN generated from the same amount in the entire uncertainty space. Validation for the former (cf. type *a)* in Fig. 13) for monitor point 2 is shown in Fig. 14. The approximation quality of the RSNN generated from 100 simulations exceeds the one of the third order PRSs, cf. Fig. 8, requiring only 15 additional simulations. The approximation quality increases when a larger amount of simulations is used. Similar results are obtained for the maximum pressure impulse.

The RSNNs for ζ_{pmax} and ζ_{pimpmax} for Test 4 in BFETS Phase 3A are generated on the basis of Latin hypercube samplings with different sizes distributed over the reduced and entire uncertainty range, i.e. $\text{lhs} = 150, 250$ and 400. The RSNNs for ζ_{pimpmax} generated on the reduced uncertainty space show better approximation behaviour than the ones on the entire uncertainty space, as for MERGE C*. Validation for RSNNs generated on the reduced uncertainty space (cf. type *a)* in Fig. 13) for monitor point 6 is shown in Fig. 15. The RSNN generated from 150 sampling points shows a higher approximation quality than the best PRS which requires 245 simulations, cf. Fig. 10. The approximation quality can be increased when using a larger amount of simulations. In contrast, the RSNN for ζ_{pmax} generated from a certain amount of sampling points

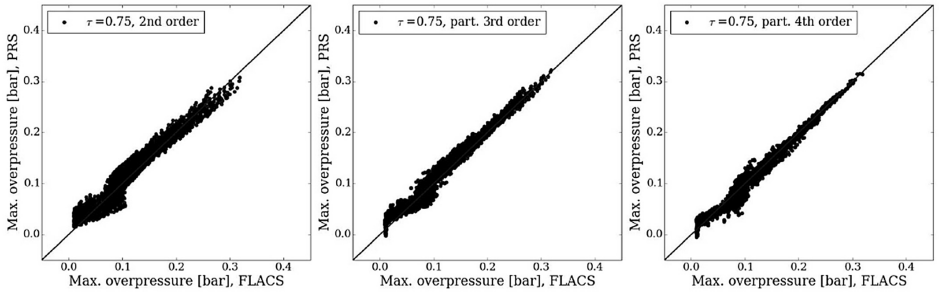

Fig. 9. PRSs for maximum overpressure vs. FLACS for BFETS Phase 3A, Test 4, $\tau = 0.75$. From left to right, the second, partial third and partial fourth order PRSs are shown, validated for the reduced uncertainty space.

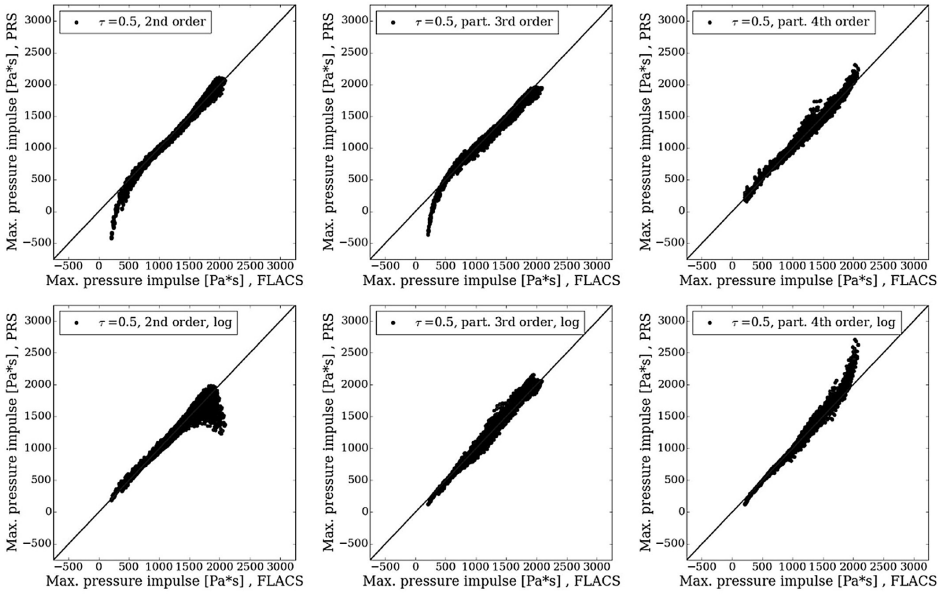

Fig. 10. PRSs for maximum pressure impulse vs. FLACS for BFETS Phase 3A, Test 4, $\tau = 0.5$. From left to right, the second, partial third and partial fourth order PRSs (upper panel) and those for the logarithmic model response (lower panel) are shown, validated for the reduced uncertainty space.

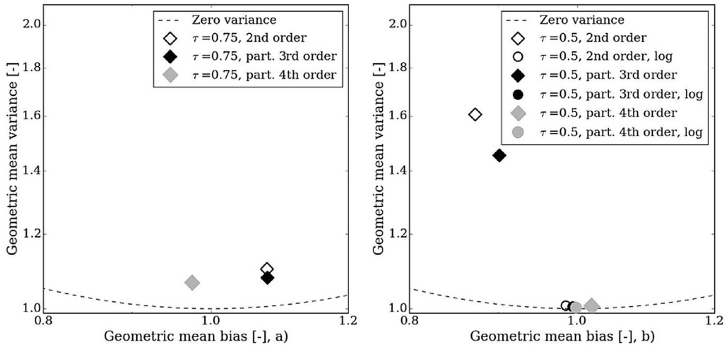

Fig. 11. Geometric mean bias and variance of truncated PRSs vs. FLACS for BFETS Phase 3A, Test 4 for a) maximum overpressure, $\tau = 0.75$ and b) maximum pressure impulse, $\tau = 0.5$, validated for the reduced uncertainty space.

distributed over the entire uncertainty space shows better approximation quality than the RSNN generated from the same amount in the reduced uncertainty space. This indicates a more complex behaviour of the maximum overpressure to model parameter perturbations. Scatter plots for both cases are presented in Fig. 16. All tested RSNNs generated for the entire uncertainty space approximate the maximum overpressure on the reduced uncertainty space (cf. type *b)* in Fig. 13) better than the PRSs. The approximation quality of the RSNNs increases to a satisfactory level if 400 sampling points within the entire uncertainty space are used for generation.

Moreover, the RSNNs generated from a sufficient amount of

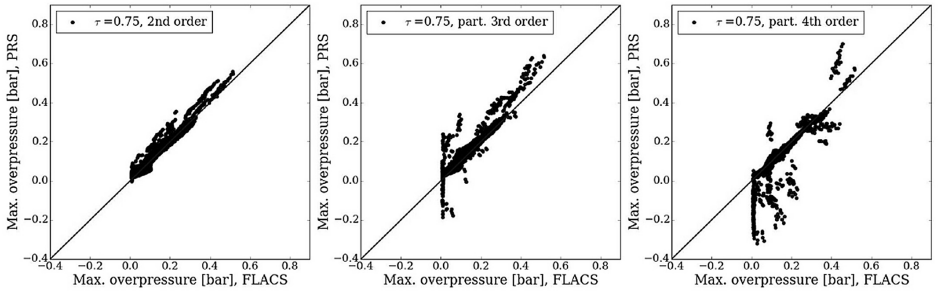

Fig. 12. PRSs for maximum overpressure vs. FLACS for BFETS Phase 3A, Test 4, for $\tau = 0.75$. From left to right, the second, partial third and partial fourth order PRSs are shown, validated for the entire uncertainty space.

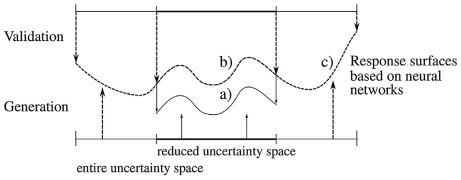

Fig. 13. Visualisation of generation and validation of RSNNs; a) generated and validated for the reduced uncertainty space, b) generated for the entire, validated for the reduced uncertainty space, c) generated and validated for the entire uncertainty space.

simulations may be trusted, i.e. evaluated, in the entire uncertainty space (cf. type *c)* in Fig. 13), as visualised in Fig. 17 for the maximum overpressure. This is of interest when employing response surfaces for optimising model parameters within their uncertainty ranges to improve the predictive capability of a CFD tool. If PRSs were applied, several iterations of optimisation may be required to converge to the optimum. In each iteration, the parameter uncertainty space has to be reduced to a space around the current iterate on which the polynomials are trusted. Applying RSNNs with global accuracy allows for a single iteration optimisation, accelerating the optimisation procedure significantly.

5.2. Extended analysis of the applicability of the RSNNs

As the RSNNs outperform the PRSs for the examples in the detailed analysis, cf. Section 5.1, the general applicability of response surfaces for industrial-scale gas explosions is investigated exclusively for the RSNNs in an extended analysis in this section. In the extended analysis, the RSNNs are generated and validated for the maximum overpressure ζ_{pmax} and the maximum pressure impulse ζ_{pimpmax} at 3–5 relevant monitor points for all experiments described in Section 4. This includes the tests studied in the detailed analysis. However, a newer development version of FLACS v10.4r1 is employed and the uncertainty ranges of some parameters are adapted accordingly. As the changes do not affect the quality of the response surfaces, the conclusions drawn from the detailed analysis in Section 5.1 remain valid.

To gain a more complete overview over the approximation quality of the RSNNs, it is measured by several metrics, i.e. MG and VG, NRMSE and NEmax defined in equations (6)–(8). Tables 2 and 3 summarise the results for RSNNs for the maximum overpressure and the maximum pressure impulse, respectively. The tables provide additional information about the considered tests, the active parameters and the size of the Latin hypercube sampling of the entire uncertainty space used to generate the RSNNs. All RSNNs are validated on a Latin hypercube sampling with 250 parameter values distributed over the entire uncertainty space, cf. type *c)* in Fig. 13. The values for MG and VG are the geometric mean bias and

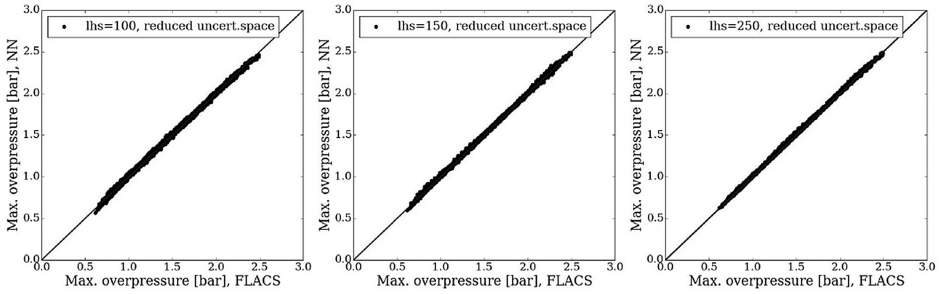

Fig. 14. RSNNs for maximum overpressure vs. FLACS for MERGE C*, propane-air, for lhs = 100, 150 and 200, generated and validated for the reduced uncertainty space.

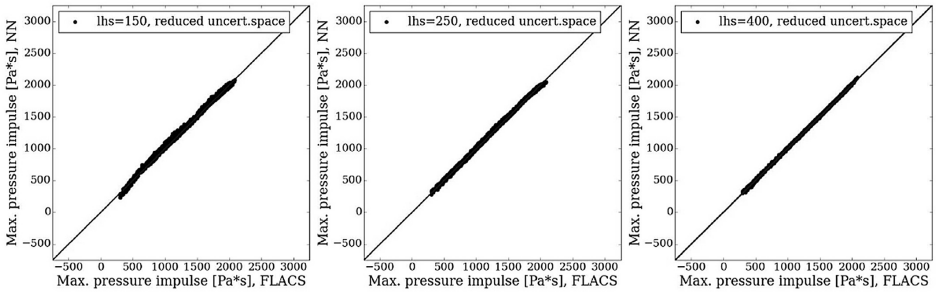

Fig. 15. RSNNs for maximum pressure impulse vs. FLACS for BFETS Phase 3A, Test 4, for lhs = 150, 250 and 400, generated and validated for the reduced uncertainty space.

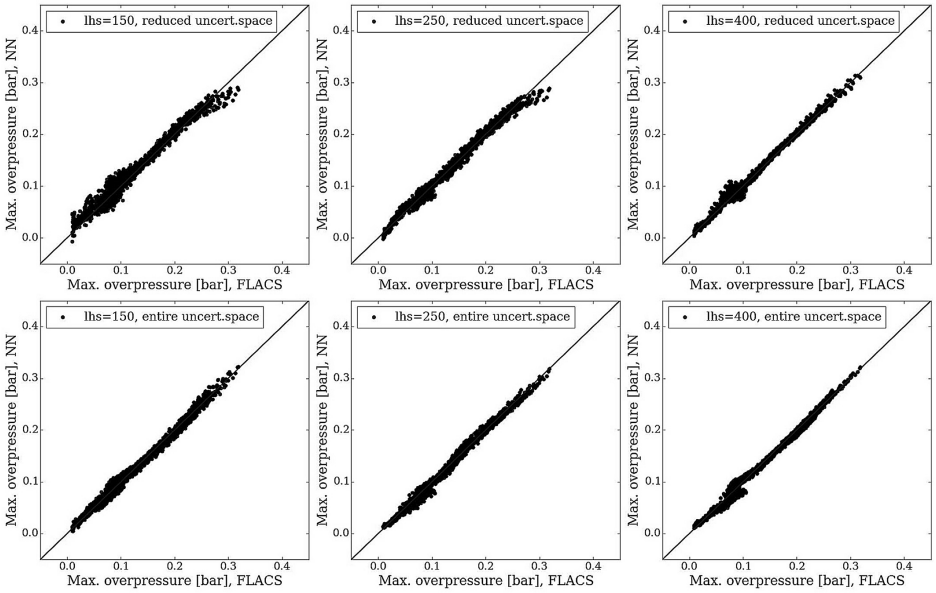

Fig. 16. RSNNs for maximum overpressure vs. FLACS for BFETS Phase 3A, Test 4, for *lhs* = 150, 250 and 400, generated from points in the reduced (upper panel) and entire (lower panel) uncertainty space, validated for the reduced uncertainty space.

variance taken over all RSNNs for the respective model response, i.e. for all tests and monitor points. The values given for NRMSE and NEmax are the average of the NRMSEs of all RSNNs and the largest NEmax of all RSNNs, respectively.

Tables 2 and 3 show that all RSNNs for ζ_{pimpmax} are more accurate approximations – in all three metrics – than the ones for ζ_{pmax}. As the RSNNs for the MERGE campaign with propane-air, called *MERGE-propane* in the following, show a high accuracy in the detailed analysis, the error measurements for those RSNNs from Tables 2 and 3 are taken as reference values. The RSNNs can be divided into three quality classes. The classification of the RSNNs is not dependent on the choice of the metric employed to measure the approximation quality, and in most cases, the RSNNs for ζ_{pmax} and ζ_{pimpmax} can be assigned to the same quality class. The first class comprises the RSNNs for the FM Global and MERGE-propane experiments which show the highest approximation quality. The RSNNs for the MERGE-methane and DNV GL experiments build the second class. Their approximation quality is only slightly worse than the one of the RSNNs from the first class. However, it is worth mentioning that generating some RSNNs for the DNV GL

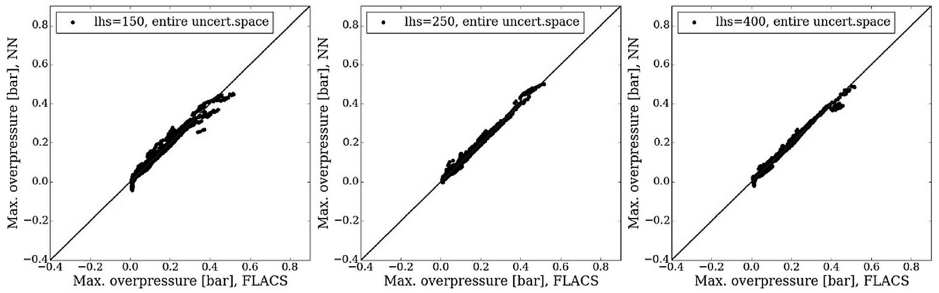

Fig. 17. RSNNs for maximum overpressure vs. FLACS for BFETS Phase 3A, Test 4, for *lhs* = 150, 250 and 400, generated and validated for points in the entire uncertainty space.

Table 2
Approximation quality of RSNNs for the maximum overpressure.

Experimental campaign	Tests	Active parameters	Sampling size	MG[a], VG[a]	NRMSE[b]	NEmax[c]
MERGE, methane-air	A, B, C, C*, D, E	α, β, C_{fl}, K_q, u_l, C_o	400	0.9972, 1.0061	0.0206	0.2136
MERGE, propane-air	A, B, C, C*, D, E	α, β, C_{fl}, K_q, u_l, C_o	400	0.9988, 1.0009	0.0180	0.2362
FM Global, 64 m^3, empty, methane-air	Back ignition, Central ignition (5.4 m^2 vent)	α, β, C_{ql}, u_l, C_o	400	1.0001, 1.0008	0.0147	0.2951
FM Global, 64 m^3, empty, propane-air	Back ignition, Central ignition (5.4 m^2 vent)	α, β, C_{ql}, u_l, C_o	400	0.9995, 1.0005	0.0116	0.1347
FM Global, 64 m^3, with obstacles, methane-air	Back ignition, Central ignition (5.4 m^2 vent)	α, β, C_{ql}, u_l, C_o	400	1.0012, 1.0011	0.0166	0.2043
FM Global, 64 m^3, with obstacles, propane-air	Back ignition, Central ignition (5.4 m^2 vent)	α, β, C_{ql}, u_l, C_o	400	1.0005, 1.0004	0.0096	0.1407
BFETS Phase 3A	Alpha, Beta, Test 1, Test 4, Test 16, Test 17	α, β, C_{fl}, C_{ql}, u_l, C_o	800	0.9857, 1.1096	0.0254	0.3130
BFETS Phase 2	Test 6, Test 7, Test 13, Test 18, Test 22	α, β, C_{fl}, u_l, C_o	800	1.0306, 1.4833	0.0498	0.5533
DNV GL, 182 m^3	Test 4, Test 12, Test 14, Test 22, Test 26, Test 38	α, β, C_{fl}, C_{ql}, u_l, C_o	400 or 800	1.0004, 1.0029	0.0266	0.2730

[a]Taken all RSNNs into account, [b]average of the NRMSEs of all RSNNs, [c]largest NEmax of all RSNNs.

Table 3
Approximation quality of RSNNs for the maximum pressure impulse.

Experimental campaign	Tests	Active parameters	Sampling size	MG[a], VG[a]	NRMSE[b]	NEmax[c]
MERGE, methane-air	A, B, C, C*, D, E	α, β, C_{fl}, K_q, u_l, C_o	400	0.9995, 1.0016	0.0096	0.1508
MERGE, propane-air	A, B, C, C*, D, E	α, β, C_{fl}, K_q, u_l, C_o	400	1.0000, 1.0000	0.0067	0.0989
FM Global, 64 m^3, empty, methane-air	Back ignition, Central ignition (5.4 m^2 vent)	α, β, C_{ql}, u_l, C_o	400	0.9996, 1.0001	0.0063	0.1007
FM Global, 64 m^3, empty, propane-air	Back ignition, Central ignition (5.4 m^2 vent)	α, β, C_{ql}, u_l, C_o	400	1.0001, 1.0001	0.0046	0.0429
FM Global, 64 m^3, with obstacles, methane-air	Back ignition, Central ignition (5.4 m^2 vent)	α, β, C_{ql}, u_l, C_o	400	0.9995, 1.0001	0.0066	0.0695
FM Global, 64 m^3, with obstacles, propane-air	Back ignition, Central ignition (5.4 m^2 vent)	α, β, C_{ql}, u_l, C_o	400	0.9994, 1.0001	0.0046	0.0390
BFETS Phase 3A	Alpha, Beta, Test 1, Test 4, Test 16, Test 17	α, β, C_{fl}, C_{ql}, u_l, C_o	800	1.0013, 1.0020	0.0091	0.1186
BFETS Phase 2	Test 6, Test 7, Test 13, Test 18, Test 22	α, β, C_{fl}, u_l, C_o	800	0.9405, 1.4069	0.0345	0.4562
DNV GL, 182 m^3	Test 4, Test 12, Test 14, Test 22, Test 26, Test 38	α, β, C_{fl}, C_{ql}, u_l, C_o	400 or 800	1.0003, 1.0004	0.0130	0.1138

[a]Taken all RSNNs into account, [b]average of the NRMSEs of all RSNNs, [c]largest NEmax of all RSNNs.

experiments requires 800 (instead of 400) sampling points to gain good results. The RSNNs for the BFETS Phase 3A experiments approximate $\zeta_{pimpmax}$ much better than ζ_{pmax}. The difference between the quality of the RSNNs for both model responses is significantly larger than for the other tests. Whereas the RSNNs for $\zeta_{pimpmax}$ can be assigned to the second class, the RSNNs for ζ_{pmax} must be assigned to a third quality class. The third class also comprises the RSNNs for the BFETS Phase 2 experiments, as they show the worst approximation quality for both model responses. For ζ_{pmax} and $\zeta_{pimpmax}$, the NRMSE is 2.8 and 5.2 times as large as for MERGE-propane, respectively. However, the values might still be acceptable, depending on the final application. It should be noted that for all BFETS experiments 800 sampling points were employed to generate the response surfaces.

The results confirm the impression gained in the detailed analysis, cf. Section 5.1, that for the realistic geometries of the BFETS campaigns the selected model responses are more complex functions of the model parameters as the ones for the idealised, symmetric modules from the other campaigns.

6. Conclusion

The main objective of this study was to present the approximation quality of response surfaces as metamodels for key model responses from CFD gas explosion simulations. The response surfaces were constructed to reproduce the maximum overpressure and the maximum pressure impulse at selected monitor points from gas explosion simulations as a function of sub-grid model parameters. The present work was motivated by the application of response surfaces in optimisation of sub-grid model parameters to improve the predictive capabilities of the CFD tool FLACS. Two response surface approaches were presented – a Taylor polynomial response surface (PRS) and a response surface based on neural

networks (RSNN). Simulations were performed with the CFD tool FLACS. The analysis was performed in two stages. The results can be summarised to 5 main findings. In the first part, the response surfaces for experiments from two experimental campaigns were analysed in detail.

i) It was demonstrated that the model responses for single gas explosion experiments can be approximated with sufficient accuracy by a PRS of up to partial fourth order. The main advantage of the PRS approach is the low amount of simulations needed to generate the response surface. However, if a model response was highly non-linear, a PRS was not able to approximate the model response with desired accuracy.
ii) For the model responses that could be approximated well by a PRS, generating an RSNN with same accuracy required more simulations than the PRS. However, it was found that the approximation quality of the RSNNs increases with increased amount of simulations used to generate the RSNNs. Therefore, more accurate RSNNs could be constructed. Furthermore, for the model responses that could not be approximated with sufficient accuracy by a PRS, RSNNs with high approximation quality were generated.
iii) Provided that the additional cost of a larger amount of simulations is feasible in the respective application, the RSNNs generated from those simulations can be trusted on the entire uncertainty space, allowing for e.g. a more efficient parameter optimisation procedure. It was found that the PRSs should in general not be trusted on the entire uncertainty space.

Second, the general applicability of the response surfaces was investigated for the RSNNs in an extended analysis, as they showed better results for the experiments in the first analysis. The RSNNs were generated for 37 tests from 5 different experimental campaigns. The approximation quality of the RSNNs was measured by three different metrics – all leading to the same conclusions.

iv) It was found that generating RSNNs for tests with large-scale geometries and non-homogeneously distributed obstacles requires larger Latin hypercube samplings to obtain the desired accuracy than for tests with more idealised, symmetric modules.
v) Taking the approximation quality of the RSNNs for the MERGE experiments with propane-air as a reference value, the RSNNs for all studied tests, except for BFETS Phase 2, showed highly satisfactory results. The approximation quality of the RSNNs for the BFETS Phase 2 experiments was slightly worse, but may still be good enough for applications such as model parameter optimisation in CFD tools.

In general, based on our findings we conclude that the PRS approach may be preferred if the model response is a less complex function of the parameters, cf. (Davis et al., 2004), or if the respective application does only allow for a low amount of simulations, accepting a lower approximation accuracy, cf. (Vianna and Cant, 2012). Otherwise, as when applying response surfaces in optimisation of sub-grid model parameters to improve the predictive capabilities of CFD tools, the RSNNs constitute more reliable response surfaces and should be preferred.

Acknowledgements

The authors acknowledge gratefully the financial support from the Research Council of Norway (project number 246167/O30) through the Industrial Ph.D. scheme.

Appendix A. Model system and parameters

In the following, the parameters from Table 1 in Section 2 and the corresponding sub-grid models for turbulence generation and premixed combustion are presented.

Appendix A.1. Turbulence production from sub-grid objects

FLACS solves conservation equations for the turbulence kinetic energy k and its dissipation rate ε according to the standard $k-\varepsilon$ model (Launder and Spalding, 1974). On differential form, the conservation equations read

$$\frac{\partial}{\partial t}(\beta_v \rho k) + \frac{\partial}{\partial x_j}\left(\beta_j \rho k u_j\right) = \frac{\partial}{\partial x_j}\left(\beta_j \Gamma_k \frac{\partial k}{\partial x_j}\right) + \beta_v P_k - \beta_v \rho \varepsilon, \tag{A.1}$$

$$\frac{\partial}{\partial t}(\beta_v \rho \varepsilon) + \frac{\partial}{\partial x_j}\left(\beta_j \rho \varepsilon u_j\right) = \frac{\partial}{\partial x_j}\left(\beta_j \Gamma_\varepsilon \frac{\partial \varepsilon}{\partial x_j}\right) + \beta_v P_\varepsilon - C_{2,\varepsilon}\beta_v \rho \frac{\varepsilon^2}{k}, \tag{A.2}$$

where P_k and P_ε define the production of k and ε, respectively (represented by S_Φ in Equation (1)), and $C_{2,\varepsilon}$ is a model constant. The production term P_k is given by

$$P_k = G_s + G_w + G_b + G_o, \tag{A.3}$$

where G_s, G_w, G_b and G_o are terms representing turbulence generation due to fluid-shear, wall-shear, buoyancy and sub-grid obstructions, respectively. The production P_ε of dissipation rate ε in Equation (A.2) is set proportional to P_k. Following Sha and Launder (1979), G_o in Equation (A.3) can be expressed as

$$G_o = C_o \beta_v \rho |\vec{u}| u_j^2 d_j, \tag{A.4}$$

where C_o is a constant specific to FLACS, and d_j is a parameter that depends on the sub-grid object. A physical interpretation of G_o relates it to energy loss due to sub-grid drag in the momentum equation (Popat et al., 1996). The model parameter C_o in Equation (A.4) is important for modelling flame acceleration in congested geometries with sub-grid obstructions, as the turbulence model provides input to the combustion model.

Appendix A.2. Combustion modelling

Premixed combustion in FLACS is modelled by the conservation equation for the fuel mass fraction Y_F according to

$$\frac{\partial}{\partial t}(\beta_v \rho Y_F) + \frac{\partial}{\partial x_j}\left(\beta_j \rho Y_F u_j\right) = \frac{\partial}{\partial x_j}\left(\beta_j \Gamma_{Y_F} \frac{\partial Y_F}{\partial x_j}\right) + w_F. \tag{A.5}$$

The sink term w_F in Equation (A.5) represents the Favre-averaged consumption rate of reactants, producing combustion products by chemical reaction. According to the analysis of Arntzen (1998), w_F and the effective diffusion coefficient Γ_{Y_F} are modelled such that the numerical flame zone propagates with a certain input burning velocity u_g. Empirical correlations relating the burning velocity u_g to the flow regime and mixture dependent variables are needed to close Equation (A.5). Burning velocity correlations are defined for laminar, quasi-laminar and turbulent flow conditions.

Appendix A.3. Laminar burning velocity

The burning velocity in all flow regimes incorporates the

laminar burning velocity u_l, which can be regarded as a fundamental property of the mixture, representing its reactivity, diffusivity and exothermicity (Ranzi et al., 2012). FLACS uses a library of laminar burning velocities to represent u_l.

Ranzi et al. (2012) present recent values for the laminar burning velocity for a range of mixtures. For example, methane and propane mixed with air, with an equivalence ratio (ER) of 1.1, burning at atmospheric pressure and an ambient temperature of 298 K, show a scatter of approximately ±0.02 m/s for methane and ±0.01 m/s for propane, using data from (Vagelopoulos and Egolfopoulos, 1998; Bosschaart and De Goey, 2004; Jomaas et al., 2005; Gu et al., 2000; Hassan et al., 1998; Rozenchan et al., 2002; Park et al., 2011; Halter et al., 2010). In the development version of FLACS used in the present study, the laminar burning velocity values from (Law et al., 1988) are applied for both methane and propane. These data sets are associated with a somewhat higher scatter than the more recent measurements listed above (Ranzi et al., 2012).

Appendix A.4. Quasi-laminar burning velocity

For an initially laminar, outwardly propagating flame, hydrodynamic (Darrieus, 1938; Landau, 1944) and thermo-diffusive flame instabilities (Barenblatt et al., 1962; Sivashinsky, 1977) will lead to the appearance of a cellular flame surface at a critical flame radius. The transition into a cellular regime of flame propagation is associated with an increase in flame surface area and a corresponding increase in the overall burning velocity (Bradley, 1999). By assuming that the flame surface in the cellular regime follows a fractal pattern with a fractal dimension of $D = 7/3$ (Gostintsev et al., 1988; Bradley, 1999), the burning velocity in the cellular regime is found to increase with the flame radius as $R_f^{1/3}$. Values for the flame radius exponent ranging from $1/3$ to $1/6$, depending on the mixture composition and experimental configuration, have been measured later (Gostintsev et al., 1999; Pan and Fursenko, 2008; Bauwens et al., 2015).

To model the regime of cellular flame propagation, a so-called quasi-laminar burning velocity u_{ql} on the form of

$$u_{ql} = u_l\left(1 + C_{ql}R_f^a\right) \tag{A.6}$$

is applied in FLACS, where C_{ql} is a mixture dependent model constant, R_f is the flame radius and a is a general model constant. Based on experiments (Arntzen, 1998), the radius exponent a was set to 0.5.

Appendix A.5. Turbulent burning velocity and its quenching limit

A range of expressions relating turbulence variables to the combustion rate in turbulent premixed flames have been proposed, see e.g. (Lipatnikov and Chomiak, 2002). There are significant uncertainties associated with such simple correlations (Verma and Lipatnikov, 2016) and with Reynolds-averaged Navier-Stokes equations (RANS) modelling of premixed turbulent combustion in general (Poinsot and Veynante, 2011).

In standard FLACS v10.4r1, the turbulent burning velocity correlation presented by Bray (1990) is used. Bray (1990) correlated the 1650 separate measurements of turbulent burning velocities for premixed gaseous mixtures consolidated by Abdel-Gayed et al. (1987), and expressed the turbulent burning velocity u_t in terms of the Karlovitz stretch factor K according to

$$\frac{u_t}{u'} = \alpha K^{\beta}, \quad K = C_K\left(\frac{u'}{u_l}\right)^2\left(\frac{u'l_l}{\nu}\right)^{-0.5}, \tag{A.7}$$

where $C_K = 0.157$, u' is the turbulence velocity fluctuation, ν is the kinematic viscosity, and l_l is the integral length scale of turbulence. Bray (1990) set the constants α and β to 0.875 and −0.393, respectively. Bradley et al. (1992) derived a correlation from the same data set on the same general form, also incorporating the Lewis number Le according to

$$\frac{u_t}{u'_k} = \alpha(KLe)^{\beta}.$$

Bradley et al. (1992) set $\alpha = 0.88$ and $\beta = -0.3$ and replaced u' with an effective turbulence velocity fluctuation u'_k representing the part of the turbulence spectrum that acts on the flame kernel, tending towards u' as the flame propagates. Bradley et al. (2011, 2013) give updated correlations on the form of Equation (A.7), where α and β are explicitly expressed in terms of the strain rate Markstein number Ma_{sr} of the mixture. There are additional uncertainties associated with the evaluation of Ma_{sr}.

At high values of the Karlovitz stretch factor K and the Reynolds number $Re = Ul/\nu$, where U is the flow speed and l is a characteristic length scale, quenching of the turbulent flame brush commences. In standard FLACS v10.4r1, the limit for u_t increasing with u' is set when K exceeds $K_q = 1.0$, i.e. the turbulent burning velocity u_t is kept constant for $K > 1.0$ (Arntzen, 1998). Meanwhile, findings from direct numerical simulations (Poinsot et al., 1991) suggest that the quenching limit may be located around $K \approx 25$, near the border between the thin reaction zones and distributed reaction zones regimes of Peters (2001), where the smallest turbulence eddies start to penetrate the reaction zone. Bradley et al. (2013) demonstrated that the critical stretch rate for flame quenching depends significantly on the local Markstein number. In summary, there are considerable uncertainties associated with the use of a quenching limit for turbulent premixed combustion.

Appendix A.6. Sub-grid flame folding

Through the modelled turbulence parameters in the burning velocity correlation of Equation (A.7), sub-grid geometry influences the rate of combustion. In addition, the flame front folding around objects will increase the flame surface area, and thereby enhance the mass burning rate further. For sub-grid objects this effect is not resolved, and must therefore be modelled. Arntzen (1998) argues that the additional flame surface area from sub-grid obstructions, ΔA, will increase with the size of the obstruction and the distance the flame front is transported downstream before the wake behind the obstruction is burned out. The analysis by Arntzen (1998) results in

$$\frac{\Delta A}{A} = C_{fl}\sqrt{U_c}\varphi_i CT_i, \tag{A.8}$$

where U_c is the normalised downstream flow velocity, φ_i is a direction vector, and CT_i denotes the total surface area of the "ending walls" of the sub-grid obstructions for flow in the ith direction. In Equation (A.8), C_{fl} is a model parameter, determined by validation against experiments.

References

Abdel-Gayed, R.G., Bradley, D., Lawes, M., 1987. Turbulent burning velocities: a general correlation in terms of straining rates. Proc. R. Soc. Lond. Ser. A, Math. Phys. Sci. 414 (1847), 389–413.

Al-Hassan, T., Johnson, D. M., 1998. Gas explosions in large scale offshore module geometries: overpressures, mitigation and repeatability. In: Seventeenth International Conference on Offshore Mechanics and Arctic Engineering (OMAE). Lisbon.

Arntzen, B.J., 1998. Modelling of Turbulence and Combustion for Simulation of Gas Explosions in Complex Geometries. Ph.D. thesis. NTNU, Trondheim.

Aven, T., Vinnem, J., 2007. Risk Management, with Applications from the Offshore Oil and Gas Industry. Springer Verlag, New York.

Barenblatt, G., Zeldovich, Y., Istratov, A., 1962. Diffusive-thermal stability of a laminar flame. Prikl. Mekh. Fiz. 2, 21.

Bauwens, C.R., 2010. Effect of ignition location, vent size, and obstacles on vented explosion overpressures in propane-air mixtures. Combust. Sci. Technol. 182 (11–12), 1915–1932.

Bauwens, C.R., Bergthorson, J.M., Dorofeev, S.B., 2015. Experimental study of spherical-flame acceleration mechanisms in large-scale propane-air flames. Proc. Combust. Inst. 35 (2), 2059–2066.

Beale, M., Hagan, M., Demuth, H., 2015. MATLAB Neural Network Toolbox User's Guide. The MathWorks, Natick, MA.

Bosschaart, K.J., De Goey, L.P.H., 2004. The laminar burning velocity of flames propagating in mixtures of hydrocarbons and air measured with the heat flux method. Combust. Flame 136, 261–269.

Box, G.E.P., Draper, N.R., 2006. Response Surfaces, Mixtures, and Ridge Analyses. John Wiley & Sons, Hoboken, NJ.

Braatz, A.-L., Hisken, H., Rückmann, J.-J., 2016. In: Surrogate-based Optimisation of Model Parameters for the Improved Modelling of Industrial-scale Gas Explosions. in: 5th International Conference on Engineering Optimization (EngOpt 2016). Iguassu Falls, Brazil, pp. 19–23. June 2016.

Bradley, D., 1999. Instabilities and flame speeds in large-scale premixed gaseous explosions. Philos. Trans. Math. Phys. Eng. Sci. 357, 3567–3581 (1764, Combustion Science at the End of the Millennium).

Bradley, D., Lau, A., Lawes, M., 1992. Flame stretch rate as a determinant of turbulent burning velocity. Philos. Trans. Phys. Sci. Eng. 338 (1650), 359–387.

Bradley, D., Lawes, M., Liu, K., Mansour, M., 2013. Measurements and correlations of turbulent burning velocities over wide ranges of fuels and elevated pressures. Proc. Combust. Inst. 34 (1), 1519–1526.

Bradley, D., Lawes, M., Mansour, M., 2011. Measurement of turbulent burning velocities in implosions at high pressures. Proc. Combust. Inst. 33 (1), 1269–1275.

Bray, K.N.C., 1990. Studies of the turbulent burning velocity. Proc. R. Soc. Lond. Math. Phys. Sci. 431 (1882), 315–335.

Chao, J., Bauwens, C.R., Dorofeev, S.B., 2011. An analysis of peak overpressures in vented gaseous explosions. Proc. Combust. Inst. 33 (2), 2367–2374.

Darrieus, G., 1938. Propagation d'un front de flamme. Presented at La Technique Moderne in 1938 (Paris) and in 1945 at Congrès de Méchanique Appliquée (Paris).

Davis, S.D., Mhadeshwar, A.B., Vlachos, D.G., Wang, H., 2004. A new approach to response surface development for detailed gas-phase and surface reaction kinetic model optimization. Int. J. Chem. Kinet. 36, 94–106.

Evans, J.A., Exon, R., Johnson, D.M., Health, G.B., Executive, S., 1999. The Repeatability of Large Scale Explosion Experiments. Offshore Technology Report. Great Britain, Health and Safety Executive available at: www.hse.gov.uk/research/otopdf/1999/oto99042.pdf (accessed 25- April- 2016).

Ferreira, T.D., Vianna, S.S.V., 2014. A novel coupled response surface for flammable gas cloud volume prediction. Int. J. Model. Simul. Petroleum Industry 8 (1).

Foisselon, P., Hansen, O.R., van Wingerden, K., 1998. Detailed Analysis of FLACS Performance in Comparison to Full-scale Experiments. CMR report no. CMR-98-F30058, Chr. Michelsen Research, Bergen, Norway.

Gant, S.E., Kelsey, A., McNally, K., Witlox, H.W.M., Bilio, M., 2013. Methodology for global sensitivity analysis of consequence models. J. Loss Prev. Process Industries 26 (4), 792–802.

Gexcon AS, 2015. FLACS v10.4r1 Users Manual. Confidential report. Gexcon AS, Bergen, Norway. information at. www.flacs.com.

Gostintsev, Y.A., Istranov, A.G., Shulenin, Y.V., 1988. Self-similar propagation of a free turbulent flame in mixed gas mixtures. Combust. Explos. Shock Waves 24, 563–569.

Gostintsev, Y.A., Istranov, A.G., Shulenin, Y.V., 1999. Autoturbulization of gas flames: analysis of experimental results. High. Temp. 37 (282).

Gu, X.J., Haq, M.Z., Lawes, M., Woolley, R., 2000. Laminar burning velocity and Markstein lengths of methane-air mixtures. Combust. Flame 121, 41–58.

Halter, F., Tahtouh, T., Mounaim-Rousselle, C., 2010. Nonlinear effects of stretch on the flame front propagation. Combust. Flame 157, 1825–1832.

Hansen, O.R., Johnson, D.M., 2014. Improved far-field blast predictions from fast deflagrations, DDTs and detonations of vapour clouds using FLACS CFD. J. Loss Prev. Process Industries 35, 293–306.

Hassan, M.I., Aung, K.T., Kwon, O.C., Faeth, G.M., 1998. Properties of laminar premixed hydrocarbon/air flames at various pressures. J. Propuls. Power 14, 478–488.

Haupt, S.E., Pasini, A., Marzban, C., 2008. Artificial Intelligence Methods in the Environmental Sciences, first ed. Springer Netherlands.

Haykin, S., 1998. Neural Networks: a Comprehensive Foundation, second ed. Prentice Hall PTR, Upper Saddle River, NJ.

Haykin, S., 1999. Neural networks: a guided tour. In: Sinha, N.K., Gupta, M.M. (Eds.), Soft Computing and Intelligent Systems: Theory and Applications. Morgan Kaufmann Publishers Inc., San Francisco, pp. 71–80.

Hjertager, B.H., 1982. Simulation of transient compressible turbulent reactive flows. Combust. Sci. Technol. 27 (5–6), 159–170.

Hjertager, B.H., 1986. Three-dimensional Modeling of Flow, Heat Transfer, and Combustion. in: Handbook of Heat and Mass Transfer. Ch. 41. Gulf Publishing, Houston, pp. 1303–1350.

Hudson, P.T.W., Postma, E.O., 1995. Choosing and using a neural net. In: Braspenning, P.J., Thuijsman, F., Weijters, A.J. (Eds.), Artificial Neural Networks. Vol. 931 of Lecture Notes in Computer Science. Springer Berlin, pp. 273–287.

Huser, A., Kvernvold, O., 2000. Explosion Risk Analysis- Development of a General Method for Gas Dispersion Analyses on Offshore Platforms. in: Parallel Computational Fluid Dynamics: Trends and Applications. Elsevier Science B.V., Trondheim. Ch. 59.

Jomaas, G., Zheng, X.L., Zhu, D.L., Law, C.K., 2005. Experimental determination of counterflow ignition temperatures and laminar flame speeds of C2-C3 hydrocarbons at atmospheric and elevated pressures. Proc. Combust. Inst. 30, 193–200.

Landau, L.D., 1944. On the theory of slow combustion. Zh. Eksp. i Theor. Fiz. 14, 240.

Launder, B.E., Spalding, D.B., 1974. The numerical computation of turbulent flows. Comput. Methods Appl. Mech. Eng. 3 (2), 269–289.

Law, C.K., Zhu, D., Yu, G., 1988. Propagation and extinction of stretched premixed flames. Symposium Int. Combust. 21 (1), 1419–1426.

Lipatnikov, A., Chomiak, J., 2002. Turbulent flame speed and thickness: phenomenology, evaluation, and application in multi-dimensional simulations. Prog. Energy Combust. Sci. 28 (1), 1–73.

Marsh, 2014. The 100 Largest Losses 1974–2013 – Large Property Damage Losses in the Hydrocarbon Industry. Tech. rep.. Marsh Global Energy Risk Engineering, London. available at: https://www.marsh.com/uk/insights/research/the-100-largest-losses-in-the-hydrocarbon-industry-1974-2013.html (accessed 25- April- 2016).

Masters, T., 1993. Practical Neural Network Recipes in C++. Academic, San Diego, CA.

McKay, M.D., Beckman, R.J., Conover, W.J., 1979. A comparison of three methods for selecting values of input variables in the analysis of output from a computer code. Technometrics 21 (2), 239–245.

Mercx, W.P.M., 1994. Modelling and Experimental Research into Gas Explosions. Overall Final Report for the MERGE Project. CEC contract STEP-CT-0111 (SMA).

Model Evaluation Group Gas Explosions (MEGGE), 1996. Gas explosion Model Evaluation Protocol. Thechnical report, version 1.

Pan, K.-L., Fursenko, R., 2008. Characteristics of cylindrical flame acceleration in outward expansion. Phys. Fluids 20 (9).

Park, O., Veloo, P.S., Liu, N., Egolfopoulos, F.N., 2011. Combustion characteristics of alternative gaseous fuels. Proc. Combust. Inst. 33, 887–894.

Patankar, S.V., Spalding, D.B., 1974. A calculation procedure for the transient and steady-state behavior of shell-and-tube heat exchangers. In: Afgan, N., Schlunder, E. (Eds.), Heat Exchangers: Design and Theory Sourcebook. McGraw-Hill, New York, pp. 155–176.

Peters, N., 2001. Turbulent Combustion. Cambridge University Press.

Poinsot, T., Veynante, D., 2011. Theoretical and Numerical Combustion. T. Poinsot, third ed.

Poinsot, T., Veynante, D., Candel, S., 1991. Diagrams of premixed turbulent combustion based on direct simulation. Symposium Int. Combust. 23 (1), 613–619.

Popat, N.R., Catlin, C.A., Arntzen, B.J., Lindstedt, R.P., Hjertager, B.H., Solberg, T., Saeter, O., den Berg, A.C.V., 1996. Investigations to improve and assess the accuracy of computational fluid dynamic based explosion models. J. Hazard. Mater. 45 (1), 1–25.

Ranzi, E., Frassoldati, A., Grana, R., Cuoci, A., Faravelli, T., Kelley, A., Law, C., 2012. Hierarchical and comparative kinetic modeling of laminar flame speeds of hydrocarbon and oxygenated fuels. Prog. Energy Combust. Sci. 38 (4), 468–501.

Rozenchan, G., Zhu, D.L., Law, C.K., Tse, S.D., 2002. Outward propagation, burning velocities, and chemical effects of methane flames up to 60 atm. Proc. Combust. Inst. 29, 1461–1469.

Rutherford, B. M., Swiler, L. P., Paez, T. L., Urbina, A., 2006. Response surface (metamodel) methods and applications. In: IMAC-XXIV: Conference & Exposition on Structural Dynamics.

Saltelli, A., Ratto, M., Andres, T., Campolongo, F., Cariboni, J., Gatelli, D., Saisana, M., Tarantola, S., 2008. Global Sensitivity Analysis. The Primer. John Wiley & Sons, Ltd.

Sha, W.T., Launder, B.E., 1979. A Model for Turbulent Momentum and Heat Transport in Large Rod Bundles. Report ANL-77–73. Argonne National Laboratory, Illinois.

Sha, W.T., Yang, C.I., Kao, T.T., Cho, S.M., 1982. Multidimensional numerical modeling of heat exchangers. J. Heat Transf. 104 (3), 417–425.

Simpson, T.W., Booker, A.J., Ghosh, D., Giunta, A.A., Koch, P.N., Yang, R.-J., 2004. Approximation methods in multidisciplinary analysis and optimization: a panel discussion. Struct. Multidiscip. Optim. 27 (5), 302–313.

Sivashinsky, G., 1977. Diffusional-thermal theory of cellular flames. Combust. Sci. Technol. 15 (3–4), 137–145.

Skjold, T., Pedersen, H.H., Bernard, L., Ichard, M., Middha, P., Narasimhamurthy, V.D., Landvik, T., Lea, T., Pesch, L., 2013. A matter of life and death: validating, qualifying and documenting models for simulating flow-related accident scenarios in the process industry. Chem. Eng. Trans. 31, 187–192.

Skjold, T., Pedersen, H.H., Narasimhamurthy, V.D., Lakshmipathy, S., Pesch, L., Atanga, G.F., Folusiak, M., Bernard, L., Siccama, D., Storvik, I.E., 2014. Pragmatic modelling of industrial explosions in complex geometries: review of the state-of-the-art and prospects for the future. In: Borisov, A.A., Frolov, S.M. (Eds.), Zel'dovich Memorial: Accomplishments in the Combustion Science in the Last Decade, vol. 1. Torus Press, Moscow, pp. 70–74.

Graphic design: Communication Division, UiB / Print: Skipnes Kommunikasjon AS

uib.no

ISBN: 9788230854983 (print)
9788230857847 (PDF)